

A Search for X-ray Counterparts of Radio Pulsars

T. Prinz¹ and W. Becker^{1,2}

Submitted for publication to ApJ on 2015 November 14. / revised and updated 1. Juli 2016

ABSTRACT

We describe a systematic search for X-ray counterparts of radio pulsars. The search was accomplished by cross-correlating the radio timing positions of all radio pulsars from the ATNF pulsar database (version 1.54) with archival XMM-Newton and Chandra observations publicly released by July 1st 2016. In total, 178 of the archival XMM-Newton observations and 213 of the archival Chandra datasets were found to have a radio pulsar serendipitously in the field of view. From the 288 radio pulsars covered by these datasets we identified 20 previously undetected X-ray counterparts. For 6 of them the statistics was sufficient to model the energy spectrum with one- or two-component models. For the remaining new detections and for those pulsars for which we determined an upper limit to their counting rate we computed the energy flux by assuming a Crab-like spectrum. Additionally, we derived upper limits on the neutron stars' surface temperature and on the non-thermal X-ray efficiency for those pulsars for which the spin-down energy was known. The temperature upper limits were compared with predictions from various neutron star cooling models and were found to be in agreement with the minimal cooling paradigm.

Subject headings: stars: neutron - pulsars: individual: PSR J0101–6422, PSR B0114+58, PSR J0337+1715, PSR J0543+2329, PSR B0919+06, PSR J1044–5737, PSR J1112–6103, PSR B1221–63, PSR J1301–6310, PSR B1338–62, PSR J1600–3053, PSR J1658–5324, PSR J1730–2304, PSR J1731–1847, PSR J1816+4510, PSR J1825–0935, PSR J1832–0836, PSR J1911–1114, PSR J2017+0603, PSR J2222–0137 - X-rays: stars - dense matter - equation of state

1. Introduction

Neutron stars (NSs) are the most dense objects accessible in the universe by direct observations. They represent unique astrophysical laboratories which allow us to explore the properties

¹Max-Planck Institut für extraterrestrische Physik, Giessenbachstrasse 1, 85741 Garching, Germany

²Max-Planck Institut für Radioastronomie, Auf dem Hügel 69, 53121 Bonn, Germany

of matter under the most extreme conditions observable in nature. Studying neutron stars is therefore an interdisciplinary field, where astronomers and astrophysicists work together with a broad community of physicists. Particle, nuclear and solid-state physicists are strongly interested in the internal structure of neutron stars which is largely uncertain because of the unknown nuclear interaction potential at matter densities above the nuclear density $\rho_{\text{nuc}} = 2.8 \times 10^{14} \text{ g cm}^{-3}$. The structure of the star is usually described by the equation of state (EOS) which is a set of non-linear coupled differential equations respecting general relativity and linking physical parameters like star composition, pressure and density as well as the energy balance, radiative energy transport, opacity and luminosity to each other.

Neutron stars are formed at very high temperatures, $\sim 10^{11} \text{ K}$, in the imploding core of supernova explosions. Much of the initial thermal energy is radiated away from the interior of the star by various processes of neutrino emission (mainly, Urca processes and neutrino bremsstrahlung), leaving a one-day-old neutron star with an internal temperature of about 10^9 – 10^{10} K . After $\sim 100 \text{ yr}$ (typical time of thermal relaxation), the star's interior is supposed to become nearly isothermal. The details of neutron star cooling, however, depend very strongly on the chemical composition and the physical behavior of the super-dense neutron star matter, described by its EOS. A very promising approach to constrain that EOS is therefore to look at the thermal evolution of neutron stars by comparing theoretical predictions from various cooling models (i.e. various EOSs) with measured surface temperatures (e.g. Becker 2009, and references therein). In this scenario, Page et al. (2004) introduced the minimal cooling paradigm, which extends and replaces the so-called standard cooling scenario (Tsuruta 1998) to include neutrino emission from the Cooper pair breaking and formation process for temperatures close to the critical temperature of superfluid pairing.

As far as non-thermal emission processes in neutron stars are concerned, several attempts have been made in recent years to explore the fraction of spin-down energy which is emitted into the X-ray band. With every new X-ray observatory and improvement in sensitivity this ratio was reinvested. Often, different authors used different approaches and different energy bands which makes it difficult to compare the various results available in the literature. Different point-spread functions and energy responses used in the various X-ray telescopes sample more or less of an eventually existing diffuse compact pulsar wind nebula. This adds to the complexity of this problem too.

Seward & Wang (1988) used the Einstein observatory to explore the X-ray efficiency of rotation-powered pulsars. Based of only a handful of mostly young and powerful pulsars they found $L_X(0.2 - 4 \text{ keV}) \approx 10^{1.39} \dot{E}$. With ROSAT data and on a much larger dataset, which for the first time included a variety of rotation-powered pulsars at various spin-down ages and energies, Becker & Trümper (1997) fitted $L_X(0.1 - 2.4 \text{ keV}) \approx 10^{1.03} \dot{E}$. Adopting the soft energy spectra measured by ROSAT and assuming that those spectra continue unchanged up to 10 keV, Possenti et al. (2002) derived $L_X(2 - 10 \text{ keV}) \approx 10^{1.34} \dot{E}$. Results from XMM-Newton and Chandra soon

showed that the emission in the soft and hard X-ray band is often based on different emission processes and hence have different efficiencies, invalidating the X-ray efficiencies derived by Possenti et al. (2002). The most recent results which are based on XMM-Newton and Chandra data yield $L_X(2 - 10 \text{ keV}) \approx 10^{0.92} \dot{E}$ (Li et al. 2008) and $L_X(0.1 - 2 \text{ keV}) \approx 10^{0.997} \dot{E}$ (Becker 2009) for the hard and soft X-ray band, respectively.

Thanks to the collecting power and sensitivity of todays X-ray satellites the sample of rotation-powered pulsars detected in X-rays is steadily increasing. At the end of the ROSAT mission 33 rotation-powered pulsars were detected (e.g. Becker & Trümper 1997, 1999). By July 1st 2016 and about 16 years after the launch of Chandra and XMM-Newton we count 188 X-ray detected neutron stars which are reported in the literature. 123 pulsars are detected in the γ -regime of which 73 are seen in both wavelength bands. Their emission properties are seen to scale with their spin-down age $\tau = P/(2\dot{P})$. Among the X-ray detected pulsars 23 turn out to be Crab-like (age $\tau \leq 10^4$ yrs), 41 Vela-like ($10^4 \text{ yrs} < \tau \leq 10^5$ yrs), 17 are classified as cooling neutron stars ($10^5 \text{ yrs} \leq \tau \leq 10^6$ yrs), 13 are so called old field pulsars ($10^6 \text{ yrs} \leq \tau \leq 10^8$ yrs) and 62 are millisecond pulsars (MSPs, $\tau \geq 10^8$ yrs and $P \leq 20$ ms). Of the X-ray detected pulsars 17 are in the category of Anomalous X-ray Pulsars (AXPs) or Soft Gamma-ray Repeaters (SGRs) and 7 are classified as Central Compact Objects (CCOs). A high-energy overview of the soft γ -ray pulsar population was given recently by Kuiper & Hermsen (2015).

Whereas with Einstein, ROSAT, ASCA and BeppoSax mostly the brighter pulsars and those which are seen under a favorable beaming geometry got detected, we now have also apparently less efficient X-ray emitting pulsars in the sample. E.g. PSR J2022+3842 has an X-ray efficiency $\mu_X = L_X/\dot{E} = 6 \times 10^{-5}$ in the 2–10 keV range (Arzoumanian et al. 2011) and Kargaltsev et al. (2012) found that μ_X of PSR J0940–5428 and PSR J1913+1011 is below 4.0×10^{-6} and 3.3×10^{-6} in the 0.5–8 keV energy range, respectively. Whether these pulsars are intrinsically less efficient X-ray emitters because of differences in the emission process or because of an unfavorable beaming geometry is still unclear. Further indications of apparently underluminous X-ray pulsars is therefore of high importance.

In this paper we report on X-ray counterpart searches for radio pulsars. The search was accomplished by correlating the ATNF Pulsar Catalogue (version 1.54, Manchester et al. 2005)¹ with the XMM-Newton and Chandra data archives to identify those observations which had a radio pulsar serendipitously in the field of view. The structure of the paper is as follows: in section 2 we describe the XMM-Newton and Chandra observations used in our correlation and provide the details of the data processing, source detection as well as counting rate upper-limit determination for undetected pulsars. The spatial and spectral analysis of the detected pulsars as well as flux

¹<http://www.atnf.csiro.au/research/pulsar/psrcat/>

estimates for those pulsars for which we just could determine a count rate upper limit are described in section 3. A discussion of the results and a concluding summary is given in section 5 and 6, respectively.

2. Observations and data reduction

In the past 16 years, Chandra² and XMM-Newton³ have proven to be extremely reliable and successful observatories (e.g. Tananbaum et al. (2014), Schartel (2012)). Both missions release their data to a public archive after a one year proprietary time. End of 2013 the XMM-Newton observatory covered already about 877 deg² of the sky (Xmm-Newton Survey Science Centre 2013). For Chandra the sky coverage is predicted to be about 550 deg² by the end of 2015 (cf. The Chandra Source Catalog⁴ Rev. 2, planned to be released in 2016, B. Wilkes, priv. com.) Many of these observations were targeted at sources located in the galactic plane, where the majority of radio pulsars is located. The chance probability that a pulsar has been covered serendipitously in one of these observations is therefore quite high. We made use of all pointed observations publicly available in these archives by July 1st 2016 and searched for datasets which had one of the ~2500 known radio pulsars listed in the ATNF Pulsar Catalogue (version 1.54, Manchester et al. 2005) in the field of view. Pulsars which were previously already detected in X-rays were neglected in our search. In total we found 178 XMM-Newton datasets and 213 Chandra datasets which had the position of a pulsar previously undetected in X-rays covered. All these datasets sum up to an on-axis observing time of 8.6 Msec. A summary of these data, listing instruments, observing modes and filters, off-axis angles of pulsar locations as well as on- and off-axis exposure times of the relevant observations is given in Table 1.

For the reduction of XMM-Newton data we used the XMM-Newton Science Analysis Software (SAS), version 15.0.0. In case of the Chandra data we used standard processed level-2 data and the Chandra Interactive Analysis of Observations (CIAO) software, version 4.8.2. In both cases we had to remove flares from the observation. As for XMM-Newton these flares are mostly coming from soft protons hitting the detector. To identify and remove these time intervals of high particle background we created light curves from MOS1/2 and PN event files at energies above 10 keV and of bin size 100s. We detected flares in almost all XMM-Newton data sets and rejected time intervals in which the count rate per bin was 3σ higher than the mean count rate without flares. Regarding Chandra observations we made use of the CIAO defflare script, which applies the

²<http://cda.harvard.edu/chaser/>

³<http://xmm.esac.esa.int/xsa/index.shtml>

⁴<http://cxc.harvard.edu/csc2/preliminary/>

criterion mentioned above by default.

The effective exposure time $t(\theta)$ (θ labels the off-axis angle a pulsar was observed under) was obtained by generating an exposure map with the SAS-tool `eexpmap` or the CIAO-tool `fluximage` after correcting for times with high background and dead time correction. In both cases the task takes into account the telescope vignetting at the respective off-axis angle. The net exposure on the source $t(\theta)$ and on the background region $t_{\text{BG}}(\theta)$ was then calculated by averaging the exposure map over the source and background region, respectively. This is required to include the effect of the CCD gaps on the exposure time. The on-axis exposure $t_{\text{on-axis}}$ and $t(\theta)$ are both listed in Table 1.

2.1. Spatial and image analysis

In order to search for X-ray sources in the selected datasets we applied a sliding box source detection algorithm for XMM-Newton data (SAS-tool `edetect_chain`) using the five standard bands (0.2–0.5 keV, 0.5–2 keV, 2–4.5 keV, 4.5–7.5 keV, and 7.5–12 keV). For Chandra data we applied a wavelet source detection algorithm (CIAO-tool `wavdetect`) in the energy range 0.1–10 keV. Both procedures turn out to be standard for the source detection in XMM-Newton and Chandra data. We accepted a source to be detected if its significance was $\geq 5\sigma$ above the background.

The angular separation in arcseconds between the radio timing position of a pulsar and the centroid of the nearest X-ray source were compared. An X-ray source was considered to be a potential counterpart of a radio pulsar if the angular distance Δ between them was

$$\Delta = \sqrt{(\Delta RA \cdot \cos(DEC_X))^2 + \Delta DEC^2} \leq 3\sigma. \quad (1)$$

Here $\Delta RA = RA_R - RA_X$ and $\Delta DEC = DEC_R - DEC_X$. (RA_X, DEC_X) and (RA_R, DEC_R) denote the positions of the X-ray source and the radio pulsar's timing position, respectively.

The uncertainty σ is obtained by deducing the error in Δ applying error propagation:

$$\sigma = \frac{\sqrt{(\Delta RA \cos(DEC_X))^2(\delta RA_R^2 + \delta RA_X^2) + \Delta DEC^2 \delta DEC_R^2 + (\Delta DEC - \Delta RA \sin(DEC_X))^2 \delta DEC_X^2}}{\Delta} \quad (2)$$

The uncertainties of the X-ray source positions in right ascension and declination $\delta RA_X, \delta DEC_X$ were determined by combining the statistical position errors and the absolute astrometric accuracy of the corresponding X-ray observatory squared. For Chandra ACIS-S, ACIS-I and HRC-S data

the 68% confidence level is $\approx 0.21''$, $\approx 0.4''$ and $\approx 0.36''$, respectively⁵. The absolute astrometric accuracy for XMM-Newton data is $\approx 2''$ (r.m.s.)⁶. We note that the uncertainties in the pulsars' radio timing position δRA_R , δDEC_R are generally at the level of milli-arcseconds. Thus, the dominant source of uncertainty in the X-ray counterpart correlation is the error in the X-ray source position.

To check whether an X-ray source has an optical counterpart we correlated all X-ray sources with the USNO-B catalog. It covers the whole sky and is thought to be complete down to a visible magnitude of $V = 21$ (Monet et al. 2003). The correlation was done using the online tool VizieR⁷ which also allowed us to constraint the X-ray-to-visual flux ratio (Maccacaro et al. 1988)

$$\log(f_X/f_V) = \log(f_X) + V/2.5 + 5.37. \quad (3)$$

for each of the detected sources. Here f_X is the X-ray flux in the 0.3–3.5 keV band in $\text{erg cm}^{-2} \text{s}^{-1}$. If no optical source could be detected within an error circle of radius 3σ we took the limiting magnitude of the USNO-B catalog as an estimate for V . Within the 3σ error box around a potential pulsar X-ray counterpart no optical source was found.

In order to compute the probability P_{coin} of a chance identification with a background source

$$P_{\text{coin}} = \frac{N_X}{l_{\text{RA}} l_{\text{Decl}}} \times \pi \delta RA_R \delta DEC_R \quad (4)$$

we computed the source density in the field of view and multiplied it with the area of the pulsar's error ellipse, where N_X is the number of sources detected within the field of view of area $l_{\text{RA}} \times l_{\text{Decl}}$. To exclude a by-chance identification of an X-ray source with the X-ray counterpart of a radio pulsar we set the criteria $P_{\text{coin}} \leq 3 \cdot 10^{-3}$.

2.2. Spectral analysis

Up to the High-Resolution Channel Plate (HRC) detector all focal plan instruments aboard Chandra and XMM-Newton provide spectral information. However, the quality of spectral fits and the constraints on the spectral model parameters are strongly dependent on the photon statistics and thus vary among the detected potential pulsar counterparts.

⁵See <http://cxc.harvard.edu/cal/ASPECT/celmon/> for more details about Chandra absolute astrometric accuracy.

⁶More information can be found at xmm.vilspa.esa.es/docs/documents/CAL-TN-0018.pdf.

⁷<http://vizier.u-strasbg.fr/viz-bin/VizieR>

For sources detected by XMM-Newton the corresponding response and effective area files for the source and background emission were extracted using the SAS-script `especget`. For the PN camera we used only those events which have a detection pattern between 1 and 4 (single and double events). For the MOS camera we included triple events as well, having a pattern between 5 and 12. The pattern value indicates which detector pixels surrounding a CCD pixel hit by a X-ray photon are taken into account for the photon energy integration. In case of Chandra observations we extracted the source and background spectra of a potential counterpart and created the corresponding response and effective area files with the CIAO-script `specextract`.

For potential pulsar counterparts (cf. Table 2) which were detected with more than 70 source counts the statistics just turned out to allow a very brief spectral analysis with mostly one-component power law or blackbody model spectra. The small photon statistics, though, strongly limited the fitting results also in those cases. Often we had to fix the hydrogen column absorption to the one deduced from the radio pulsar’s dispersion measure DM which is listed in the ATNF Pulsar Catalogue (Manchester et al. 2005). This value was estimated by assuming a 10% ionization degree of the interstellar medium (ISM) along the line of sight towards the pulsar. The latter corresponds to a ratio of one free electron per ten neutral hydrogen atoms in the ISM, as commonly assumed in the literature.

For a consistency check we deduced $N_{\text{H}}^{\text{LAB}}$ from the LAB Survey of Galactic HI (Kalberla et al. 2005). $N_{\text{H}}^{\text{LAB}}$ is based on HI emission line measurements at a radio frequency of 21 cm and refers to the entire hydrogen column density along the line of sight. For all pulsars for which it turned out that N_{H} towards the source is higher than $N_{\text{H}}^{\text{LAB}}$ we used the latter.

The used DM and N_{H} for the potential X-ray counterparts are listed in Table 4. Additionally, N_{H} and $N_{\text{H}}^{\text{LAB}}$ are given in Table 5 for all analyzed potential counterparts.

As mentioned before, for sources observed with the HRC cameras no spectral information can be obtained from the pulsar. The only informations we have are the position and the counting rate in the energy range of the camera where it is sensitive to incoming photons. In this case and in the case of observations with less than 70 source counts we obtained constraints on the X-ray flux and luminosity by converting the pulsar counting rate into an equivalent flux. First, we obtained the net counting rate for these pulsar counterparts by dividing the source counts derived with the source detection software by the effective exposure time $t(\theta)$. The X-ray flux was then deduced for a typical pulsar spectrum using the method described in Section 2.4. As a typical pulsar spectrum we assumed a power law model with photon index 1.7 (Becker 2009) and a hydrogen column density based on the radio pulsar’s dispersion measure as mentioned previously. As the assumption of a spectral shape introduces an extra uncertainty when converting the photon flux to an energy flux we doubled the statistical error in the flux numbers off all potential counterparts which we detected with less than 70 source counts.

2.3. Timing analysis

The timing resolution of the ACIS and the EPIC-MOS cameras (~ 1 s) were insufficient to study the pulsed emission of the pulsars. Additionally, the time resolution of the EPIC-PN CCDs depends on the used observation mode. For all observations that had a high enough time resolution to study the temporal properties of a rotating neutron star we converted the event time tags to the Barycentric Dynamical Time using the SAS-tool `barycen`. For this we used the radio timing position. After folding the events with the pulsar’s rotation frequency given by the ATNF Pulsar Catalogue (Manchester et al. 2005) we searched for a periodic signal by applying the H-test (de Jager et al. 1989). However, for none of the detected counterparts pulsed emission could be found with a significance higher than a confidence level of 95%.

2.4. Upper limits

For all observations in which no source was detected sufficiently close to the radio position we derived an upper limit on the count rate as follows: First, we extracted the counts N_i including the background contribution for every single data set from XMM-Newton or Chandra within a circle of radius $r = 30''$ or $r = 2''$ around the radio position in the energy band E_{\min} to $E_{\max} = 4.5$ keV. E_{\min} is 0.2 keV for XMM-Newton and 0.1 keV for Chandra events. For Chandra data sets were the pulsar was observed far off-axis the radius had to be adjusted, because above $\approx 4'$ the point-spread-function broadens significantly. Hence, for an off-axis angle $4' < \theta \leq 8'$ the applied radius $r = 5''$ and for $\theta > 8'$ the radius $r = 10''$. The background counts B_i were extracted from an annulus of inner radius $r_{\text{inner}} = 1.5r$ and outer radius $r_{\text{outer}} = 2.5r$. To obtain the background counts in the source region, we had to normalize these counts to the source region by the fraction c_1 between source region area and annulus area and by the fraction c_2 between $t(\theta)$ and $t_{\text{BG}}(\theta)$. Because we used a finite region, we had to correct for the missing flux in the unselected wings of the point-spread function. This encircled energy fraction (EEF_i) was calculated with the help of the `eregionanalyse`- (XMM-Newton) and `psf`-tool (Chandra).

If $\sum_i^n N_i > 20$ counts, where n is the number of X-ray observations of a single pulsar, we derived the $x \cdot \sigma$ upper limit on the count rate with the following equation:

$$UL(x \cdot \sigma) = \frac{\max\left(\sum_i^n \frac{N_i - c_1 c_2 \cdot B_i}{EEF_i}, 0\right) + x \cdot \sum_i^n \frac{\sqrt{N_i + c_1^2 c_2^2 B_i}}{EEF_i}}{\sum_i^n t_i(\theta_i)}. \quad (5)$$

Otherwise, the upper limit was derived using the Bayesian approach introduced by Kraft et al. (1991) which has its advantage for observations with very small numbers of counts in the presence of background when compared with the classical method.

Assuming a pure blackbody (BB) spectrum we deduced the 3σ upper limit on the effective temperature $T_e = T_\infty(1+z)$ ⁸ by minimizing the difference $UL(3\sigma) - UL_{\text{BB}}(T_e)$ (Becker et al. 1993; Becker 1995), where

$$UL_{\text{BB}}(T_e) = \text{const.} \cdot \int_{E_{\min}}^{E_{\max}} \frac{E^2 A_{\text{eff}}(E) \cdot \exp(-\sigma(E) \cdot N_{\text{H}}^{\text{ul}})}{\exp(E(1+z)/k_B T_e)} dE. \quad (6)$$

Here $\text{const.} = \frac{2\pi(1+z)^2 R_0^2}{h^3 c^2 d_{\text{ul}}^2}$ with z the gravitational red shift for a neutron star with radius $R_0 = 11.43$ km and mass $M = 1.4M_\odot$, h the Planck constant, c the speed of light and d_{ul} the upper limit of the distance to the pulsar. Furthermore, $\sigma(E)$ is the interstellar photoelectric absorption cross section (Morrison & McCammon 1983), N_{H}^{ul} the upper limit of the hydrogen column density, k_B is the Boltzmann constant and A_{eff} is the weighted effective area of all used instruments with which a certain source was observed:

$$A_{\text{eff}}(E) = \frac{\sum_i^n A_i(E) t_i(\theta_i)}{\sum_i^n t_i(\theta_i)}, \quad (7)$$

where A_i is the on-axis effective area of the instrument used in the i th observation of the pulsar. Because the count rate is already vignetting corrected we used the on-axis effective area obtained with the SAS-task calview for the XMM-Newton EPIC cameras with different filters. The Chandra ACIS and HRC effective area were taken from the Portable, Interactive Multi-Mission Simulator (WebPIMMS), version 4.6.⁹ N_{H}^{ul} is calculated as described in Section 2.2, except that we add the error of DM to obtain the upper limit of N_{H} .

The distance estimate is based on the work by Verbiest et al. (2012), where they present a detailed analysis of all measured distances to pulsars. For all other sources we used the NE2001 model of Cordes & Lazio (2002) to transform the measured DM to a distance. We apply a distance error of 20 % to 120 % depending on their Galactic coordinates. According to this work the large difference in the used uncertainties is because the error in d is larger for a pulsar in a region of small electron density than in a region with higher density (Cordes & Lazio 2002).

To estimate the 2σ upper limit of the non-thermal X-ray efficiency we derived an expression for UL_{model} in a similar way as for the blackbody spectrum, except that we inserted a power law model (PL) with photon index $\Gamma = 1.7$ (Becker 2009) and minimizing $UL(2\sigma) - UL_{\text{PL}}(K)$ with

$$UL_{\text{PL}}(K) = K \int_{E_{\min}}^{E_{\max}} E^{-\Gamma} \exp(-\sigma(E) \cdot N_{\text{H}}^{\text{ul}}) \cdot A_{\text{eff}}(E) dE. \quad (8)$$

Using the resulting value for the normalization constant K and the assumed photon index we

⁸ T_∞ denotes the temperature measured by a distant observer.

⁹See <http://heasarc.nasa.gov/docs/software/tools/pimms.html>

can derive the flux upper limit in a certain energy range by integrating the power law model with the derived normalization over this energy band.

In the following, all given uncertainties represent the 1σ confidence range for one parameter of interest, unless stated otherwise.

3. Potential X-ray counterparts of radio pulsars

In our search for X-ray counterparts of radio pulsars we found 20 X-ray point sources sufficiently close to the corresponding radio pulsar’s timing positions to claim a match. The X-ray images of these sources are displayed in Figure 1. Their coordinates, the offset between their X-ray position and the radio pulsar’s timing position, Δ , as well as the chance probability P_{coin} and the X-ray to visual flux ratio for each of this sources are displayed in Table 2. Due to a limitation in the photon statistics a detailed spectral analysis was possible only for six of the 20 counterparts. The results of this spectral analysis are summarized in Table 3. In Table 4 the relevant parameters of the radio pulsars are listed along with the flux, the luminosity and the X-ray efficiency $\mu_{0.1-2 \text{ keV}}$ of their potential counterparts.

The following subsections highlight the results for the 20 potential X-ray counterparts and provide background information on the corresponding radio pulsars.

3.1. PSR J0101-6422

The binary millisecond pulsar PSR J0101-6422 was discovered with the Parkes radio telescope in an identification campaign for unidentified Fermi sources (Kerr et al. 2012). It was in the focus of the Chandra telescope for 9.0 ksec. In this observation we detected a faint X-ray point source only $0''.2 \pm 0''.4$ off from the pulsar’s radio position, making it a very likely X-ray counterpart of the pulsar. This point source has 34 ± 6 source counts. Converting the photon flux to an energy flux yields $F_X^{0.1-2 \text{ keV}} = (3.0 \pm 1.0) \times 10^{-14} \text{ erg s}^{-1} \text{ cm}^{-2}$ in the 0.1 to 2 keV range.

3.2. PSR B0114+58

The pulsar PSR B0114+58 (PSR J0117+5914) was first detected in the Princeton-NRAO pulsar survey (Stokes et al. 1985). In the XMM-Newton data archive we found a 9 ksec observation which had the pulsar in the focus of the telescope. Analyzing this data we detected a point source with 113 ± 13 source counts in the PN- and MOS1/2 cameras. It is located only $1''.6 \pm 2''.1$ off

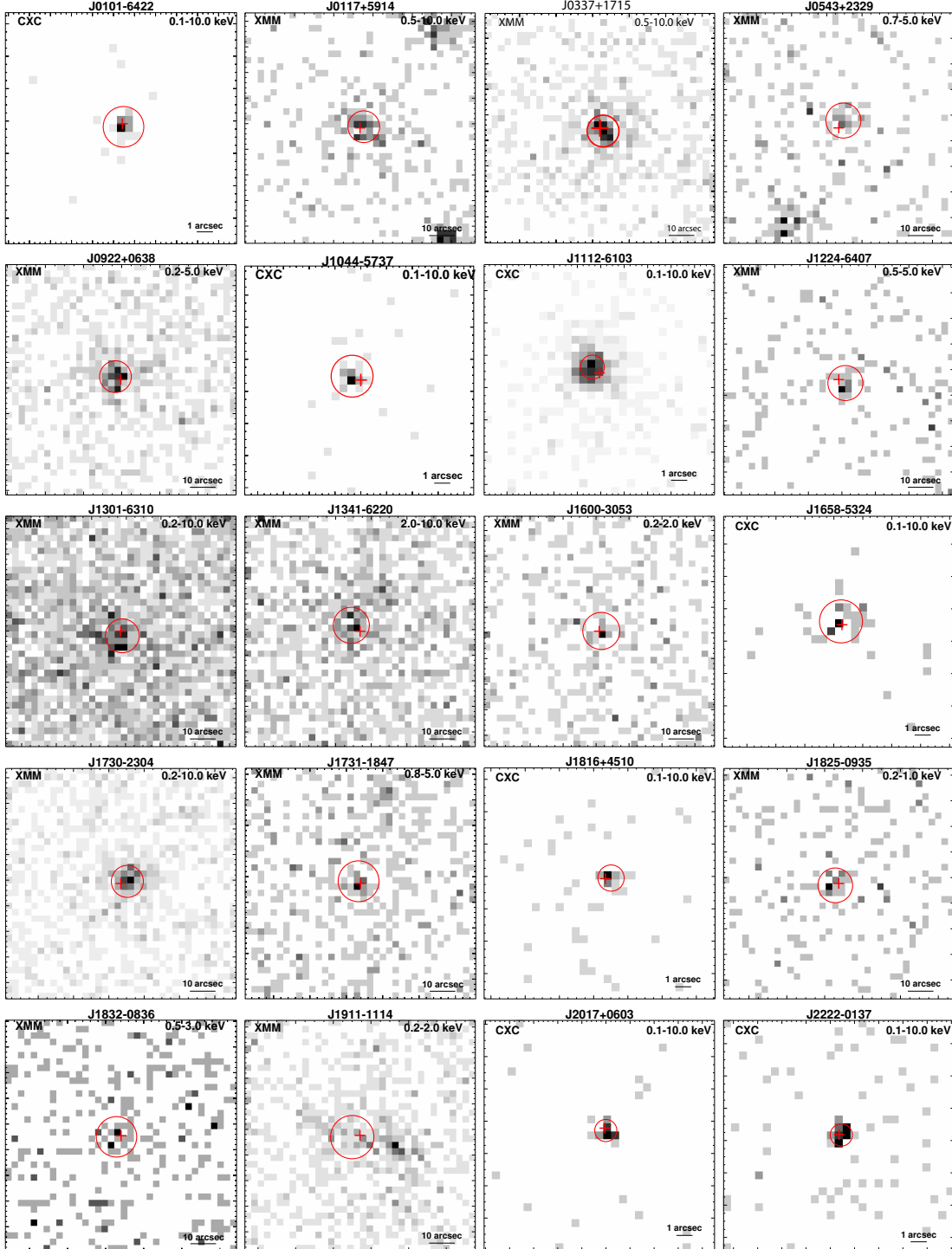


Fig. 1.— X-ray images of the region around all radio pulsars where an X-ray counterpart was detected in our correlation. Each panel has a size of $1'5 \times 1'5$ for XMM-Newton observations and $15'' \times 15''$ for Chandra observations. North is up and east is to the left. The cross marks the radio position of the pulsar and the red circle indicates the 3σ uncertainty in the measured X-ray position.

from the radio pulsar’s timing position, making it a positional match with the pulsar. The detected photons allowed a very brief spectral analysis. To do so we extracted the source counts from a circle of radius $20''$ centered on the counterpart. The background spectra were extracted from an annulus with inner and outer radius $45''$ and $75''$, respectively. The extracted counts were binned with at least 8 counts/bin in case of the PN data and 5 counts/bin for the MOS1/2 data sets. We first fitted the energy spectra with an absorbed power law and free varying N_{H} . This resulted in a fit with $\chi^2 = 12.1$ for 12 d.o.f. and $N_{\text{H}} = 0.5^{+0.7}_{-0.5} \times 10^{22} \text{ cm}^{-2}$, in agreement with the $N_{\text{H}} = 0.15 \times 10^{22} \text{ cm}^{-2}$ as deduced from the radio dispersion measurement DM and the model for the galactic distribution of free electrons by Cordes & Lazio (2002). To put better constraints on the remaining parameters we fixed N_{H} to the *DM*-based value. This gave an acceptable fit ($\chi^2 = 13.2$, 13 d.o.f.) with a photon index $\Gamma = 3.3 \pm 0.5$. Modeling the spectrum with a blackbody fitted the data as well and yielded a $\chi^2 = 12.2$ (13 d.o.f.). The resulting blackbody temperature is $2.1^{+0.4}_{-0.3} \times 10^6 \text{ K}$ with a normalization factor $K = 3.7^{+1.3}_{-1.1} \times 10^{-7}$. Using the normalization factor $K = L_{39}/D_{10}^2$ ($L_{39} = L/10^{39} \text{ erg/s}$ and $D_{10} = d/10 \text{ kpc}$) we deduced the emitting blackbody radius R_{BB} to be:

$$R_{BB} = \sqrt{\frac{K \cdot D_{10}^2 \times 10^{39} \text{ erg/s}}{4\pi\sigma_B T^4}} = (0.4 \pm 0.2) \text{ km.} \quad (9)$$

Herein σ_B is the Stefan-Boltzmann constant.

3.3. PSR J0337+1715

J0337+1715 is a millisecond pulsar in a triple system (Ransom et al. 2014). In an ~ 18 ksec archival XMM-Newton observation which had the pulsar in the focus of the telescope we detected a central point source with 303 ± 21 source counts in the PN and MOS1/2 data. The position of this source matches the radio pulsar’s timing position by only $1.''7 \pm 2.''1$ making it a positional counterpart of the pulsar. During the publication process of this paper a detailed analysis of the PSR J0337+1775 was published on astro-ph by Spiewak et al. (2016). We therefore refer to this publication for further analysis details and source properties.

3.4. PSR B0540+23

PSR B0540+23 (PSR J0543+2329) was first detected by Davies et al. (1972). In archival XMM-Newton data of ~ 20 ksec observing time in which the pulsar was in the focus of the telescope we detected a faint point source $3.''4 \pm 4.''8$ near to the radio pulsar’s timing position. The positional coincidence makes this X-ray source a very likely counterpart of the radio pulsar. It is

detected with 17 ± 4 source counts in the PN and MOS1/2 data. Converting the photon flux to an energy flux yields $F_X^{0.1-2 \text{ keV}} = (8 \pm 4) \times 10^{-15} \text{ erg s}^{-1} \text{ cm}^{-2}$ in the 0.1 to 2 keV range.

3.5. PSR B0919+06

The pulsar PSR B0919+06 (PSR J0922+0638) was discovered in the second Molonglo pulsar survey (Manchester et al. 1978). It has a measured parallax which places it at a distance of 1.1 ± 0.2 kpc (Verbiest et al. 2012). In archival XMM-Newton data of ~ 65 ksec observing time, taken with the pulsar position in the focus of the telescope, we detected a point source $2.^{\circ}4 \pm 2.^{\circ}1$ near to the radio pulsar’s timing position. Merging the PN and MOS1/2 data yielded 171 ± 18 source counts which supported a brief spectral analysis.

The energy spectrum was extracted by selecting all events from within a circle of radius $15''$ centered on the potential pulsar counterpart. The background spectrum was extracted by selecting all events from an annulus with radii $5''$ and $75''$, respectively. The spectra were binned so as to have at least 20 counts/bin in the PN data and 10 counts/bin in the MOS1/2 data. Fitting a power law model to this spectral data gave a $\chi^2 = 4.0$ for 8 d.o.f. and an $N_{\text{H}} < 1.2 \times 10^{21} \text{ cm}^{-2}$. The column absorption is in agreement with the value estimated from the radio pulsar’s dispersion measure, $N_{\text{H}}^{DM} = 8.42 \times 10^{20} \text{ cm}^{-2}$, using the model of Cordes & Lazio (2002). The fitted photon index Γ is $2.3_{-0.4}^{+0.8}$. We also tested a single blackbody model but did not find it to fit the data ($\chi^2 = 15.9$ for 8 d.o.f.).

3.6. PSR J1044–5737

PSR J1044–5737 is a young and energetic pulsar. It was discovered in a blind frequency search of Fermi LAT data (Saz Parkinson et al. 2010). No radio dispersion measure has been reported for this pulsar in the literature so far. Its distance is therefore still unconstrained. The Chandra data archive has a 10 ksec deep observation with the pulsar in the telescope focus. Analyzing this data we detected a point source matching the pulsar’s radio timing position by $0.^{\circ}6 \pm 0.^{\circ}9$. This source is detected with 30 ± 6 source counts. Converting the photon flux to an energy flux yields $F_X^{0.1-2 \text{ keV}} = 2.4 \pm 1.0 \times 10^{-14} \text{ erg s}^{-1} \text{ cm}^{-2}$ in the 0.1 to 2 keV range.

3.7. PSR J1112–6103

PSR J1112–6103 was discovered in the Parkes multi-beam pulsar survey (Manchester et al. 2001). Two Chandra observations are covering the radio position of the pulsar. In the first one (Obs.ID 6706) the pulsar position was in the focus of the telescope. The second observation (Obs.ID 8905) was pointed on the HII region NGC 3576 in which the pulsar position was observed $2''.4$ off-axis. In the combined data we detected a point source $0''.6 \pm 0''.5$ near to the pulsar’s timing position which makes it a very likely counterpart of the pulsar. From both observations we have 331 ± 19 source counts which allowed a brief spatial and spectral analysis.

The CIAO-tool `srcextent` indicated that the source is extended at a 90% confidential level. To explore the existence of a possible PWN around PSR J1112–6103 we produced radial profiles centered on the deduced X-ray position for both ACIS observations. The profiles were obtained by integrating all counts in 12 concentric, equally-spaced annuli with a minimum radius of $0''.5$ and maximum radius $6''$ and dividing the selected counts by the respective ring area. This profiles were then compared with the profile of a point source at the same off-axis angle, simulated with MARX¹⁰ and convolved with a Gaussian with a full width at half maximum (FWHM) of $1''$ as used by Romani & Ng (2003) to detect a faint PWN surrounding PSR J0538+2817. Figure 2 shows the resulting diagram obtained for obs.ID 6706. No extension of the X-ray source is visible with a significance of 3σ . Therefore, we see no evidence for a PWN surrounding J1112–6103.

To extract the source counts for spectral analysis we selected all events within an aperture of $3''$ centered on the counterpart. All counts were binned to have at least 20 cts/bin.

Testing a power law model yields an excellent fit with $\chi^2 = 9.7$ for 11 d.o.f. and a power law index of 1.5 ± 0.7 (see Figure 3). The fitted column density $N_{\text{H}} = 1.2_{-1.0}^{+1.1} \times 10^{22} \text{ cm}^{-2}$ is in agreement with both, the results of the LAB Survey of Galactic HI (Kalberla et al. 2005), where the column density in the direction to PSR J1112–6103 is between $(1.0 - 1.3) \times 10^{22} \text{ cm}^{-2}$ and $1.8 \times 10^{22} \text{ cm}^{-2}$ as estimated from the pulsar’s radio dispersion measure DM.

Although a blackbody model fit gives an acceptable description of the spectrum as well ($\chi^2 = 12.7$ for 11 d.o.f.), the resulting blackbody temperature $T = (1.4 \pm 0.2) \times 10^7 \text{ K}$ for an emitting radius $R_{\text{BB}} \sim 157 \pm 28 \text{ m}$ is almost an order of magnitude higher than what is observed in other X-ray detected rotation powered pulsars. The blackbody model is rejected for this reason.

¹⁰See <http://space.mit.edu/cxc/marx/>

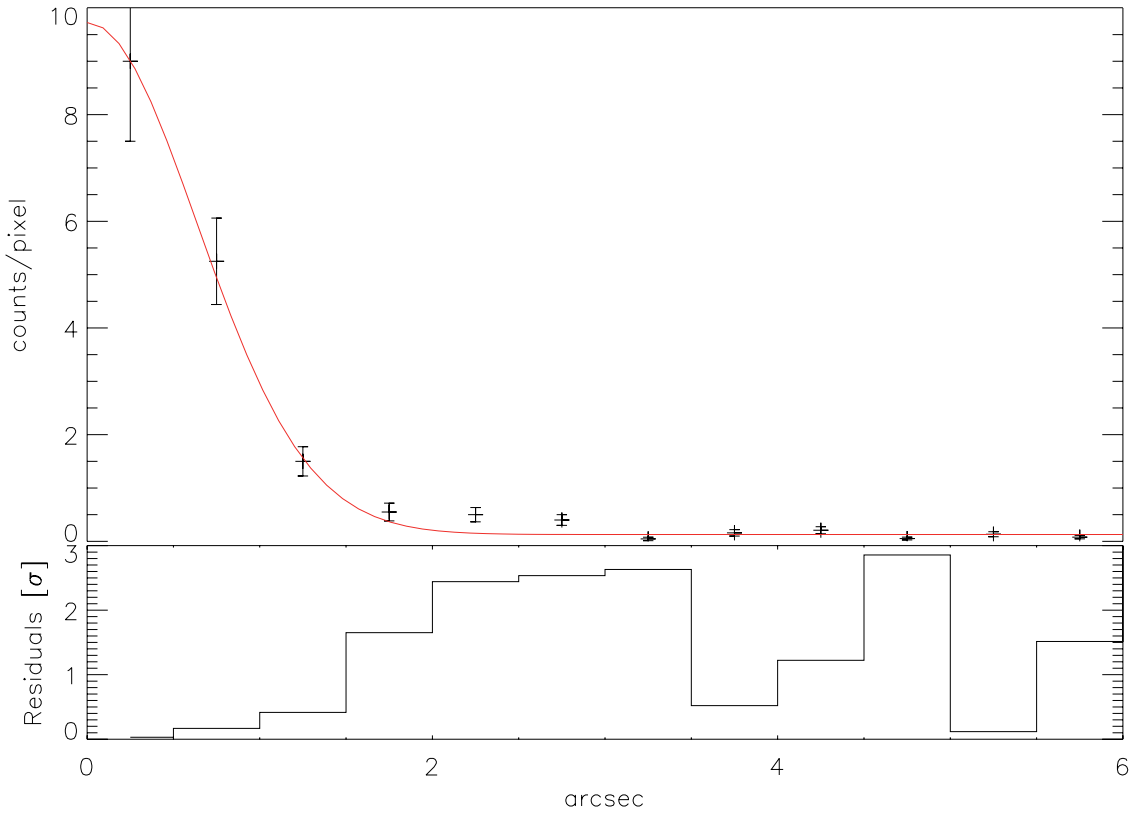


Fig. 2.— *Top:* Radial intensity distribution around PSR J1112–6103 in obs.ID 6706. The red line shows the simulated distribution for a point source convolved with a Gaussian with a FWHM=1''. *Bottom:* Difference between this two profiles, expressed in terms of the 1σ uncertainty in the derived counts per annulus.

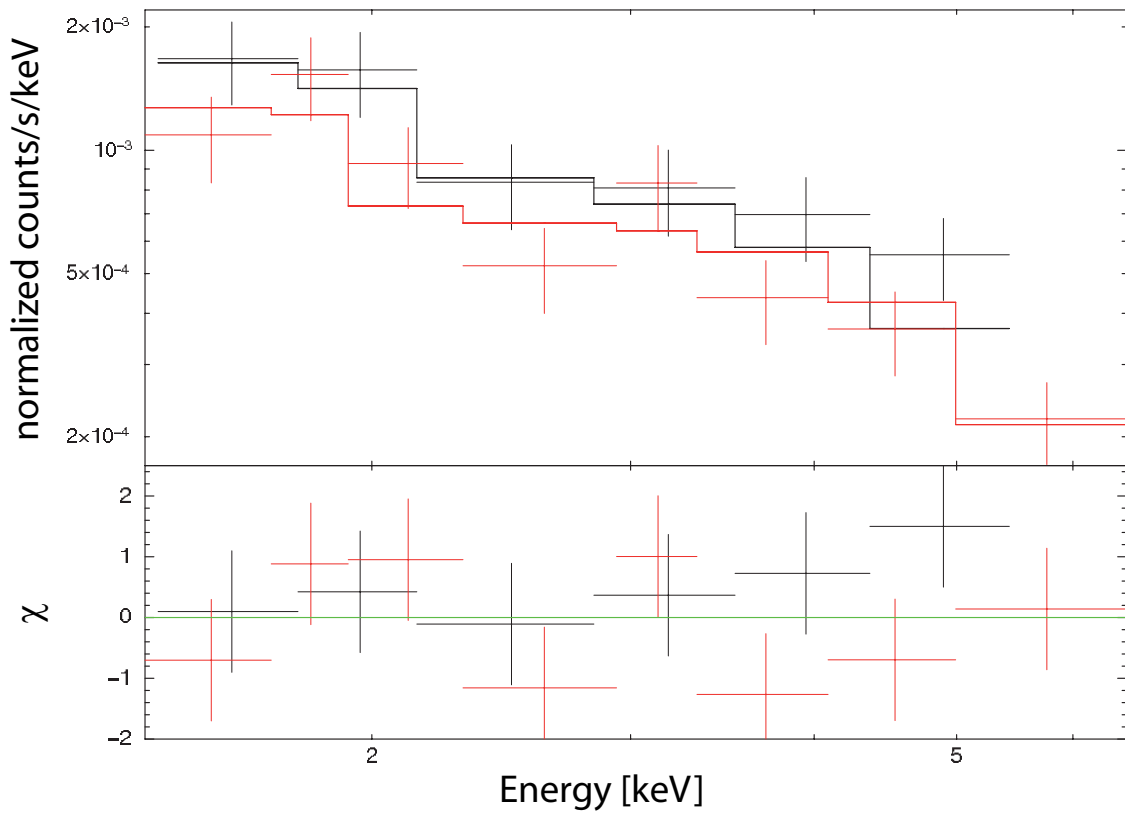


Fig. 3.— X-ray spectrum of PSR J1112–6103 fitted with a power law model. The χ^2 statistic is shown for comparison.

3.8. PSR B1221–63

The radio pulsar PSR B1221–63 (PSR J1224–6407) was first detected by Komesaroff et al. (1973). It was observed on-axis by XMM-Newton with an exposure time of ~ 7 ksec. Combining the MOS1/2 and PN data we detected a faint X-ray source which matches the pulsar position by $0''.6 \pm 0''.9$. In total we detected (30 ± 8) source counts in the PN and MOS1/2 detectors. Using the net exposure time on this source of 3.9 and 6.4 ksec for the PN and the two MOS1/2 cameras, respectively, the photon flux converts to an energy flux of $F_X^{0.1-2 \text{ keV}} = (1 \pm 0.6) \times 10^{-14} \text{ erg s}^{-1} \text{ cm}^{-2}$ in the 0.1 to 2 keV range.

3.9. PSR J1301–6310

The middle-aged pulsar PSR J1301–6310 was discovered in the Parkes multi-beam survey (Kramer et al. 2003b). XMM-Newton observed the pulsar position twice for a total of ~ 60 ksec. In the combined data we detected a X-ray point source with 78 ± 13 source counts in the PN- and MOS1/2 cameras $1''.9 \pm 2''.3$ near to the radio pulsar’s timing position. The recorded events allow for a very coarse spectral analysis for which we extracted the events from within a circle of $20''$ radius, centered on the position of the counterpart. Due to the small data statistics both a blackbody and power law spectrum fitted equally good. The fit of a power law results in $\chi^2 = 15.2$ for 15 d.o.f., an $N_{\text{H}} < 3.9 \times 10^{21} \text{ cm}^{-2}$ and a spectral index of $3.4^{+0.8}_{-0.6}$. Using a blackbody spectrum leads to $\chi^2 = 17.0$ for 15 d.o.f. and $N_{\text{H}} \leq 9 \times 10^{20} \text{ cm}^{-2}$. After fixing N_{H} to the DM based value of $2.6 \times 10^{21} \text{ cm}^{-2}$ both fits still appear to be reasonable (see Table 3), albeit the blackbody radius computed from the blackbody normalization resulted in an unreasonable small value of $R_{BB} = 0.09 \pm 0.03 \text{ km}$.

3.10. PSR B1338–62

PSR B1338–62 (PSR J1341-6220) is a young, Vela-like pulsar which was discovered in 1985 at the Parkes radio telescope (Manchester et al. 1985). The pulsar is associated with the supernova remnant G308.8–0.1 (Kaspi et al. 1992) and according to Wang et al. (2000) among the most actively glitching pulsars known. The pulsar position was in the field of view of the XMM-Newton telescope for about 42 ksec during two different epochs and with different off-axis angles. Merging the PN- and MOS1/2 data we detected two faint X-ray sources close to the radio pulsar’s timing position: S_1 with the coordinates RA= $13^h 41^m 43.1^s \pm 0.3^s$, DEC= $-62^\circ 20' 18'' \pm 2''$ and S_2 with RA= $13^h 41^m 43.3^s \pm 0.3^s$, DEC= $-62^\circ 20' 06'' \pm 2''$.

Source S_1 is close to the pulsar position, the difference is $4''.2 \pm 2''.4$. This source is only

distinguishable from S_2 at energies above ~ 2 keV (see Figure 1). Thus, it has a hard spectrum. For S_2 we found a possible counterpart in the 2MASS All-Sky Catalog of Point Sources, 2MASS J13414307-6220063 with a positional discrepancy of only $1''.5 \pm 2''.2$.

In order to fit the energy spectrum of the detected X-ray source S_1 we extracted the counts from within a radius of $12''.5$, centered on the point source, and excluding events from the region around S_2 . The background spectrum was extracted from a region close to S_1 . Using a power law to fit the energy spectrum gave an acceptable fit ($\chi^2 = 3.1$ for 8 d.o.f.) with $N_H = 4 \pm 3 \times 10^{22} \text{ cm}^{-2}$. The column absorption is in agreement with the DM based value of $2.2 \times 10^{22} \text{ cm}^{-2}$ (Cordes & Lazio 2002). Fixing N_H to this value yields $\chi^2 = 3.2$ for 9 d.o.f. and a photon index $\Gamma = 1.1 \pm 0.7$. A blackbody model fit gave $\chi^2 = 2.8$ for 7 d.o.f. with fixed N_H , but the resulting blackbody temperature $T = 1.3_{-0.4}^{+1.8} \times 10^7 \text{ K}$ is too high to be consistent with neutron star cooling emission or coming from a hot spot on the neutron star surface.

3.11. PSR J1600–3053

The high galactic latitude binary pulsar PSR J1600–3053 was detected by Jacoby et al. (2007). The XMM-Newton archive contains data from an observation in which the pulsar was in the focus of the telescope for ~ 25 ksec. As in this observation the PN camera was operated in timing mode, not providing suitable spatial resolution for source detection, we analysed only the two MOS1/2 data sets and detected a faint X-ray source with 37 ± 10 source counts which matches the pulsar’s radio timing position by $0''.8 \pm 2''.4$, making it a very likely counterpart. Converting the photon flux to energy flux results in $F_X^{0.1-2 \text{ keV}} = (6 \pm 4) \times 10^{-15} \text{ erg s}^{-1} \text{ cm}^{-2}$.

3.12. PSR J1658–5324

This pulsar was detected in a survey of unidentified Fermi LAT sources with the Parkes radio telescope (Kerr et al. 2012). It is an isolated millisecond pulsar. In the Chandra data archive we found an observation in which this pulsar was in the telescope focus for ~ 10 ksec. Analyzing this data we detected a faint X-ray point source with 26 ± 5 counts which matches the pulsar position by $0''.22 \pm 0''.28$ what makes it a potential counterpart of the pulsar. Converting the photon flux of this counterpart to energy flux yields $F_X^{0.1-2 \text{ keV}} = (1.6 \pm 0.6) \times 10^{-14} \text{ erg s}^{-1} \text{ cm}^{-2}$.

3.13. PSR J1730–2304

The solitary millisecond pulsar J1730–2304 was discovered by Lorimer et al. (1995). The XMM-Newton data archive holds data from an observation in which the pulsar was in the focus of the telescope for ~ 23 ksec. Analyzing this data we detected an X-ray source with in total 248 ± 21 counts in the PN and MOS1/2 data. It matches the pulsar position by $2.^{\circ}7 \pm 2.^{\circ}1$ which makes it a potential X-ray counterpart of the pulsar.

The data statistics allows for a brief spectral analysis for which we extracted the source counts from a circle of radius $20''$, centered on the position of the point source. For the spectral binning we used at least 20 cts/bin and 10 cts/bin for the PN and MOS1/2 data, respectively.

Fitting a single power law or blackbody model to the data showed systematic deviations at ≈ 1.4 keV and did not result in acceptable fits. Adding a Gaussian emission line profile to the power law model improved the fit to yield $\chi^2 = 17.0$ for 16 d.o.f., though the statistical justification for the need of such a spectral line component is barely significant due to the low photon statistics in the spectrum. The line center was fitted to be $1.36_{-0.1}^{+0.08}$ keV. The blackbody model still showed systematic deviations even after adding a spectral emission line component to the model spectrum. Deeper Chandra observations which provide better data statistics are required to further explore the source spectrum with higher significance.

3.14. PSR J1731–1847

The binary pulsar PSR J1731–1847 was discovered in the High Time Resolution Universe Pulsar survey (Bates et al. 2011). It was observed on axis, both with XMM-Newton and Chandra for ~ 40 ksec and ~ 10 ksec, respectively. In the merged XMM-Newton MOS1/2 data a point source is clearly detected $1.^{\circ}2 \pm 2.^{\circ}7$ arcsec from the radio position with in total 47 ± 13 counts. The photon flux corresponds to an energy flux of $F_X^{0.1-2 \text{ keV}} = (6 \pm 4) \times 10^{-15} \text{ erg s}^{-1} \text{ cm}^{-2}$. The XMM-Newton PN data were not usable for the analysis because of high background flares which strongly reduced the S/N ratio in that data. An optical source with visible magnitude $V = 17.34^{\text{mag}}$ is within the 1σ error circle around the position obtained in the XMM-Newton data. However, using the Chandra data we can rule out the possibility that the optical source is the X-ray counterpart of the detected XMM source. The Chandra source position is more than $3''$ away from the optical source whereas the positional uncertainty is only $0.^{\circ}5$.

3.15. PSR J1816+4510

This eclipsing millisecond pulsar was studied in detail in the optical, UV and γ -ray band by Kaplan et al. (2012). The Chandra data archive holds an observation in which the pulsar position was in the focus of the telescope for ~ 34 ksec. Using this observation we detected a faint potential X-ray counterpart $0\rlap{.}^{\prime}4 \pm 0\rlap{.}^{\prime}3$ near to the pulsars timing position. It has 16 ± 4 source counts. The photon flux converts to an energy flux of $F_X^{0.1-2 \text{ keV}} = (3.1 \pm 1.6) \times 10^{-15} \text{ erg s}^{-1} \text{ cm}^{-2}$.

3.16. PSR B1822-09

The middle-aged pulsar B1822-09 (PSR J1825–0935) was first mentioned in the literature by Davies et al. (1972). In the XMM-Newton data archive we found a short ~ 5 ksec deep observation targeted on this pulsar. Using this data we detected an X-ray source $1\rlap{.}^{\prime\prime}5 \pm 2\rlap{.}^{\prime\prime}3$ near to the pulsar’s timing position which makes it a potential counterpart of the pulsar. The X-ray source has 46 ± 11 source counts in the merged PN and MOS1/2 data. The photon flux corresponds to an energy flux of $F_X^{0.1-2 \text{ keV}} = (1.7 \pm 0.8) \times 10^{-14} \text{ erg s}^{-1} \text{ cm}^{-2}$.

3.17. PSR J1832–0836

This isolated millisecond pulsar was discovered in the radio band during the High Time Resolution Universe Pulsar survey (Burgay et al. 2013). In an archival observation of AX J1832.3–0840, a low luminous X-ray pulsator (Kaur et al. 2010), the pulsar was observed $\sim 4'$ off-axis. In the merged EPIC-PN and MOS1/2 data a faint X-ray source was detected $1\rlap{.}^{\prime\prime}8 \pm 2\rlap{.}^{\prime\prime}6$ near to the radio timing position with 34 ± 9 counts, making it a potential pulsar counterpart. Its photon flux converts to an energy flux of $F_X^{0.1-2 \text{ keV}} = (3.8 \pm 2.0) \times 10^{-15} \text{ erg s}^{-1} \text{ cm}^{-2}$.

3.18. PSR J1911–1114

Radio emission from the binary millisecond pulsar PSR J1911–1114 was discovered by Lorimer et al. (1996). The XMM-Newton data archive holds a ~ 50 ksec deep observation of this pulsar in which the PN was operated in timing mode. Using the EPIC MOS1/2 data we detected an X-ray source $3\rlap{.}^{\prime\prime}1 \pm 2\rlap{.}^{\prime\prime}8$ near to the pulsars position. It has 54 ± 13 source counts in the merged MOS1 and MOS2 data. The photon flux converts to an energy flux of $F_X^{0.1-2 \text{ keV}} = 3.7 \pm 1.8 \times 10^{-15} \text{ erg s}^{-1} \text{ cm}^{-2}$.

3.19. PSR J2017+0603

PSR J2017+0603 is a millisecond pulsar in a binary system. It was first detected by its pulsed γ -ray emission with the Fermi satellite (Cognard et al. 2011). In the discovery paper the authors derived an upper limit on the X-ray flux in the 0.5–8 keV band of $F_X^{0.5-8 \text{ keV}} < 6 \times 10^{-14} \text{ erg s}^{-1} \text{ cm}^{-2}$. Using an archival Chandra ACIS-S observation aimed on this pulsar we detected an X-ray source $0'2 \pm 0'2$ near to the radio pulsar’s timing position, making it a potential X-ray counterpart of the pulsar. It has 19 ± 5 source counts which we convert to an energy flux of $F_X^{0.1-2 \text{ keV}} = (1.1 \pm 0.6) \times 10^{-14} \text{ erg s}^{-1} \text{ cm}^{-2}$.

3.20. PSR J2222–0137

The binary millisecond pulsar PSR J2222–0137 (Boyles et al. 2012) was observed on-axis for ~ 30 ksec with the Chandra ACIS-S camera. In this data we detected an X-ray source with 26 ± 5 source counts 0.1 ± 0.2 arcsec near to the pulsar’s radio position, making it a potential pulsar counterpart. The photon flux corresponds to an energy flux of $F_X^{0.1-2 \text{ keV}} = 4.5 \pm 2.0 \times 10^{-15} \text{ erg s}^{-1} \text{ cm}^{-2}$.

4. Upper limits on the X-ray counterparts of radio pulsars

In Table 5 the non-thermal flux $F_{0.1-2 \text{ keV}}^{\text{PL}}$ and the upper limits on the blackbody temperature T_∞ , as measured by a distant observer at infinity, are listed for all rotation-powered pulsars for which no X-ray counterpart was detected in the archival data. Furthermore, the non-thermal luminosity $L_{0.1-2 \text{ keV}}^{\text{PL}} = 4\pi d_{UL}^2 F_{0.1-2 \text{ keV}}^{\text{PL}}$ and the X-ray efficiency $\mu_{0.1-2 \text{ keV}}^{\text{PL}} = L_{0.1-2 \text{ keV}}^{\text{PL}} / \dot{E}$ are listed there as well. Therein $\dot{E} = -4\pi^2 I \dot{P} P^{-3}$ is the spin-down luminosity and $I = 10^{45} \text{ g cm}^2$ the canonical moment of inertia for a neutron star with a mass of $1.4 M_\odot$ and a radius of 10 km. In Table 6 the pulsars with the lowest X-ray efficiency upper-limit are displayed separately.

Figure 4 displays the correlation of the isotropic X-ray luminosity $L_X^{0.1-2}$ in the 0.1–2 keV band with the pulsar’s spin-down luminosity \dot{E} . In red color we plotted the X-ray luminosity for all potential pulsar counterparts for which we were able to perform a brief spectral analysis. Blue error bars indicate the X-ray luminosity of potential counterparts for which we had to assume the spectral shape to convert the photon flux to an energy flux resp. X-ray luminosity. In addition we added the 2σ upper limits on the non-thermal X-ray luminosity for all pulsars, for which at least a dispersion measure based distance estimate is known. The gray shaded region in this graph shows the correlation between $L_X^{0.1-2}$ and \dot{E} as found by Becker (2009):

$$L_X^{0.1-2} = 10^{-3.24_{-0.66}^{+0.26}} \dot{E}^{-0.997_{-0.001}^{+0.008}}. \quad (10)$$

For this fit the authors used ≈ 80 rotation-powered pulsars for which spectral information was obtained in XMM-Newton and Chandra observations, respectively.

If no association between a pulsar and e.g. a hosting supernova remnant is possible, the only way to estimate the age of a pulsar is by its spin-down age $\tau = 2P/\dot{P}$. The Crab pulsar is the only pulsar for which the true historic age is known (Green & Stephenson 2003). In this case the difference between the spin-down age τ and the true historic age is of the order of $\approx 20\%$. In Figure 5 we plotted the derived 3σ temperature upper limits T_∞ against the spin-down age of the pulsars. In this figure we show an error bar for the pulsar age only if kinematic informations are available, i.e., the age is known with accurately determined errors.

To compare the data with actual cooling models we used the cooling curves of Page et al. (2009). For the computation of the curves Page et al. (2009) used a $1.4 M_\odot$ neutron star with the equation of state taken from Akmal et al. (1998), different neutron 1S_0 , proton 1S_0 , and neutron 3P_2 gap models were taken from Page et al. (2004). The authors showed that the cooling of a neutron star in the minimal cooling paradigm is only slightly dependent on the neutron star mass and the used neutron and proton 1S_0 gap model. The main uncertainties in the minimal cooling paradigm are a possible evolution of the chemical composition of the envelope of the neutron star and hence its opacity, as well as the number of different gap models that are allowed by current measurements. In Figure 5 we therefore compare our data with the allowed temperature range of these models.

The lower panel in Figure 5 shows the bolometric luminosity plotted against the pulsars' spin-down age. We added all pulsars from the literature for which thermal emission from their surface has been detected or upper limits on the temperature have been published. In this plot the upper limits derived in this paper are indicated by gray arrows. The cooling models shown are computed for a $1.4 M_\odot$ star with the equation of state adopted from Akmal et al. (1998), different neutron 1S_0 , proton 1S_0 , and neutron 3P_2 gap models as introduced by Page et al. (2004). The area in dark and light gray contain cooling models computed with heavy- and light-element dominated envelopes, respectively. The error bars indicate the error range in temperature or bolometric luminosity of all pulsars with detected thermal emission, e.g. (1) Cas A: Shternin et al. (2011); Fesen et al. (2006); (2) J0822–4300: Zavlin et al. (1999); Becker et al. (2012); (3) J1210–5226: Zavlin et al. (1998); Roger et al. (1988); (4) B0833–45: Pavlov et al. (2001); Aschenbach et al. (1995); (5) B1706–44: McGowan et al. (2004); Koribalski et al. (1995); (6) B0656+14: Marshall & Schulz (2002); Brisken et al. (2003); (7) J0633+1748: Halpern & Wang (1997); Caraveo et al. (2001); (8) B1055–52: De Luca et al. (2005); Kramer et al. (2003b); (9) J1856–3754: Burwitz et al. (2003); Mignani et al. (2013); (10) J0720–3125: Kaplan et al. (2003); Tetzlaff et al. (2011);

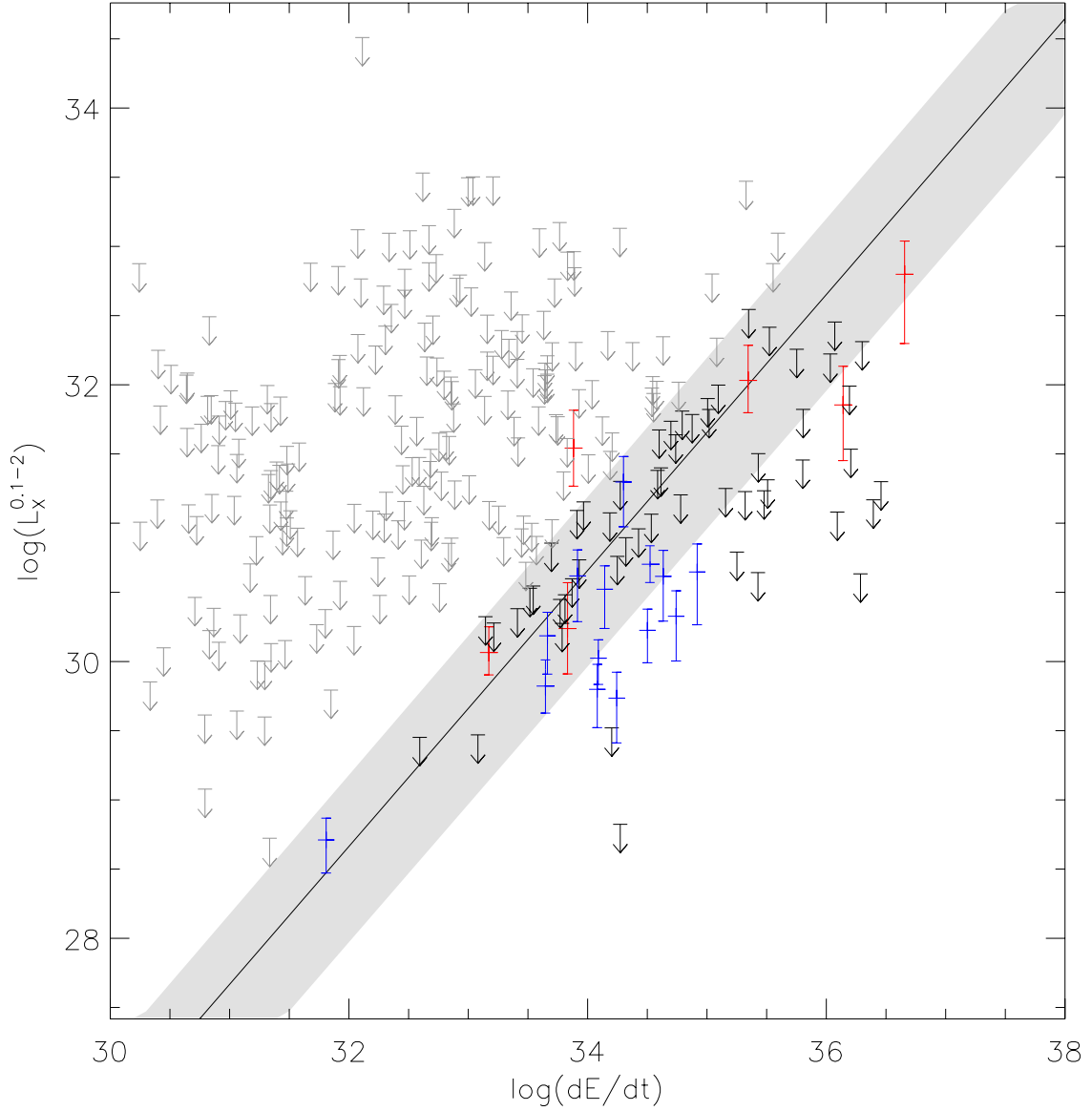


Fig. 4.— Spin-down luminosity dE/dt plotted against the isotropic X-ray luminosity $L_X^{0.1-2}$ in the 0.1–2 keV band. The red error bars represent the 1σ confidence range and indicate those potential pulsar counterparts for which we could perform a brief spectral analysis in order to obtain the energy flux and X-ray luminosity. Values for the remaining potential counterparts are plotted in blue. In the case of the non-detected pulsars the 2σ upper limit is indicated by an arrow. The straight line represent the relation found by Becker (2009) with an uncertainty range indicated by the gray shaded region.

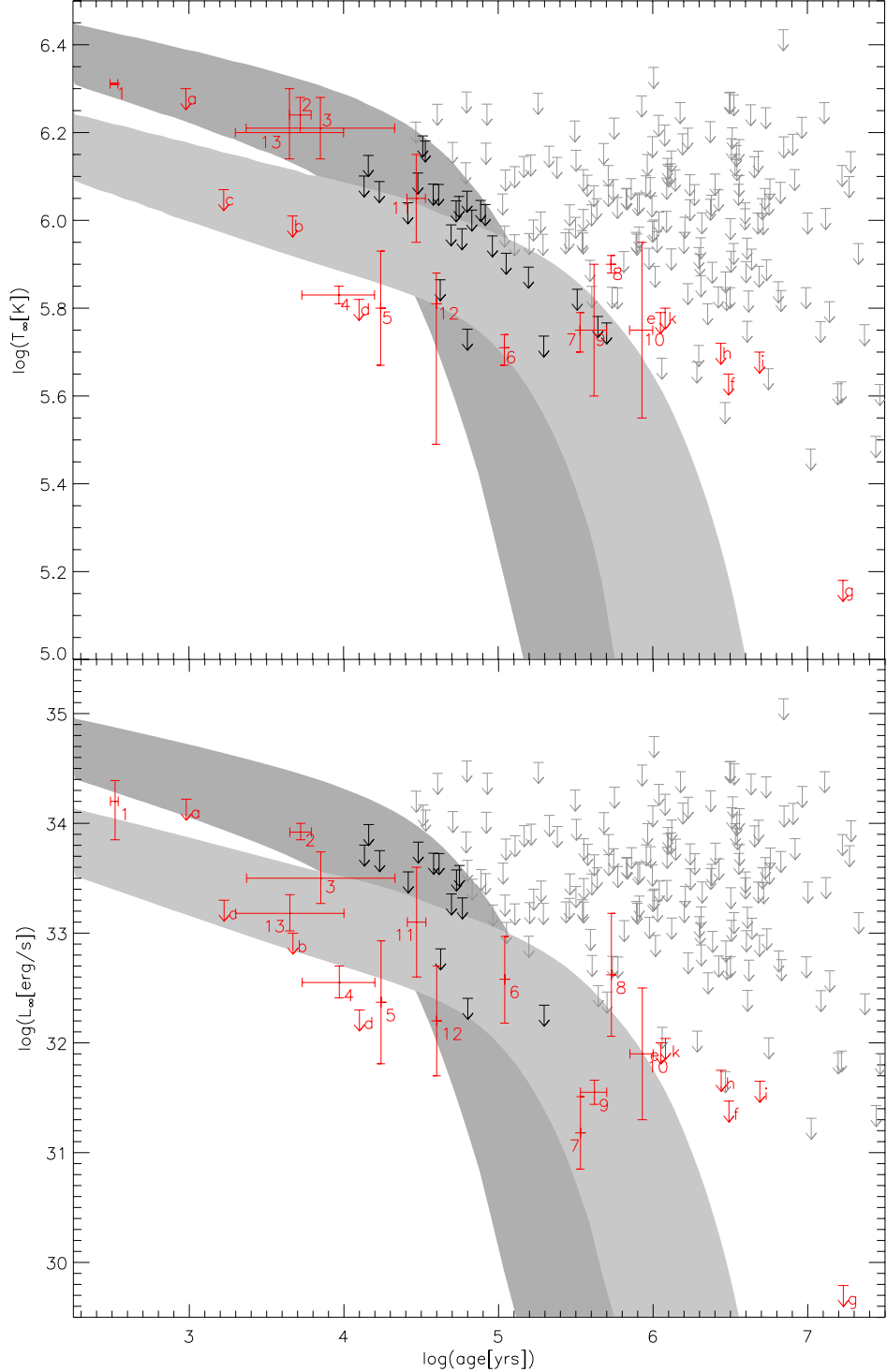


Fig. 5.— Comparison of the derived upper limits on the temperature (*upper panel*) and bolometric luminosity (*lower panel*) of the radio pulsars for which data were found in the XMM-Newton or Chandra archives. The plotted cooling curves were taken from Page et al. (2009) (see text for more informations).

(11) J0538+2817: Zavlin & Pavlov (2004b); Kramer et al. (2003a); (12) B2334+61: McGowan et al. (2006); Yar-Uyaniker et al. (2004); (13) J1119–6127: Safi-Harb & Kumar (2008); Kumar et al. (2012).

All pulsars with derived temperature upper limit are indicated by a red arrow, e.g. (a) Crab: Weisskopf et al. (2011); (b) J0205+6449: Slane et al. (2004a); Fesen et al. (2008); (c) J1124–5916: Hughes et al. (2003); Camilo et al. (2002); (d) RX J0007.0+7302: Halpern et al. (2004); Slane et al. (2004b); (e) B2224+65: Gonzalez et al. (2004); (f) B1929+10: Hui & Becker (2007); (g) B0950+08: Becker et al. (2006); Chatterjee et al. (2004); (h) B0628–28: Zavlin & Pavlov (2004a); Brisken et al. (2002); (i) B0823+26: Becker et al. (2005); (k) J2043+2740: Becker et al. (2004); Brisken et al. (2002). We added the error in the age for pulsars with known kinematic age. These data are taken from Page et al. (2004, 2009), Özel (2013), and Zhu et al. (2011). Additionally, for the central compact object in Puppis-A we adopted the new age estimate of $(5.2 \pm 1.0) \times 10^3$ years (Becker et al. 2012). In Table 7 we summarize the neutron stars which have the lowest 3σ upper limit on the surface temperature in our sample. They are indicated by a black arrow in the upper panel of Figure 5.

The ATNF Pulsar Catalog (Catalogue version number = 1.54) which we used to searched for potential X-ray counterparts in the XMM-Newton or Chandra data archives has currently about 2500 rotation-powered pulsars in its database (Manchester et al. 2005). However, only about 2000 of them have published period derivatives and spindown energies. For some others no dispersion measure has been published so far, so that it is not possible to get an estimate on their distance and hence no estimate on their X-ray luminosity or luminosity upper limit and/or X-ray efficiency.

5. Conclusion

We have systematically searched the archives of the X-ray observatories Chandra and XMM-Newton for serendipitous datasets which include a radio pulsar in the field of view. All 20 detected X-ray counterparts of radio pulsars fulfill the following criteria (see also Section 2): The discrepancy between the radio and X-ray source position is less than 3σ , the probability that an X-ray source is by-chance at the pulsar’s position is below 3σ and no optical source having a X-ray-to-visual flux ratio typical for stars is found within the 3σ error box around the pulsar’s counterpart.

The non-thermal X-ray efficiency of all potential counterparts and or their upper limits are in agreement with the predictions made by Becker (2009). Only a small scatter is noticeable which is in agreement with statistical fluctuations (e.g. Becker et al. 2010, figure 18) and the uncertainties introduced by e.g. assuming the spectral parameters for the pulsars with less than 70 detected counts. The uncertainties that can cause the scatter in equation 10 is addressed separately in the

next section.

Four of the 20 potential counterpart which we detected in our correlation were mentioned in the literature during the analysis and publication process of this paper. J1341–6220 is listed as radio pulsar with X-ray counterpart in Kaplan et al. (2004) and Smith et al. (2008), but no detailed analysis of the X-ray properties of PSR J1341–6220 was presented by the authors. For the radio pulsars PSR J1112–6103 and PSR J2222–0137 a detection is claimed by Townsley et al. (2011) and Boyles et al. (2011), respectively, but these authors did not investigate the X-ray data in detail too. In any case, we consider this as a confirmation of our findings which strengthens the detections of the other potential counterparts too.

5.1. Non-thermal X-ray emission

In a first step, the consistency of the measured upper limits on the non-thermal X-ray emission was verified. This was done by comparing the values derived in Section 2.4 with upper limits found in the literature. The limits on μ_X of Kargaltsev et al. (2012) were confirmed, even though a different energy band and a larger confidential level of 95.4 % was used in this work. Only in the case of PSR J1837–0604 our derived upper limit on the flux is three times higher. However, this can be explained by the fact that in Kargaltsev et al. (2012) the counts were not corrected for the encircled energy fraction.

Thereafter, the non-thermal X-ray luminosity for the 20 X-ray counterparts and the upper limits derived for the 262 remaining pulsars were used to further study the scatter in the relation of the non-thermal X-ray luminosity to the spin-down power. Eleven sources were found with upper limits on $\mu_{0.1-2 \text{ keV}}$ below 10^{-4} . This confirms the trend for finding smaller X-ray efficiencies with increasing sample size and higher sensitivity of X-ray observatories. The X-ray efficiency of a rotation-powered pulsar can be as high as 1.9×10^{-3} , e.g., for the Crab pulsar (Becker 2009), but also be below 2.2×10^{-6} as for PSR J0940–5428.

It should be noted that young pulsars with $\dot{E} > \dot{E}_c \approx 4 \times 10^{36}$ erg/s could manifest a distinct pulsar wind nebula (PWN, Gotthelf 2004). If such a PWN exists and/or thermal emission from the pulsar’s surface is hot enough to contribute to the X-ray emission, the non-thermal X-ray efficiency of several pulsars could be even lower than the determined upper limit.

Theory predicts a distinct relation between the X-ray efficiency and the spin-down power (e.g. Wang & Zhao 2004). The detected large scatter contradicts such a tight relation and favors the interpretation of Becker (2009) that the efficiency of $\mu_X \sim 10^{-3}$ represents more the maximum efficiency rather than a fixed correlation. It might be seen for pulsars which are seen with an optimal viewing geometry. Because the orientation of the pulsar’s magnetic axes with respect to the

observer’s line of sight might not have been optimal for observation and no beaming correction can be applied to the observed luminosity, the X-ray efficiency of pulsars observed with an unfavorable viewing geometry appears to be smaller than that for pulsars observed with an optimal viewing geometry. A reason for the large dispersion in μ_X then would be mostly caused by the viewing geometry and the inability to apply a beaming correction (Becker 2009, and references therein).

Kargaltsev & Pavlov (2010) reviewed all known PWNe and investigated their X-ray efficiency. They found a scatter in the measured luminosities too, despite of the fact that PWN emission is thought to be unbeamed (Gaensler & Slane 2006). Therefore, the beaming angle might be only one of several parameters which might cause the observed scatter in μ_X for pulsars.

Certainly, erroneous distances contribute to the uncertainty in the derived X-ray luminosities too. Although the errors in the distance measurement were included in our μ_X calculations, most distances used in this work are based on the radio dispersion measure DM and large fluctuations in it are not included in the model calculations. This could easily introduce a scatter of roughly one order of magnitude in the derived X-ray luminosity for some sources.

Finally, another reason for the scatter in μ_X could be a wrongly determined spin-down luminosity. In the last years several intermittent pulsars have been discovered (e.g., Kramer et al. 2006; Camilo et al. 2012; Lorimer et al. 2012), which at first seemed to be ordinary radio pulsars, but later have been seen to switch their radio emission off quasi-periodically, then showing different spin-down rates at time scales from months to years. In the so called on-state the spin-down rate increases by a factor of 2 to 3 compared to the off-state. Because the spin-down luminosity is proportional to the spin-down rate and for some radio pulsars only a few observations exist, it can not be excluded that some sources have indeed a lower \dot{E} than calculated from their period and period derivatives.

5.2. Thermal X-ray emission

As for the non-thermal X-ray emission, the consistency of the measured upper limits were tested. Temperature upper limits for eight pulsars can be found in the literature (Gonzalez et al. 2004; Kaplan et al. 2009; Olausen et al. 2013; Keane et al. 2013), including the coolest pulsar in the sample presented in this work, PSR J2144–3933. For six pulsars similar values for the temperature upper limit were found, with a minor deviation of $\pm 10\%$. This small discrepancy may be due to the fact that Olausen et al. (2013) did not include the distance error in their calculations. Additionally, it is difficult to compare the results in detail because all aforementioned authors used slightly different methods to calculate the upper limits and no detailed information is given in Olausen et al. (2013) about the effective exposure time and radius of the annulus they used to compute the

upper limits for PSRs J1814–1744 and J1847–0130. However, the method used in this work makes use of all archival observations of a pulsar and, thus, in general derives deeper upper limits. In the case of PSR B1845–19 (Olausen et al. 2013) and PSR J0157+6212 (Gonzalez et al. 2004) the temperature upper limits we deduced in this work are 32% and 36% lower than what is reported in the literature. For PSR B1845–19 this is because two archival XMM-Newton observations were used rather than one as in Olausen et al. (2013). In the case of PSR J0157+6212 the difference appears partly due to a different N_{H} value, though a large, and yet unexplained, difference remains between the measured upper limit in our work and that by Gonzalez et al. (2004).

In total, 3σ upper limits on the blackbody temperature for 263 pulsars were derived, ranging from 2.2×10^5 K for PSR J2144–3933 to 2.7×10^6 K for PSR J1822–1617. All measured temperature upper limits are in agreement with current cooling models, which assume only nuclear matter in the core of a neutron star and Cooper-pair breaking and formation as the main source of neutrino emission. These models include the uncertainties regarding the allowed amounts of light elements in the envelope of the star and the different possible neutron ${}^3\text{P}_2$ gap models. A comparison of the upper limits with other cooling curves (e.g. Tsuruta 1998; Yakovlev & Pethick 2004; Tsuruta 2009) shows that they are in agreement with models that assume standard cooling with Cooper-pair breaking and formation too.

6. Future prospects

In Table 6 and 7 we list those pulsars which appear to have a rather low X-ray efficiency or 3σ temperature upper limit. Further observations of these sources will allow to explore them in more detail which might result in even tighter constraints on the cooling models or the theories that try to explain the pulsar’s non-thermal X-ray efficiency. Detecting, for example, thermal X-ray emission from a neutron star with a surface temperature lower than what is predicted by the minimal cooling paradigm would require to include enhanced cooling mechanisms in those models to explain that observation.

In fall 2017 the eROSITA Observatory (extended ROentgen Survey with an Imaging Telescope Array) is scheduled for launch on the Russian Spectrum X-Gamma Satellite. Three month after the start it will begin to survey the X-ray sky with an XMM-Newton like sensitivity (Merloni et al. 2012). This data will enable us to study all ≈ 2500 known pulsars in the X-ray band with three times better spatial resolution and ≈ 20 times higher sensitivity than possible in the ROSAT All-Sky Survey. The eROSITA survey will provide unique X-ray data which enables us to investigate a larger and even more unbiased pulsar sample than possible with the data available in the XMM-Newton and Chandra data archives.

Acknowledgments

We acknowledge the use of the XMM-Newton and Chandra data archive. T.P. acknowledges support from and participation in the International Max Planck Research School on Astrophysics at the Ludwig Maximilian University of Munich, Germany, IMPRS.

REFERENCES

- Akmal, A., Pandharipande, V. R., & Ravenhall, D. G. 1998, Phys. Rev. C, 58, 1804
- Arzoumanian, Z., Gotthelf, E. V., Ransom, S. M., et al. 2011, ApJ, 739, 39
- Aschenbach, B., Egger, R., & Trümper, J. 1995, Nature, 373, 587
- Bates, S. D., Bailes, M., Bhat, N. D. R., et al. 2011, MNRAS, 416, 2455
- Becker, W. 1995, PhD thesis, LMU, Germany
- Becker, W. 2009, in Astrophysics and Space Science Library, Vol. 357, Astrophysics and Space Science Library, ed. W. Becker, 91
- Becker, W., Huang, H. H., & Prinz, T. 2010, ArXiv e-prints, arXiv:1006.0335
- Becker, W., Jessner, A., Kramer, M., Testa, V., & Howaldt, C. 2005, ApJ, 633, 367
- Becker, W., Prinz, T., Winkler, P. F., & Petre, R. 2012, ApJ, 755, 141
- Becker, W., & Trümper, J. 1997, A&A, 326, 682
- . 1999, A&A, 341, 803
- Becker, W., Trümper, J., & Ögelman, H. 1993, in Isolated Pulsars, ed. K. A. van Riper, R. I. Epstein, & C. Ho, 104
- Becker, W., Weisskopf, M. C., Tennant, A. F., et al. 2004, ApJ, 615, 908
- Becker, W., Kramer, M., Jessner, A., et al. 2006, ApJ, 645, 1421
- Boyles, J., Lorimer, D. R., McLaughlin, M. A., et al. 2011, in American Institute of Physics Conference Series, Vol. 1357, American Institute of Physics Conference Series, ed. M. Burgay, N. D’Amico, P. Esposito, A. Pellizzoni, & A. Possenti, 32–35
- Boyles, J., Lynch, R. S., Ransom, S. M., et al. 2012, ArXiv e-prints, arXiv:1209.4293

- Brisken, W. F., Benson, J. M., Goss, W. M., & Thorsett, S. E. 2002, ApJ, 571, 906
- Brisken, W. F., Thorsett, S. E., Golden, A., & Goss, W. M. 2003, ApJ, 593, L89
- Burgay, M., Bailes, M., Bates, S. D., et al. 2013, MNRAS, 433, 259
- Burwitz, V., Haberl, F., Neuhäuser, R., et al. 2003, A&A, 399, 1109
- Camilo, F., Manchester, R. N., Gaensler, B. M., Lorimer, D. R., & Sarkissian, J. 2002, ApJ, 567, L71
- Camilo, F., Ransom, S. M., Chatterjee, S., Johnston, S., & Demorest, P. 2012, ApJ, 746, 63
- Caraveo, P. A., De Luca, A., Mignani, R. P., & Bignami, G. F. 2001, ApJ, 561, 930
- Chatterjee, S., Cordes, J. M., Vlemmings, W. H. T., et al. 2004, ApJ, 604, 339
- Cognard, I., Guillemot, L., Johnson, T. J., et al. 2011, ApJ, 732, 47
- Cordes, J. M., & Lazio, T. J. W. 2002, ArXiv Astrophysics e-prints, arXiv:astro-ph/0207156
- Davies, J. G., Lyne, A. G., & Seiradakis, J. H. 1972, Nature, 240, 229
- de Jager, O. C., Raubenheimer, B. C., & Swanepoel, J. W. H. 1989, A&A, 221, 180
- De Luca, A., Caraveo, P. A., Mereghetti, S., Negroni, M., & Bignami, G. F. 2005, ApJ, 623, 1051
- Fesen, R., Rudie, G., Hurford, A., & Soto, A. 2008, ApJS, 174, 379
- Fesen, R. A., Hammell, M. C., Morse, J., et al. 2006, ApJ, 645, 283
- Gaensler, B. M., & Slane, P. O. 2006, ARA&A, 44, 17
- Gonzalez, M. E., Kaspi, V. M., Lyne, A. G., & Pivovaroff, M. J. 2004, ApJ, 610, L37
- Gotthelf, E. V. 2004, in IAU Symposium, Vol. 218, Young Neutron Stars and Their Environments, ed. F. Camilo & B. M. Gaensler, 225
- Green, D. A., & Stephenson, F. R. 2003, in Lecture Notes in Physics, Berlin Springer Verlag, Vol. 598, Supernovae and Gamma-Ray Bursters, ed. K. Weiler, 7–19
- Halpern, J. P., Gotthelf, E. V., Camilo, F., Helfand, D. J., & Ransom, S. M. 2004, ApJ, 612, 398
- Halpern, J. P., & Wang, F. Y.-H. 1997, ApJ, 477, 905
- Hughes, J. P., Slane, P. O., Park, S., Roming, P. W. A., & Burrows, D. N. 2003, ApJ, 591, L139

- Hui, C. Y., & Becker, W. 2007, A&A, 467, 1209
- Jacoby, B. A., Bailes, M., Ord, S. M., Knight, H. S., & Hotan, A. W. 2007, ApJ, 656, 408
- Kalberla, P. M. W., Burton, W. B., Hartmann, D., et al. 2005, A&A, 440, 775
- Kaplan, D. L., Esposito, P., Chatterjee, S., et al. 2009, MNRAS, 400, 1445
- Kaplan, D. L., Frail, D. A., Gaensler, B. M., et al. 2004, ApJS, 153, 269
- Kaplan, D. L., van Kerkwijk, M. H., Marshall, H. L., et al. 2003, ApJ, 590, 1008
- Kaplan, D. L., Stovall, K., Ransom, S. M., et al. 2012, ApJ, 753, 174
- Kargaltsev, O., Durant, M., Pavlov, G. G., & Garmire, G. 2012, ApJS, 201, 37
- Kargaltsev, O., & Pavlov, G. G. 2010, X-ray Astronomy 2009; Present Status, Multi-Wavelength Approach and Future Perspectives, 1248, 25
- Kaspi, V. M., Manchester, R. N., Johnston, S., Lyne, A. G., & D'Amico, N. 1992, ApJ, 399, L155
- Kaur, R., Wijnands, R., Paul, B., Patruno, A., & Degenaar, N. 2010, MNRAS, 402, 2388
- Keane, E. F., McLaughlin, M. A., Kramer, M., et al. 2013, ApJ, 764, 180
- Kerr, M., Camilo, F., Johnson, T. J., et al. 2012, ApJ, 748, L2
- Komesaroff, M. M., Ables, J. G., Cooke, D. J., Hamilton, P. A., & McCulloch, P. M. 1973, Astrophys. Lett., 15, 169
- Koribalski, B., Johnston, S., Weisberg, J. M., & Wilson, W. 1995, ApJ, 441, 756
- Kraft, R. P., Burrows, D. N., & Nousek, J. A. 1991, ApJ, 374, 344
- Kramer, M., Lyne, A. G., Hobbs, G., et al. 2003a, ApJ, 593, L31
- Kramer, M., Lyne, A. G., O'Brien, J. T., Jordan, C. A., & Lorimer, D. R. 2006, Science, 312, 549
- Kramer, M., Bell, J. F., Manchester, R. N., et al. 2003b, MNRAS, 342, 1299
- Kuiper, L., & Hermsen, W. 2015, MNRAS, 449, 3827
- Kumar, H. S., Safi-Harb, S., & Gonzalez, M. E. 2012, ApJ, 754, 96
- Li, X.-H., Lu, F.-J., & Li, Z. 2008, ApJ, 682, 1166
- Lorimer, D. R., Lyne, A. G., Bailes, M., et al. 1996, MNRAS, 283, 1383

- Lorimer, D. R., Lyne, A. G., McLaughlin, M. A., et al. 2012, ApJ, 758, 141
- Lorimer, D. R., Nicastro, L., Lyne, A. G., et al. 1995, ApJ, 439, 933
- Maccacaro, T., Gioia, I. M., Wolter, A., Zamorani, G., & Stocke, J. T. 1988, ApJ, 326, 680
- Manchester, R. N., Damico, N., & Tuohy, I. R. 1985, MNRAS, 212, 975
- Manchester, R. N., Hobbs, G. B., Teoh, A., & Hobbs, M. 2005, AJ, 129, 1993
- Manchester, R. N., Lyne, A. G., Taylor, J. H., et al. 1978, MNRAS, 185, 409
- Manchester, R. N., Lyne, A. G., Camilo, F., et al. 2001, MNRAS, 328, 17
- Marshall, H. L., & Schulz, N. S. 2002, ApJ, 574, 377
- McGowan, K. E., Zane, S., Cropper, M., et al. 2004, ApJ, 600, 343
- McGowan, K. E., Zane, S., Cropper, M., Vestrand, W. T., & Ho, C. 2006, ApJ, 639, 377
- Merloni, A., Predehl, P., Becker, W., et al. 2012, ArXiv e-prints, arXiv:1209.3114
- Mignani, R. P., Vande Putte, D., Cropper, M., et al. 2013, MNRAS, 429, 3517
- Monet, D. G., Levine, S. E., Canzian, B., et al. 2003, AJ, 125, 984
- Morrison, R., & McCammon, D. 1983, ApJ, 270, 119
- Olausen, S. A., Zhu, W. W., Vogel, J. K., et al. 2013, ApJ, 764, 1
- Özel, F. 2013, Reports on Progress in Physics, 76, 016901
- Page, D., Lattimer, J. M., Prakash, M., & Steiner, A. W. 2004, ApJS, 155, 623
- . 2009, ApJ, 707, 1131
- Pavlov, G. G., Zavlin, V. E., Sanwal, D., Burwitz, V., & Garmire, G. P. 2001, ApJ, 552, L129
- Possenti, A., Cerutti, R., Colpi, M., & Mereghetti, S. 2002, A&A, 387, 993
- Ransom, S. M., Stairs, I. H., Archibald, A. M., et al. 2014, Nature, 505, 520
- Roger, R. S., Milne, D. K., Kesteven, M. J., Wellington, K. J., & Haynes, R. F. 1988, ApJ, 332, 940
- Romani, R. W., & Ng, C.-Y. 2003, ApJ, 585, L41

- Safi-Harb, S., & Kumar, H. S. 2008, ApJ, 684, 532
- Saz Parkinson, P. M., Dormody, M., Ziegler, M., et al. 2010, ApJ, 725, 571
- Schartel, N. 2012, Mem. Soc. Astron. Italiana, 83, 97
- Seward, F. D., & Wang, Z.-R. 1988, ApJ, 332, 199
- Shternin, P. S., Yakovlev, D. G., Heinke, C. O., Ho, W. C. G., & Patnaude, D. J. 2011, MNRAS, 412, L108
- Slane, P., Helfand, D. J., van der Swaluw, E., & Murray, S. S. 2004a, ApJ, 616, 403
- Slane, P., Zimmerman, E. R., Hughes, J. P., et al. 2004b, ApJ, 601, 1045
- Smith, D. A., Guillemot, L., Camilo, F., et al. 2008, A&A, 492, 923
- Spiewak, R., Kaplan, D. L., Archibald, A., et al. 2016, ArXiv e-prints, arXiv:1602.00655
- Stokes, G. H., Taylor, J. H., Welsberg, J. M., & Dewey, R. J. 1985, Nature, 317, 787
- Tananbaum, H., Weisskopf, M. C., Tucker, W., Wilkes, B., & Edmonds, P. 2014, Reports on Progress in Physics, 77, 066902
- Taylor, J. H., & Cordes, J. M. 1993, ApJ, 411, 674
- Tetzlaff, N., Eisenbeiss, T., Neuhäuser, R., & Hohle, M. M. 2011, MNRAS, 417, 617
- Townsley, L. K., Broos, P. S., Chu, Y.-H., et al. 2011, ApJS, 194, 16
- Tsuruta, S. 1998, Phys. Rep., 292, 1
- Tsuruta, S. 2009, in Astrophysics and Space Science Library, Vol. 357, Astrophysics and Space Science Library, ed. W. Becker, 289
- Verbiest, J. P. W., Weisberg, J. M., Chael, A. A., Lee, K. J., & Lorimer, D. R. 2012, ApJ, 755, 39
- Wang, N., Manchester, R. N., Pace, R. T., et al. 2000, MNRAS, 317, 843
- Wang, W., & Zhao, Y. 2004, ApJ, 601, 1038
- Weisskopf, M. C., Tennant, A. F., Yakovlev, D. G., et al. 2011, ApJ, 743, 139
- Xmm-Newton Survey Science Centre, C. 2013, VizieR Online Data Catalog, 9044, 0
- Yakovlev, D. G., & Pethick, C. J. 2004, ARA&A, 42, 169

- Yar-Uyaniker, A., Uyaniker, B., & Kothes, R. 2004, ApJ, 616, 247
- Zavlin, V. E., & Pavlov, G. G. 2004a, ApJ, 616, 452
- . 2004b, Mem. Soc. Astron. Italiana, 75, 458
- Zavlin, V. E., Pavlov, G. G., & Trumper, J. 1998, A&A, 331, 821
- Zavlin, V. E., Trümper, J., & Pavlov, G. G. 1999, ApJ, 525, 959
- Zhu, W. W., Kaspi, V. M., McLaughlin, M. A., et al. 2011, ApJ, 734, 44

Table 1:: Used observations.

PSR	satellite ^(α)	obsID	date	instrument ^(β)	filter	$t_{\text{on-axis}}$ ksec	$t(\theta)$ ksec	$\theta^{(\gamma)}$ arcmin	count rate ^(δ) cts/ksec	flag ^(δ)
J0051+0423	C	15968	2013-12-22	ACIS-S	-	3.6	3.5	0.2	0.83	ul
J0101-6422	C	15363	2013-02-17	ACIS-I	-	9.8	9.0	0.7	-	d
J0117+5914	X	0112200201	2002-07-09	PN/FF	Medium	5.8	5.1	1.7	-	d
	X	0112200201	2002-07-09	MOS1	Medium	7.9	7.7	1.7	-	d
	X	0112200201	2002-07-09	MOS2	Medium	8.1	7.9	1.7	-	d
J0134-2937	X	0654800501	2010-12-30	PN/FF	Medium	30.4	11.8	11.4	3.44	ul
	X	0654800501	2010-12-30	MOS1	Medium	39.0	2.1	11.4	1.44	ul
	X	0654800501	2010-12-30	MOS2	Medium	39.5	19.1	11.4	1.55	ul
J0137+1654	C	15969	2013-12-27	ACIS-S	-	3.6	3.5	0.2	0.83	ul
J0139+5814	X	0103262501	2003-01-16	PN/FF	Medium	2.7	2.4	1.7	2.86	ul
	X	0103262501	2003-01-16	MOS1	Medium	4.4	4.3	1.7	1.95	ul
	X	0103262501	2003-01-16	MOS2	Medium	4.4	4.2	1.7	0.74	ul
J0157+6212	X	0150820201	2003-03-06	PN/SW	Thin	12.1	8.4	1.8	4.06	ul
	X	0150820201	2003-03-06	MOS1	Medium	12.8	12.6	1.8	0.94	ul
	X	0150820201	2003-03-06	MOS2	Medium	13.3	11.4	1.8	1.23	ul
J0248+6021	C	13289	2012-09-25	ACIS-I	-	9.3	8.6	0.3	1.15	ul
J0335+4555	C	15970	2013-12-25	ACIS-S	-	3.6	3.5	0.2	0.89	ul
J0337+1715	X	0722920101	2013-08-01	PN/FF	Thin	16.8	14.8	1.8	-	d
	X	0722920101	2013-08-01	MOS1	Thin	18.4	17.2	1.8	-	d
	X	0722920101	2013-08-01	MOS2	Thin	18.2	17.2	1.8	-	d
J0520-2553	C	15971	2013-12-28	ACIS-S	-	3.6	3.5	0.2	0.83	ul
J0543+2329	X	0103262801	2003-10-09	PN/FF	Medium	5.5	4.9	1.7	-	d
	X	0103262801	2003-10-09	MOS1	Medium	7.6	7.5	1.7	-	d
	X	0103262801	2003-10-09	MOS2	Medium	7.5	7.1	1.7	-	d
J0609+2130	C	12687	2011-04-14	ACIS-S	-	5.1	5.0	0.3	0.62	ul
J0622+3749	C	12842	2011-01-29	ACIS-I	-	2.1	1.9	2.2	1.56	ul
J0636+5129	X	0722920201	2013-10-12	MOS1	Thin	16.4	15.0	1.7	4.49	ul
	X	0722920201	2013-10-12	MOS2	Thin	16.2	15.4	1.7	3.98	ul
J0645+5158	X	0722920301	2014-03-29	MOS1	Thin	18.8	17.2	1.7	0.86	ul
	X	0722920301	2014-03-29	MOS2	Thin	18.4	16.5	1.7	0.71	ul
J0656-5449	C	15972	2014-04-06	ACIS-S	-	3.6	3.5	0.2	0.83	ul
J0742-2822	X	0103262401	2002-10-11	PN/FF	Medium	2.7	2.4	1.7	14.54	ul
	X	0103262401	2002-10-11	MOS1	Medium	5.1	5.0	1.7	3.54	ul
	X	0103262401	2002-10-11	MOS2	Medium	5.7	5.5	1.7	2.22	ul
J0828-3417	X	0400020101	2006-11-13	PN/FF	Thin	35.4	30.6	1.7	1.34	ul
	X	0400020101	2006-11-13	MOS1	Thin	41.5	40.7	1.7	0.58	ul
	X	0400020101	2006-11-13	MOS2	Thin	42.3	40.8	1.7	0.54	ul
J0847-4316	C	7626	2007-02-08	ACIS-I	-	10.8	8.6	1.1	0.54	ul
J0907-5157	X	0112930101	2001-12-11	PN/EFF	Thin	12.1	5.5	9.0	8.10	ul
	X	0112930101	2001-12-10	MOS1	Thin	23.0	11.2	9.0	2.91	ul
	X	0112930101	2001-12-10	MOS2	Thin	23.8	13.2	9.0	3.77	ul
	C	9147	2008-08-26	ACIS-I	-	42.2	20.7	9.3	1.44	ul
	C	10572	2008-08-27	ACIS-I	-	23.1	11.1	9.3	1.45	ul
J0922+0638	X	0502920101	2007-11-09	PN/LW	Thin	15.5	14.2	1.7	-	d
	X	0502920101	2007-11-09	MOS1	Thin	25.2	24.7	1.7	-	d
	X	0502920101	2007-11-09	MOS2	Thin	24.9	23.5	1.7	-	d
J0940-5428	C	9077	2008-08-20	ACIS-I	-	10.2	9.1	0.8	0.34	ul
J0943+1631	X	0046940201	2001-05-07	MOS1	Medium	5.2	1.8	11.6	1.72	ul
	X	0046940201	2001-05-07	MOS2	Medium	4.9	2.0	11.6	1.54	ul
	X	0046940401	2001-11-02	MOS1	Medium	14.9	5.3	14.7	0.58	ul
	X	0046940401	2001-11-02	MOS2	Medium	14.7	4.4	14.7	0.71	ul

Continued on next page

Table 1 – continued from previous page

PSR	satellite ^(a)	obsID	date	instrument ^(β)	filter	$t_{\text{on-axis}}$	$t(\theta)$	$\theta^{(γ)}$	count rate ^(δ)	flag ^(δ)
J1001–5939	C	12561	2011-10-08	ACIS-S	-	19.0	17.2	0.2	0.24	ul
J1038+0032	C	13801	2012-01-18	ACIS-S	-	3.5	3.5	0.2	0.89	ul
J1044–5737	C	15361	2013-08-25	ACIS-I	-	10.1	9.5	0.7	-	d
J1055–6022	X	0600030101	2010-01-21	PN/FF	Medium	16.5	10.5	4.4	3.56	ul
	X	0600030101	2010-01-21	MOS1	Medium	18.9	9.2	4.4	1.90	ul
	X	0600030101	2010-01-21	MOS2	Medium	20.0	11.8	4.4	1.33	ul
J1055–6028	X	0600030101	2010-01-21	PN/FF	Medium	16.5	10.8	5.5	3.52	ul
	X	0600030101	2010-01-21	MOS1	Medium	18.9	14.6	5.5	1.48	ul
	X	0600030101	2010-01-21	MOS2	Medium	20.0	14.6	5.5	1.36	ul
J1103–5403	C	12538	2011-09-08	ACIS-S	-	10.0	9.9	0.2	0.80	ul
J1104–6103	C	4380	2002-10-01	ACIS-S	-	11.9	8.0	7.6	1.55	ul
	C	2780	2002-09-29	ACIS-S	-	11.8	7.9	7.6	0.30	ul
J1105–6107	C	4380	2002-10-01	ACIS-S	-	11.9	11.5	2.0	1.15	ul
	C	2780	2002-09-29	ACIS-S	-	11.8	11.4	2.0	0.53	ul
J1107–5907	C	12688	2011-03-31	ACIS-S	-	5.1	5.0	0.3	1.67	ul
J1112–6103	C	6706	2006-09-16	ACIS-S	-	34.6	33.3	0.1	-	d
	C	8905	2007-11-10	ACIS-I	-	59.1	53.0	2.4	-	d
J1115+5030	C	15021	2013-07-07	ACIS-S	-	22.1	19.5	6.4	0.16	ul
J1157–6224	X	0503780301	2008-02-16	PN/FF	Medium	15.9	4.5	12.8	12.20	ul
	X	0503780301	2008-02-16	MOS1	Medium	18.8	5.3	12.8	3.80	ul
	X	0503780301	2008-02-16	MOS2	Medium	17.6	5.2	12.8	2.99	ul
	X	0550170101	2008-08-16	MOS1	Medium	45.3	15.0	14.2	2.51	ul
	X	0550170101	2008-08-16	MOS2	Medium	45.9	18.8	14.2	1.58	ul
J1159–7910	X	0550120601	2009-03-16	PN/FF	Medium	2.9	0.6	11.7	15.38	ul
	X	0550120601	2009-03-16	MOS1	Medium	9.7	3.0	11.7	4.30	ul
	X	0550120601	2009-03-16	MOS2	Medium	9.2	1.1	11.7	8.11	ul
J1224–6407	X	0103260901	2002-08-10	PN/FF	Medium	4.3	3.9	1.7	-	d
	X	0103260901	2002-08-10	MOS1	Medium	6.6	6.4	1.7	-	d
	X	0103260901	2002-08-10	MOS2	Medium	6.6	6.4	1.7	-	d
J1225–6408	X	0103260901	2002-08-10	MOS1	Medium	6.6	3.2	9.2	0.95	ul
	X	0103260901	2002-08-10	MOS2	Medium	6.6	2.7	9.2	3.64	ul
	X	0653030501	2010-08-08	MOS2	Thick	17.7	7.7	5.7	0.40	ul
	X	0653030601	2010-08-14	MOS1	Medium	18.5	2.4	5.7	1.28	ul
	X	0653030601	2010-08-14	MOS2	Thick	18.6	8.7	5.7	2.14	ul
	X	0653030701	2010-08-16	MOS1	Medium	18.3	4.7	5.8	3.19	ul
	X	0653030701	2010-08-16	MOS2	Thick	18.6	8.5	5.8	1.32	ul
J1253–5820	X	0720300401	2013-08-20	PN/FF	Medium	4.8	2.7	9.5	8.72	ul
	X	0720300401	2013-08-20	MOS1	Medium	5.7	3.7	9.5	6.03	ul
	X	0720300401	2013-08-20	MOS2	Medium	7.3	4.6	9.5	2.51	ul
J1300+1240	C	5518	2005-05-22	ACIS-S	-	20.1	19.8	0.7	0.23	ul
	C	7577	2007-05-03	ACIS-S	-	18.5	18.2	0.4	0.27	ul
J1301–6310	X	0303440101	2005-07-12	PN/LW	Thin	27.1	24.9	1.8	-	d
	X	0303440101	2005-07-12	MOS1	Medium	29.8	27.3	1.8	-	d
	X	0303440101	2005-07-12	MOS2	Medium	29.7	28.5	1.8	-	d
	X	0302340101	2005-07-14	PN/FF	Medium	24.2	11.4	11.3	-	d
	X	0302340101	2005-07-14	MOS1	Medium	30.1	15.0	11.3	-	d
	X	0302340101	2005-07-14	MOS2	Medium	30.5	16.3	11.3	-	d
J1302–6313	X	0302340101	2005-07-14	MOS1	Medium	30.0	25.6	5.2	0.74	ul
	X	0302340101	2005-07-14	MOS2	Medium	30.7	26.0	5.2	1.35	ul
	X	0303440101	2005-07-12	MOS1	Medium	29.8	19.7	5.3	0.90	ul
	X	0303440101	2005-07-12	MOS2	Medium	29.7	20.0	5.3	1.26	ul
	C	6098	2004-09-25	ACIS-I	-	4.7	3.8	3.9	0.76	ul
J1303–6305	X	0302340101	2005-07-14	MOS1	Medium	30.3	19.2	8.5	1.40	ul
	X	0302340101	2005-07-14	MOS2	Medium	30.6	17.6	8.5	1.24	ul

Continued on next page

Table 1 – continued from previous page

PSR	satellite ^(α)	obsID	date	instrument ^(β)	filter	$t_{\text{on-axis}}$	$t(\theta)$	$\theta^{(γ)}$	count rate ^(δ)	flag ^(δ)
	X	0303440101	2005-07-12	MOS1	Medium	29.8	10.4	12.3	1.44	ul
	X	0303440101	2005-07-12	MOS2	Medium	29.8	10.5	12.3	1.59	ul
	C	6098	2004-09-25	ACIS-I	-	4.7	3.6	6.2	1.30	ul
J1305-6256	X	0303100201	2005-08-25	PN/FF	Medium	5.1	1.4	13.1	45.55	ul
J1306-6242	X	0303100201	2005-08-25	PN/FF	Medium	8.1	4.6	6.9	6.12	ul
	X	0303100201	2005-08-25	MOS1	Medium	7.3	4.9	6.9	2.78	ul
	X	0303100201	2005-08-25	MOS2	Medium	10.7	7.0	6.9	2.14	ul
J1309-6526	X	0090030201	2004-07-20	PN/FF	Thick	75.7	33.8	8.1	1.31	ul
	X	0090030201	2004-07-20	MOS1	Thick	84.9	39.8	8.1	0.98	ul
	X	0090030201	2004-07-20	MOS2	Thick	90.4	36.2	8.1	0.95	ul
	X	0605670201	2009-07-19	PN/FF	Thick	52.3	22.5	8.1	1.74	ul
	X	0605670201	2009-07-19	MOS1	Thick	53.7	25.0	8.1	1.11	ul
	X	0605670201	2009-07-19	MOS2	Thick	53.2	20.9	8.1	1.27	ul
J1317-5759	X	0406450101	2006-07-16	PN/SW	Thin	25.1	17.3	1.8	3.80	ul
	X	0406450101	2006-07-16	MOS1	Thin	29.7	28.7	1.8	1.36	ul
	X	0406450101	2006-07-16	MOS2	Thin	30.6	28.9	1.8	1.03	ul
J1317-6302	C	9049	2008-09-11	ACIS-I	-	5.1	4.1	7.9	0.69	ul
J1320-3512	C	13797	2012-03-20	ACIS-S	-	3.5	3.4	0.2	0.90	ul
J1322-6329	X	0691550101	2013-03-02	PN/FF	Medium	33.6	16.4	4.6	2.21	ul
	X	0691550101	2013-03-02	MOS1	Medium	44.8	4.2	4.6	0.73	ul
	X	0691550101	2013-03-02	MOS2	Medium	48.5	26.9	4.6	0.91	ul
	C	14812	2013-09-24	ACIS-S	-	47.8	42.0	5.9	0.07	ul
J1324-6302	C	1913	2001-09-10	ACIS-S	-	5.1	3.2	11.4	2.09	ul
J1333-4449	C	13800	2012-03-28	ACIS-S	-	3.5	3.4	0.2	0.85	ul
J1334-5839	C	15973	2014-01-02	ACIS-S	-	3.6	3.5	0.2	1.42	ul
J1339-4712	C	13799	2012-05-13	ACIS-S	-	3.5	3.4	0.2	0.85	ul
J1341-6220	X	0301740101	2005-07-26	PN/LW	Thick	35.5	32.6	1.7	-	d
	X	0301740101	2005-07-26	MOS1	Thick	37.3	34.1	1.7	-	d
	X	0301740101	2005-07-26	MOS2	Thick	36.9	35.8	1.7	-	d
	X	0143400201	2003-07-17	PN/LW	Thick	6.2	5.7	1.7	-	d
	X	0143400201	2003-07-17	MOS1	Thick	6.6	6.5	1.7	-	d
	X	0143400201	2003-07-17	MOS2	Thick	6.5	6.3	1.7	-	d
	X	0143400101	2003-02-11	PN/LW	Thick	5.3	4.9	1.7	-	d
	X	0143400101	2003-02-11	MOS1	Thick	4.9	4.8	1.7	-	d
	X	0143400101	2003-02-11	MOS2	Thick	5.3	5.0	1.7	-	d
J1355-5925	X	0007422301	2001-02-08	PN/FF	Medium	12.1	3.1	12.5	7.56	ul
	X	0007422301	2001-02-08	MOS1	Medium	14.8	4.7	12.5	0.66	ul
	X	0007422301	2001-02-08	MOS2	Medium	14.6	4.6	12.5	3.21	ul
J1355-6206	C	13806	2012-05-28	ACIS-S	-	3.5	3.4	0.2	0.85	ul
J1359-6038	X	0007421101	2002-02-13	MOS1	Medium	10.3	3.4	14.6	0.90	ul
	X	0007421101	2002-02-13	MOS2	Medium	10.5	3.7	14.6	0.83	ul
J1406-6121	C	14888	2013-09-19	ACIS-I	-	13.1	9.7	9.9	1.34	ul
J1410-7404	C	15974	2014-01-03	ACIS-S	-	3.6	3.5	0.2	0.88	ul
J1412-6145	C	1985	2001-07-26	ACIS-I	-	9.4	8.5	0.3	0.36	ul
J1413-6141	C	1985	2001-07-26	ACIS-I	-	9.4	6.9	8.7	0.81	ul
J1425-5723	C	12686	2011-06-02	ACIS-S	-	5.1	5.0	0.3	0.62	ul
J1432-5032	X	0690210101	2012-08-10	PN/FF	Thick	11.5	7.7	3.8	2.32	ul
	X	0690210101	2012-08-10	MOS1	Thick	13.1	8.8	3.8	1.39	ul
	X	0690210101	2012-08-10	MOS2	Thick	13.1	10.4	3.8	1.68	ul
J1444-5941	C	8235	2007-10-19	ACIS-S	-	1.8	0.9	9.6	3.35	ul
J1453-6413	X	0103261001	2001-02-28	PN/SW	Medium	4.8	3.3	1.8	5.82	ul
	X	0103261001	2001-02-28	MOS1	Medium	5.7	5.6	1.8	2.35	ul
	X	0103261001	2001-02-28	MOS2	Medium	5.6	4.9	1.8	0.63	ul
J1457-5900	C	11880	2010-05-05	ACIS-S	-	10.2	9.9	0.6	0.31	ul

Continued on next page

Table 1 – continued from previous page

PSR	satellite ^(α)	obsID	date	instrument ^(β)	filter	$t_{\text{on-axis}}$	$t(\theta)$	$\theta^{(\gamma)}$	count rate ^(δ)	flag ^(δ)
J1457–5902	C	11880	2010-05-05	ACIS-S	-	10.2	10.0	1.0	0.31	ul
J1507–6640	X	0551430301	2009-02-02	PN/FF	Medium	26.3	7.6	11.2	5.41	ul
	X	0551430301	2009-02-02	MOS1	Medium	30.6	9.4	11.2	2.08	ul
	X	0551430301	2009-02-02	MOS2	Medium	30.9	10.7	11.2	2.00	ul
J1511–5835	C	11881	2010-06-14	ACIS-S	-	10.0	6.7	13.0	0.46	ul
J1514–5925	X	0207050101	2004-09-14	PN/FF	Medium	4.7	0.9	9.9	35.44	ul
	X	0207050101	2004-09-14	MOS1	Medium	10.5	4.1	9.9	10.17	ul
	X	0207050101	2004-09-14	MOS2	Medium	10.6	4.6	9.9	8.28	ul
	X	0302730101	2005-08-07	PN/FF	Medium	15.9	4.7	10.1	19.55	ul
	X	0302730101	2005-08-07	MOS2	Medium	13.9	6.5	10.1	5.93	ul
J1517–4636	X	0204710901	2004-08-03	PN/FF	Medium	6.4	2.2	11.3	18.10	ul
	X	0204710901	2004-08-03	MOS1	Medium	14.1	6.6	11.3	10.31	ul
	X	0204710901	2004-08-03	MOS2	Medium	15.5	8.1	11.3	3.41	ul
J1524–5706	C	2784	2002-07-16	ACIS-I	-	28.2	21.2	8.8	0.15	ul
J1529–5611	C	12417	2011-06-22	ACIS-I	-	5.2	3.6	2.8	0.80	ul
J1535–4114	X	0652610201	2011-02-25	PN/FF	Thick	72.4	33.6	6.1	1.59	ul
	X	0652610201	2011-02-25	MOS1	Thick	102.3	80.3	6.1	0.62	ul
	X	0652610201	2011-02-25	MOS2	Thick	80.9	64.3	6.1	0.60	ul
J1538–5551	C	10509	2009-01-24	ACIS-S	-	4.6	2.8	8.8	1.12	ul
	C	9600	2008-05-24	HRC-I	-	1.2	0.9	10.6	10.56	ul
J1542–5034	C	12429	2011-10-09	ACIS-I	-	5.1	4.8	13.0	1.49	ul
J1548–4821	C	13805	2012-07-28	ACIS-S	-	3.5	3.4	0.2	0.85	ul
J1549–4848	X	0740970101	2014-09-03	MOS1	Medium	89.5	81.4	1.7	0.43	ul
	X	0740970101	2014-09-03	MOS2	Medium	92.0	85.9	1.7	0.42	ul
J1549+2113	X	0136040101	2002-02-18	PN/FF	Thin	15.6	4.4	14.2	5.82	ul
	X	0136040101	2002-02-18	MOS1	Thin	17.7	6.5	14.2	1.83	ul
	X	0136040101	2002-02-18	MOS2	Thin	17.8	5.5	14.2	2.10	ul
J1553–5456	C	1955	2001-07-15	ACIS-I	-	49.9	40.4	7.1	0.08	ul
J1554–5512	C	13767	2012-05-24	ACIS-I	-	143.5	120.8	7.1	0.03	ul
	C	13768	2012-05-22	ACIS-I	-	161.5	135.9	7.1	0.02	ul
	C	14430	2012-05-27	ACIS-I	-	37.1	31.5	7.1	0.18	ul
J1555–2341	X	0112380101	2000-08-26	PN/FF	Medium	34.8	13.8	12.6	2.21	ul
	X	0112380101	2000-08-26	MOS1	Medium	37.8	17.1	12.6	1.22	ul
	X	0112380101	2000-08-26	MOS2	Medium	39.4	12.6	12.6	1.23	ul
J1600–3053	X	0503190401	2008-02-17	MOS1	Medium	25.0	24.5	1.7	-	d
	X	0503190401	2008-02-17	MOS2	Medium	25.3	23.5	1.7	-	d
J1604–4909	X	0724700101	2013-09-17	PN/FF	Thin	28.1	14.6	6.5	1.77	ul
	X	0724700101	2013-09-17	MOS1	Thin	0.3	0.1	6.5	109.62	ul
	X	0724700101	2013-09-17	MOS2	Thin	0.4	0.2	6.5	53.62	ul
J1607–6449	C	15975	2014-01-16	ACIS-S	-	3.6	3.5	0.2	1.42	ul
J1611–5847	C	13802	2012-05-21	ACIS-S	-	3.5	3.4	0.2	0.91	ul
J1613–5211	X	0555660101	2008-08-15	PN/FF	Medium	21.6	18.1	2.9	3.78	ul
	X	0555660101	2008-08-15	MOS1	Medium	32.3	29.1	2.9	1.20	ul
	X	0555660101	2008-08-15	MOS2	Medium	31.7	30.0	2.9	1.08	ul
J1614–5144	X	0406650101	2006-08-15	PN/EFF	Medium	19.7	14.8	3.3	2.61	ul
	X	0406650101	2006-08-15	MOS1	Medium	30.9	27.8	3.3	0.97	ul
	X	0406650101	2006-08-15	MOS2	Thin	30.7	28.2	3.3	1.04	ul
	X	0406550101	2007-02-13	PN/FF	Medium	7.7	2.9	4.5	7.73	ul
	X	0406550101	2007-02-13	MOS1	Medium	12.0	10.0	4.5	6.55	ul
	X	0406550101	2007-02-13	MOS2	Medium	11.7	10.1	4.5	1.86	ul
J1616–5109	X	0302390101	2005-08-23	MOS1	Medium	60.8	25.7	12.3	1.45	ul
	X	0302390101	2005-08-23	MOS2	Medium	60.1	28.3	12.3	1.72	ul
J1616–5208	C	2546	2002-10-23	ACIS-S	-	41.4	30.5	11.7	0.70	ul
J1620–4927	X	0406750201	2007-02-25	PN/FF	Medium	6.0	1.3	11.5	13.71	ul

Continued on next page

Table 1 – continued from previous page

PSR	satellite ^(a)	obsID	date	instrument ^(β)	filter	$t_{\text{on-axis}}$	$t(\theta)$	$\theta^{(\gamma)}$	count rate ^(δ)	flag ^(δ)
	X	0406750201	2007-02-25	MOS1	Medium	7.6	2.4	11.5	3.92	ul
	X	0406750201	2007-02-25	MOS2	Medium	3.7	0.7	11.5	11.14	ul
J1621-5039	C	14531	2013-06-25	ACIS-I	-	61.1	50.9	3.6	0.06	ul
J1622-4944	C	10929	2009-07-10	ACIS-I	-	20.1	15.8	6.1	0.20	ul
	C	8161	2007-06-13	ACIS-S	-	2.9	2.5	3.0	1.23	ul
J1623-4949	X	0654110101	2011-02-22	MOS1	Thin	55.6	25.1	12.3	2.99	ul
	X	0654110101	2011-02-22	MOS2	Thin	55.6	27.1	12.3	1.56	ul
	C	8161	2007-06-13	ACIS-S	-	2.9	1.3	10.9	3.12	ul
J1625-4904	X	0403280201	2007-02-14	MOS1	Medium	15.2	5.3	10.2	7.59	ul
	X	0403280201	2007-02-14	MOS2	Medium	15.6	5.8	10.2	4.78	ul
J1625-4913	X	0403280201	2007-02-14	PN/FF	Medium	7.6	2.7	10.7	8.39	ul
	X	0403280201	2007-02-14	MOS1	Medium	15.2	5.8	10.7	4.49	ul
	X	0403280201	2007-02-14	MOS2	Medium	17.7	6.4	10.7	3.50	ul
J1627-4845	X	0724560101	2013-08-14	PN/FF	Medium	18.7	13.7	4.5	1.77	ul
	X	0724560101	2013-08-14	MOS1	Medium	21.6	18.9	4.5	0.90	ul
	X	0724560101	2013-08-14	MOS2	Medium	21.5	18.0	4.5	0.88	ul
J1627-5936	C	15976	2014-01-19	ACIS-S	-	3.6	3.5	0.2	0.89	ul
J1632-4757	X	0128531101	2003-03-04	PN/LW	Medium	4.8	3.0	8.9	5.03	ul
	X	0128531101	2003-03-04	MOS2	Medium	5.0	2.8	8.9	3.61	ul
	X	0201700301	2004-08-19	PN/FF	Thin	35.2	22.8	4.0	1.92	ul
	X	0556140101	2008-08-14	PN/FF	Thin	5.5	3.6	4.0	4.86	ul
	X	0556140101	2008-08-14	MOS1	Thin	9.4	6.3	4.0	1.93	ul
	X	0556140101	2008-08-14	MOS2	Thin	9.1	6.9	4.0	1.82	ul
	X	0556140201	2008-08-16	PN/FF	Thin	2.5	1.7	3.9	11.80	ul
	X	0556140201	2008-08-16	MOS1	Thin	3.5	2.4	3.9	1.30	ul
	X	0556140201	2008-08-16	MOS2	Thin	3.5	2.8	3.9	2.08	ul
	X	0556140301	2008-08-18	PN/FF	Thin	5.0	3.3	4.0	8.47	ul
	X	0556140301	2008-08-18	MOS1	Thin	6.7	4.5	4.0	2.69	ul
	X	0556140301	2008-08-18	MOS2	Thin	6.1	4.8	4.0	4.00	ul
	X	0556140401	2008-08-20	PN/FF	Thin	8.3	5.1	4.0	3.87	ul
	X	0556140401	2008-08-20	MOS1	Thin	12.5	8.5	4.0	1.63	ul
	X	0556140401	2008-08-20	MOS2	Thin	12.5	9.9	4.0	1.48	ul
	X	0556140501	2008-08-21	PN/FF	Thin	2.0	1.3	4.0	10.54	ul
	X	0556140501	2008-08-21	MOS1	Thin	4.9	3.4	4.0	0.92	ul
	X	0556140501	2008-08-21	MOS2	Thin	4.3	3.4	4.0	0.91	ul
	X	0556140601	2008-08-22	PN/FF	Thin	10.7	5.7	4.1	3.17	ul
	X	0556140601	2008-08-22	MOS1	Thin	14.0	9.5	4.1	1.55	ul
	X	0556140601	2008-08-22	MOS2	Thin	13.4	10.4	4.1	1.49	ul
	X	0556140701	2008-08-24	PN/FF	Thin	6.2	3.3	3.9	10.42	ul
	X	0556140701	2008-08-24	MOS1	Thin	10.0	6.9	3.9	1.71	ul
	X	0556140701	2008-08-24	MOS2	Thin	9.8	7.7	3.9	1.73	ul
	X	0556140801	2008-08-26	PN/FF	Thin	8.9	4.5	4.0	3.94	ul
	X	0556140801	2008-08-26	MOS1	Thin	11.1	7.7	4.0	1.77	ul
	X	0556140801	2008-08-26	MOS2	Thin	11.2	8.8	4.0	1.56	ul
	X	0556141001	2008-09-17	PN/FF	Thin	4.2	2.5	4.0	5.02	ul
	X	0556141001	2008-09-17	MOS1	Thin	7.0	4.9	4.0	2.68	ul
	X	0556141001	2008-09-17	MOS2	Thin	6.4	5.0	4.0	0.62	ul
	C	10088	2009-06-22	ACIS-I	-	9.8	7.0	8.3	0.44	ul
	C	8155	2007-10-23	HRC-I	-	2.7	1.9	12.7	1.65	ul
J1633-4805	C	10982	2010-06-05	ACIS-S	-	100.0	65.1	8.2	0.25	ul
J1636-4803	C	9007	2008-05-27	HRC-I	-	1.2	0.9	14.3	3.57	ul
J1637-4553	X	0103261101	2002-02-23	PN/FF	Medium	4.0	3.5	1.8	14.91	ul
	X	0103261101	2002-02-23	MOS1	Medium	5.3	5.2	1.8	3.97	ul
	X	0103261101	2002-02-23	MOS2	Medium	6.2	5.8	1.8	3.88	ul

Continued on next page

Table 1 – continued from previous page

PSR	satellite ^(α)	obsID	date	instrument ^(β)	filter	$t_{\text{on-axis}}$	$t(\theta)$	$\theta^{(γ)}$	count rate ^(δ)	flag ^(δ)
J1637–4642	C	12518	2011-06-11	ACIS-I	-	19.8	15.1	8.6	0.93	ul
J1637–4721	X	0204500201	2004-02-16	MOS1	Thin	18.1	6.6	14.4	2.18	ul
	X	0204500201	2004-02-16	MOS2	Thin	18.0	7.1	14.4	2.42	ul
	X	0204500301	2004-09-04	PN/FF	Thin	28.7	7.8	13.9	3.42	ul
	X	0204500301	2004-09-04	MOS1	Thin	32.2	5.5	13.9	4.61	ul
	X	0307170201	2005-08-19	PN/FF	Medium	42.2	18.0	12.8	2.34	ul
	X	0307170201	2005-08-19	MOS1	Medium	63.8	28.8	12.8	1.96	ul
	X	0307170201	2005-08-19	MOS2	Medium	69.9	32.0	12.8	0.91	ul
	C	12525	2011-06-14	ACIS-I	-	19.8	18.5	13.1	1.00	ul
	C	12522	2011-06-13	ACIS-I	-	19.3	15.8	5.4	0.20	ul
	C	12523	2011-06-14	ACIS-I	-	19.3	16.0	6.6	0.19	ul
	C	12503	2011-02-05	HRC-I	-	1.2	0.8	13.8	3.64	ul
J1638–4725	C	12522	2011-06-13	ACIS-I	-	19.3	16.1	6.4	0.19	ul
	C	6261	2005-05-04	ACIS-S	-	10.2	9.9	0.6	0.42	ul
J1640–4648	C	12510	2011-06-09	ACIS-I	-	20.2	17.9	0.7	0.28	ul
	C	12513	2011-06-27	ACIS-I	-	20.4	19.2	12.7	0.88	ul
J1643–1224	X	0742520101	2014-09-12	MOS1	Medium	11.3	10.3	1.7	3.68	ul
	X	0742520101	2014-09-12	MOS2	Medium	11.4	10.6	1.7	4.01	ul
J1646–4346	X	0553110201	2009-03-09	PN/FF	Medium	2.7	1.5	2.2	21.27	ul
	X	0553110201	2009-03-09	MOS1	Medium	3.1	3.0	2.2	9.41	ul
	X	0553110201	2009-03-09	MOS2	Medium	2.8	2.7	2.2	21.95	ul
J1648–4458	X	0512180101	2008-03-21	MOS2	Medium	27.2	10.0	12.3	1.91	ul
J1648–4611	C	11836	2010-01-24	ACIS-I	-	10.2	8.7	4.9	0.35	ul
J1649–4349	C	6270	2005-10-21	HRC-I	-	4.2	4.1	0.2	0.75	ul
J1650–4341	C	13777	2012-06-22	ACIS-S	-	8.1	7.9	0.2	0.39	ul
J1652–4406	C	8145	2007-10-25	ACIS-S	-	2.2	1.0	11.2	3.13	ul
J1653–4315	C	13774	2012-07-07	ACIS-S	-	5.1	5.0	0.2	0.62	ul
J1654–4140	X	0109490101	2001-09-05	PN/FF	Thick	29.8	12.1	10.7	3.05	ul
	X	0109490101	2001-09-05	MOS1	Thick	32.9	16.4	10.7	1.01	ul
	X	0109490101	2001-09-05	MOS2	Thick	32.5	15.6	10.7	1.61	ul
	X	0109490201	2001-09-06	PN/FF	Thick	16.4	6.9	10.7	5.14	ul
	X	0109490201	2001-09-06	MOS1	Thick	19.3	9.6	10.7	1.79	ul
	X	0109490201	2001-09-06	MOS2	Thick	19.4	9.3	10.7	1.49	ul
	X	0109490301	2001-09-07	PN/FF	Thick	28.7	12.5	10.8	2.46	ul
	X	0109490301	2001-09-07	MOS1	Thick	33.2	16.6	10.8	1.24	ul
	X	0109490301	2001-09-07	MOS2	Thick	34.0	16.3	10.8	1.23	ul
	X	0109490401	2001-09-08	PN/FF	Thick	11.8	5.3	10.7	3.86	ul
	X	0109490401	2001-09-08	MOS1	Thick	19.7	10.0	10.7	2.30	ul
	X	0109490401	2001-09-08	MOS2	Thick	19.4	9.3	10.7	2.83	ul
	X	0109490501	2001-09-09	PN/FF	Thick	24.9	11.1	10.8	2.50	ul
	X	0109490501	2001-09-09	MOS1	Thick	30.9	15.5	10.8	1.46	ul
	X	0109490501	2001-09-09	MOS2	Thick	30.9	14.8	10.8	1.32	ul
	X	0109490601	2001-09-10	PN/FF	Thick	30.3	13.4	10.8	3.22	ul
	X	0109490601	2001-09-10	MOS1	Thick	32.8	16.4	10.8	1.30	ul
	X	0109490601	2001-09-10	MOS2	Thick	32.8	15.7	10.8	1.80	ul
	C	5372	2005-07-03	ACIS-I	-	77.2	58.6	9.6	0.22	ul
J1658–5324	C	12535	2011-01-25	ACIS-S	-	10.0	9.4	4.4	-	d
J1702–4217	C	13776	2012-06-24	ACIS-S	-	8.7	8.5	0.2	0.57	ul
J1702–4306	C	9083	2009-01-30	ACIS-I	-	9.8	9.4	3.2	0.33	ul
J1702–4310	C	9083	2009-01-30	ACIS-I	-	9.8	9.6	0.8	0.32	ul
J1703–4851	C	4446	2004-02-04	ACIS-S	-	29.8	18.2	11.9	0.57	ul
J1705–1906	X	0112200501	2002-03-14	PN/FF	Medium	3.6	3.2	1.7	9.64	ul
	X	0112200501	2002-03-14	MOS1	Medium	6.0	5.9	1.7	3.67	ul
	X	0112200501	2002-03-14	MOS2	Medium	6.2	5.7	1.7	2.76	ul

Continued on next page

Table 1 – continued from previous page

PSR	satellite ^(a)	obsID	date	instrument ^(β)	filter	$t_{\text{on-axis}}$	$t(\theta)$	$\theta^{(γ)}$	count rate ^(δ)	flag ^(δ)
J1705–4108	X	0406750301	2007-02-25	PN/FF	Medium	5.9	5.2	2.3	2.54	ul
	X	0406750301	2007-02-25	MOS1	Medium	7.6	7.0	2.3	1.40	ul
	X	0406750301	2007-02-25	MOS2	Medium	7.4	6.4	2.3	0.48	ul
J1706–4310	C	3791	2003-06-19	HRC-I	-	1.0	0.9	8.1	3.60	ul
J1707–4053	X	0144080101	2002-09-27	PN/FF	Medium	10.9	9.6	0.9	1.94	ul
	X	0144080101	2002-09-27	MOS1	Medium	17.0	16.5	0.9	0.89	ul
	X	0144080101	2002-09-27	MOS2	Medium	17.0	16.0	0.9	1.94	ul
J1709–3626	C	12505	2011-03-06	HRC-I	-	1.1	1.0	7.7	6.23	ul
J1709–4401	X	0105470201	2000-09-11	MOS1	Medium	13.4	5.9	9.9	3.89	ul
	X	0105470201	2000-09-11	MOS2	Medium	13.4	4.8	9.9	8.16	ul
	X	0105470501	2001-08-28	MOS1	Medium	6.0	2.5	9.8	9.93	ul
	X	0105470501	2001-08-28	MOS2	Medium	6.8	2.2	9.8	10.93	ul
J1711–3826	C	13621	2012-06-30	ACIS-I	-	49.8	35.3	8.3	0.32	ul
	C	13276	2013-02-11	ACIS-I	-	30.1	23.4	7.5	0.13	ul
J1712–2715	X	0206610101	2004-08-29	PN/EFF	Thin	43.3	9.6	14.1	3.30	ul
	X	0206610101	2004-08-29	MOS1	Thin	47.9	15.5	14.1	1.30	ul
	X	0206610101	2004-08-29	MOS2	Thin	47.8	15.9	14.1	1.26	ul
J1715–3859	C	8976	2008-09-22	ACIS-I	-	1.2	0.9	6.4	3.52	ul
J1716–3720	C	9607	2008-09-20	ACIS-S	-	1.4	0.8	12.8	4.11	ul
J1717–3737	C	2785	2002-05-13	ACIS-S	-	56.5	18.0	15.2	1.15	ul
J1717–4043	C	7536	2007-10-23	HRC-I	-	1.2	1.1	4.8	4.19	ul
J1718–3714	C	2785	2002-05-13	ACIS-S	-	56.5	43.0	11.8	0.37	ul
	C	10768	2009-10-23	ACIS-S	-	37.7	32.5	5.0	0.10	ul
J1718–4539	X	0200680201	2004-09-22	MOS1	Medium	14.0	5.3	14.4	2.73	ul
	X	0200680201	2004-09-22	MOS2	Thick	22.6	9.1	14.4	1.59	ul
J1719–1438	X	0674950201	2012-02-20	PN/FF	Thin	3.3	2.9	1.7	5.99	ul
	X	0674950201	2012-02-20	MOS1	Thin	3.9	3.8	1.7	0.80	ul
	X	0674950201	2012-02-20	MOS2	Thin	3.9	3.5	1.7	0.87	ul
J1720–3659	C	10525	2009-02-08	ACIS-S	-	7.8	4.7	8.8	0.66	ul
J1721–1936	C	9957	2009-07-10	ACIS-S	-	16.0	6.7	2.5	0.46	ul
J1723–3659	X	0103261201	2002-02-24	MOS1	Medium	6.4	2.4	11.7	6.51	ul
	X	0103261201	2002-02-24	MOS2	Medium	6.1	2.7	11.7	3.35	ul
J1725–3546	C	10514	2009-02-06	ACIS-S	-	5.5	3.3	12.9	0.94	ul
	C	8222	2007-10-23	HRC-I	-	1.2	0.9	13.2	14.82	ul
J1726–3530	C	8154	2007-10-26	ACIS-S	-	2.3	1.5	13.3	2.01	ul
	C	10514	2009-02-06	ACIS-S	-	5.5	3.9	5.0	0.75	ul
J1730–2304	X	0650140101	2011-03-29	PN/FF	Thin	9.1	7.8	1.7	-	d
	X	0650140101	2011-03-29	MOS1	Thin	22.6	20.7	1.7	-	d
	X	0650140101	2011-03-29	MOS2	Thin	22.6	21.1	1.7	-	d
J1730–3350	C	9080	2008-10-27	ACIS-I	-	10.1	9.8	0.8	0.31	ul
J1730–3353	C	9080	2008-10-27	ACIS-I	-	10.1	9.0	5.5	0.82	ul
J1731–1847	X	0694710101	2012-08-31	MOS1	Medium	36.5	33.4	1.7	-	d
	X	0694710101	2012-08-31	MOS2	Medium	38.3	37.2	1.7	-	d
	C	13290	2013-02-19	ACIS-I	-	9.8	9.6	0.8	-	d
J1732–3426	X	0405680201	2007-03-21	MOS2	Medium	24.6	7.9	12.1	5.95	ul
J1733–3030	C	8686	2008-05-22	ACIS-I	-	2.2	2.0	14.1	6.54	ul
J1733–3322	X	0553850101	2009-03-09	MOS1	Medium	10.5	1.3	11.5	2.38	ul
	X	0553850101	2009-03-09	MOS2	Medium	10.6	3.8	11.5	8.10	ul
	X	0653320101	2011-03-11	MOS2	Medium	39.7	14.5	11.4	1.69	ul
	C	674	2000-08-02	HRC-I	-	15.1	13.1	6.8	0.70	ul
J1733–3716	C	12683	2011-05-06	ACIS-S	-	2.0	1.3	8.5	2.36	ul
J1735–3258	X	0654190101	2011-03-06	PN/FF	Medium	18.0	11.8	8.1	3.06	ul
	X	0654190101	2011-03-06	MOS1	Medium	21.4	15.4	8.1	1.22	ul
	X	0654190101	2011-03-06	MOS2	Medium	21.3	13.9	8.1	1.39	ul

Continued on next page

Table 1 – continued from previous page

PSR	satellite ^(α)	obsID	date	instrument ^(β)	filter	$t_{\text{on-axis}}$	$t(\theta)$	$\theta^{(γ)}$	count rate ^(δ)	flag ^(δ)
J1736–2843	C	9050	2009-02-06	ACIS-I	-	4.8	3.9	8.1	0.79	ul
	C	9993	2009-02-03	ACIS-I	-	2.2	2.0	4.9	1.56	ul
J1739–2903	X	0304220101	2005-09-29	MOS1	Medium	6.8	3.6	10.5	0.86	ul
	X	0304220101	2005-09-29	MOS2	Medium	6.4	3.6	10.5	0.85	ul
	C	8678	2008-05-18	ACIS-I	-	2.2	1.8	7.1	1.71	ul
	C	8679	2008-05-18	ACIS-I	-	2.2	1.6	7.7	1.80	ul
J1739–3023	X	0554720101	2008-10-01	PN/LW	Medium	32.8	14.7	5.3	5.24	ul
	X	0554720101	2008-10-01	MOS1	Medium	39.3	25.1	5.3	0.96	ul
	X	0561580101	2009-03-11	MOS1	Thin	34.0	24.4	8.1	1.85	ul
	X	0561580101	2009-03-11	MOS2	Thin	33.2	21.7	8.1	1.12	ul
J1739–3049	C	2687	2002-05-07	ACIS-I	-	21.0	14.2	13.9	0.22	ul
J1739–3951	C	12685	2011-02-01	ACIS-S	-	5.1	5.0	0.3	0.62	ul
J1740–3052	X	0301730101	2006-03-05	PN/FF	Thick	55.6	25.2	10.7	1.61	ul
	X	0301730101	2006-03-05	MOS1	Thick	61.3	31.7	10.7	0.84	ul
	X	0301730101	2006-03-05	MOS2	Thick	60.7	32.9	10.7	0.95	ul
	C	11837	2010-07-24	ACIS-I	-	10.0	8.1	7.5	0.38	ul
J1741–2719	C	8667	2008-05-17	ACIS-I	-	2.2	1.7	5.9	1.83	ul
J1741–2733	C	8666	2008-05-18	ACIS-I	-	2.2	0.8	4.9	3.49	ul
J1743–3150	C	13573	2011-11-02	ACIS-I	-	2.0	0.4	9.5	7.90	ul
	C	13576	2011-11-02	ACIS-I	-	2.0	1.8	6.1	1.64	ul
J1743–3153	C	13576	2011-11-02	ACIS-I	-	2.0	1.9	0.9	1.51	ul
J1744–3130	C	8751	2008-05-15	ACIS-I	-	2.2	1.9	3.3	1.52	ul
J1744–3922	X	0304960301	2006-02-28	PN/SW	Medium	3.8	2.6	1.7	11.88	ul
	X	0304960301	2006-02-28	MOS2	Medium	4.5	4.3	1.7	2.69	ul
J1745–3040	X	0103261301	2001-03-21	PN/FF	Medium	4.3	3.8	1.7	3.57	ul
	X	0103261301	2001-03-21	MOS1	Medium	7.3	7.2	1.7	1.69	ul
	X	0103261301	2001-03-21	MOS2	Medium	7.4	6.7	1.7	1.75	ul
J1747–2802	C	1036	2000-10-27	ACIS-S	-	35.5	22.3	9.0	0.53	ul
	C	2274	2001-07-16	ACIS-I	-	10.6	10.0	12.5	0.31	ul
J1748–3009	C	8756	2008-05-13	ACIS-I	-	2.2	1.5	10.0	1.91	ul
	C	8755	2008-05-13	ACIS-I	-	2.2	2.0	13.0	3.20	ul
	C	8744	2008-05-15	ACIS-I	-	2.2	1.9	4.0	1.49	ul
J1749–3002	C	8755	2008-05-13	ACIS-I	-	2.2	1.9	3.6	1.53	ul
J1751–2857	X	0603850201	2010-04-07	MOS1	Medium	18.6	10.0	12.1	2.96	ul
	X	0603850201	2010-04-07	MOS2	Medium	19.1	8.6	12.1	4.01	ul
	C	7562	2008-02-05	ACIS-S	-	4.8	3.0	11.2	4.39	ul
	C	8722	2008-05-13	ACIS-I	-	2.2	2.0	12.9	1.51	ul
	C	8710	2008-05-13	ACIS-I	-	2.2	1.6	1.9	3.07	ul
J1753–1914	C	13803	2012-07-18	ACIS-S	-	3.5	3.4	0.2	0.85	ul
J1754–3443	X	0300690101	2006-04-02	PN/FF	Thick	38.3	19.1	10.1	2.50	ul
	X	0300690101	2006-04-02	MOS1	Thick	42.0	23.8	10.1	1.18	ul
	X	0300690101	2006-04-02	MOS2	Thick	41.8	22.8	10.1	1.18	ul
J1755–2725	C	8717	2008-05-14	ACIS-I	-	2.2	1.5	8.7	2.00	ul
	C	8718	2008-05-14	ACIS-I	-	2.2	1.9	6.1	1.66	ul
J1757–2421	X	0112201501	2002-09-09	PN/FF	Medium	4.2	1.8	3.9	9.20	ul
	X	0112201501	2002-09-09	MOS1	Medium	5.8	5.6	3.9	2.08	ul
	X	0112201501	2002-09-09	MOS2	Medium	5.7	5.1	3.9	3.13	ul
J1759–2205	C	7471	2007-10-23	HRC-I	-	1.2	1.1	6.6	2.89	ul
	C	12506	2011-02-20	HRC-I	-	1.1	1.0	6.6	3.12	ul
J1759–2302	X	0135742301	2003-03-20	PN/FF	Medium	2.9	1.1	3.8	2.73	ul
	X	0135742301	2003-03-20	MOS1	Medium	4.0	3.7	3.8	2.42	ul
	X	0135742301	2003-03-20	MOS2	Medium	4.2	3.9	3.8	0.79	ul
J1759–2307	X	0135742301	2003-03-20	PN/FF	Medium	2.9	1.9	5.7	6.33	ul
	X	0135742301	2003-03-20	MOS1	Medium	4.0	3.2	5.7	0.96	ul

Continued on next page

Table 1 – continued from previous page

PSR	satellite ^(a)	obsID	date	instrument ^(β)	filter	$t_{\text{on-axis}}$	$t(\theta)$	$\theta^{(γ)}$	count rate ^(δ)	flag ^(δ)
J1759–3107	X	0135742301	2003-03-20	MOS2	Medium	4.2	3.0	5.7	1.02	ul
	C	10083	2009-08-05	HRC-I	-	1.2	0.7	14.4	32.44	ul
J1801–2304	X	0135742501	2003-03-20	PN/FF	Medium	2.3	1.8	5.5	11.30	ul
	X	0135742501	2003-03-20	MOS1	Medium	3.3	2.8	5.5	1.09	ul
	X	0135742501	2003-03-20	MOS2	Medium	3.2	2.6	5.5	1.19	ul
J1804–0735	C	8949	2008-10-31	ACIS-S	-	15.2	15.0	0.2	0.37	ul
J1805–1504	X	0405390301	2007-03-03	MOS1	Medium	13.1	7.2	11.5	2.28	ul
	C	7275	2006-03-28	HRC-I	-	1.1	0.9	10.0	4.10	ul
J1806–2125	X	0405750201	2007-03-02	PN/FF	Medium	10.7	4.9	11.3	5.09	ul
	X	0405750201	2007-03-02	MOS1	Medium	14.9	8.5	11.3	3.99	ul
	X	0405750201	2007-03-02	MOS2	Medium	15.4	6.5	11.3	2.49	ul
J1807–0847	C	15979	2014-02-21	ACIS-S	-	3.6	3.5	0.2	0.88	ul
J1808–2701	X	0692210101	2012-09-15	PN/FF	Thin	4.8	4.2	1.7	4.48	ul
	X	0692210101	2012-09-15	MOS1	Medium	16.5	15.1	1.7	1.60	ul
	X	0692210101	2012-09-15	MOS2	Medium	16.7	16.1	1.7	1.93	ul
J1809–1850	X	0152835701	2003-10-09	PN/FF	Medium	7.3	2.3	11.4	10.88	ul
	X	0152835701	2003-10-09	MOS1	Medium	9.2	4.3	11.4	4.79	ul
	X	0152835701	2003-10-09	MOS2	Medium	9.9	5.0	11.4	2.62	ul
J1809–2004	X	0152832901	2003-10-12	PN/FF	Medium	6.3	4.4	7.2	4.78	ul
	X	0152832901	2003-10-12	MOS1	Medium	7.7	6.2	7.2	1.82	ul
	X	0152832901	2003-10-12	MOS2	Medium	8.0	5.6	7.2	1.51	ul
J1810–1820	C	13775	2012-04-22	ACIS-S	-	5.1	5.0	0.2	0.97	ul
J1811–1049	C	9005	2009-02-15	HRC-I	-	1.2	1.0	9.4	7.83	ul
J1811–1835	C	8167	2007-10-26	ACIS-S	-	3.0	1.8	12.7	1.69	ul
	C	8162	2007-05-04	ACIS-S	-	2.8	1.8	8.4	5.49	ul
J1812–1910	X	0152835501	2003-09-12	MOS2	Medium	2.9	1.0	11.6	3.00	ul
J1813+1822	C	15980	2014-02-21	ACIS-S	-	3.3	3.2	0.2	0.90	ul
J1814–1744	X	0207010101	2004-09-14	PN/FF	Medium	0.9	0.7	1.5	38.36	ul
	X	0207010101	2004-09-14	MOS1	Medium	6.0	5.7	1.5	3.60	ul
	X	0207010101	2004-09-14	MOS2	Medium	5.9	5.7	1.5	6.61	ul
J1815–1738	X	0207010101	2004-09-14	PN/FF	Medium	0.9	0.1	10.3	25.56	ul
	X	0207010101	2004-09-14	MOS1	Medium	6.0	2.6	10.3	10.08	ul
	X	0207010101	2004-09-14	MOS2	Medium	5.9	2.5	10.3	6.16	ul
J1816+4510	C	13724	2012-12-09	ACIS-S	-	34.0	33.4	0.2	-	d
J1816–5643	C	13804	2012-04-24	ACIS-S	-	3.5	3.4	0.2	0.91	ul
J1817–3618	C	2011	2001-10-24	ACIS-S	-	29.0	28.6	0.6	0.24	ul
J1818–1448	C	5530	2005-05-23	ACIS-S	-	9.2	6.9	11.9	0.87	ul
	C	6288	2005-05-25	ACIS-S	-	5.0	3.7	11.9	0.82	ul
	C	6289	2005-05-28	ACIS-S	-	15.1	11.4	11.9	1.29	ul
J1818–1519	X	0152834901	2003-04-04	PN/FF	Medium	5.6	2.1	10.2	19.92	ul
	X	0152834901	2003-04-04	MOS1	Medium	7.6	2.8	10.2	4.31	ul
	X	0152834901	2003-04-04	MOS2	Medium	7.2	2.9	10.2	1.06	ul
J1818–1541	X	0152834801	2003-04-06	PN/FF	Medium	5.8	1.7	12.8	13.53	ul
	X	0152834801	2003-04-06	MOS1	Medium	6.8	1.9	12.8	7.97	ul
	X	0152834801	2003-04-06	MOS2	Medium	7.0	1.4	12.8	8.46	ul
J1818–1556	C	7617	2007-10-21	ACIS-S	-	5.1	4.6	6.5	0.67	ul
	C	9609	2008-02-19	ACIS-S	-	1.7	1.2	3.1	2.38	ul
J1819–1008	X	0403410101	2006-09-18	MOS1	Thin	2.6	1.4	12.2	10.90	ul
	X	0403410101	2006-09-18	MOS2	Medium	2.6	1.2	12.2	2.49	ul
	X	0403410101	2006-09-18	MOS1	Thin	44.6	23.2	12.2	1.89	ul
	X	0403410101	2006-09-18	MOS2	Medium	45.9	22.3	12.2	1.26	ul
J1819–1510	X	0505240101	2008-03-31	PN/FF	Medium	52.3	16.0	14.8	3.36	ul
	X	0505240101	2008-03-31	MOS1	Medium	65.7	24.7	14.8	2.23	ul
	X	0505240101	2008-03-31	MOS2	Medium	65.8	21.0	14.8	2.57	ul

Continued on next page

Table 1 – continued from previous page

PSR	satellite ^(α)	obsID	date	instrument ^(β)	filter	$t_{\text{on-axis}}$	$t(\theta)$	$\theta^{(γ)}$	count rate ^(δ)	flag ^(δ)
J1821–1419	X	0004210201	2001-03-08	PN/FF	Medium	3.5	1.5	10.1	8.47	ul
	X	0004210201	2001-03-08	MOS1	Medium	6.4	3.7	10.1	0.83	ul
	X	0004210201	2001-03-08	MOS2	Medium	6.5	3.8	10.1	2.09	ul
J1821–1432	C	11835	2010-08-14	ACIS-I	-	10.0	9.0	3.5	0.34	ul
J1822–1617	C	13511	2011-07-28	HRC-I	-	1.2	0.8	13.7	25.76	ul
J1823–1347	X	0040140201	2002-03-23	PN/FF	Medium	11.8	8.1	6.6	4.87	ul
	X	0040140201	2002-03-23	MOS1	Medium	15.2	12.4	6.6	1.48	ul
	X	0040140201	2002-03-23	MOS2	Medium	15.4	11.7	6.6	1.85	ul
J1824–1159	X	0051940101	2001-03-08	PN/FF	Medium	4.7	1.0	10.1	12.07	ul
	X	0051940101	2001-03-08	MOS1	Medium	7.5	3.4	10.1	3.99	ul
	X	0051940101	2001-03-08	MOS2	Medium	7.6	3.5	10.1	2.57	ul
J1825–0935	X	0112201001	2002-04-08	PN/FF	Medium	1.5	1.3	1.6	-	d
	X	0112201001	2002-04-08	MOS1	Medium	3.8	3.8	1.6	-	d
	X	0112201001	2002-04-08	MOS2	Medium	4.7	4.3	1.6	-	d
J1825–1446	X	0505530101	2008-04-10	PN/FF	Medium	29.0	10.8	11.0	2.80	ul
	X	0505530101	2008-04-10	MOS1	Medium	33.6	13.9	11.0	1.77	ul
	X	0505530101	2008-04-10	MOS2	Medium	33.6	13.7	11.0	1.30	ul
J1826–1131	C	5341	2004-07-11	ACIS-I	-	18.2	15.4	5.9	0.91	ul
	C	4600	2004-07-09	ACIS-I	-	11.2	9.5	5.9	1.60	ul
J1828–1007	X	0051940301	2001-03-10	PN/FF	Medium	5.8	4.7	5.0	4.45	ul
	X	0051940301	2001-03-10	MOS1	Medium	8.5	7.3	5.0	0.42	ul
	X	0051940301	2001-03-10	MOS2	Medium	8.5	6.9	5.0	0.45	ul
J1828–1057	X	0135741201	2001-09-10	PN/FF	Medium	1.2	0.6	7.1	5.04	ul
	X	0135741201	2001-09-10	MOS1	Medium	3.1	2.3	7.1	2.74	ul
	X	0135741201	2001-09-10	MOS2	Medium	3.3	2.5	7.1	3.51	ul
	X	0135745701	2002-09-27	PN/FF	Medium	5.6	3.0	7.3	3.73	ul
	X	0135745701	2002-09-27	MOS1	Medium	7.4	4.6	7.3	0.67	ul
J1828–1101	X	0135745701	2002-09-27	MOS2	Medium	7.4	5.5	7.3	0.56	ul
	X	0104460401	2000-10-12	PN/FF	Medium	3.3	1.3	11.4	2.36	ul
	X	0104460401	2000-10-12	MOS1	Medium	6.6	2.9	11.4	1.06	ul
	X	0104460401	2000-10-12	MOS2	Medium	7.6	3.2	11.4	3.83	ul
	X	0135747001	2003-09-15	PN/FF	Medium	4.1	1.6	11.5	8.64	ul
	X	0135747001	2003-09-15	MOS1	Medium	6.4	2.9	11.5	1.07	ul
J1830–1059	X	0135747001	2003-09-15	MOS2	Medium	6.5	2.7	11.5	1.16	ul
	X	0104460401	2000-10-12	PN/FF	Medium	3.3	2.2	6.8	5.30	ul
	X	0104460401	2000-10-12	MOS1	Medium	6.6	4.2	6.8	2.02	ul
	X	0104460401	2000-10-12	MOS2	Medium	6.7	3.6	6.8	0.86	ul
	X	0135747001	2003-09-15	PN/FF	Medium	4.1	2.3	6.9	9.05	ul
	X	0135747001	2003-09-15	MOS1	Medium	6.4	4.0	6.9	2.11	ul
J1831–0952	X	0135747001	2003-09-15	MOS2	Medium	6.5	3.3	6.9	0.95	ul
	X	0135745901	2002-10-03	MOS1	Medium	8.9	3.0	12.3	1.02	ul
	X	0135745901	2002-10-03	MOS2	Medium	7.6	2.9	12.3	8.33	ul
	X	0135741701	2002-03-29	PN/FF	Medium	3.3	1.5	11.5	14.95	ul
	X	0135741701	2002-03-29	MOS1	Medium	6.8	3.4	11.5	6.72	ul
J1831–1223	X	0135741701	2002-03-29	MOS2	Medium	6.9	3.3	11.5	3.98	ul
	X	0601270501	2010-03-11	PN/FF	Thin	20.7	9.5	9.9	3.24	ul
	X	0601270501	2010-03-11	MOS1	Thin	28.3	4.2	9.9	3.31	ul
	X	0601270501	2010-03-11	MOS2	Thin	28.8	16.2	9.9	2.33	ul
	C	9055	2008-04-27	ACIS-I	-	4.8	3.6	10.3	0.87	ul
J1832+0029	C	9145	2007-10-19	ACIS-S	-	20.1	19.8	0.3	0.20	ul
	C	12556	2011-03-28	ACIS-S	-	23.0	22.7	0.3	0.18	ul
J1832–0836	X	0511010801	2007-10-16	PN/FF	Medium	25.3	4.7	5.0	-	d
	X	0511010801	2007-10-15	MOS1	Medium	28.3	20.7	5.0	-	d
	X	0511010801	2007-10-15	MOS2	Medium	28.7	22.6	5.0	-	d

Continued on next page

Table 1 – continued from previous page

PSR	satellite ^(α)	obsID	date	instrument ^(β)	filter	$t_{\text{on-axis}}$	$t(\theta)$	$\theta^{(\gamma)}$	count rate ^(δ)	flag ^(δ)
J1832–1021	X	0122700401	2000-04-15	PN/FF	Medium	15.4	4.0	10.1	7.89	ul
	X	0122700401	2000-04-15	MOS1	Medium	15.4	5.9	10.1	2.79	ul
	X	0122700401	2000-04-15	MOS2	Medium	15.5	5.7	10.1	2.93	ul
J1833–1055	X	0122700201	2000-04-09	PN/FF	Medium	24.5	8.7	13.8	2.39	ul
J1835–1106	C	9082	2008-10-27	ACIS-I	-	10.1	9.0	0.8	0.34	ul
J1837–0559	C	1986	2001-07-02	ACIS-S	-	9.1	5.4	9.5	0.57	ul
J1837–0604	C	1986	2001-07-02	ACIS-S	-	9.1	8.5	5.1	1.48	ul
J1837–0653	X	0400910301	2006-10-18	MOS2	Medium	8.5	3.3	11.9	2.88	ul
	X	0400910401	2006-10-18	PN/FF	Medium	7.5	3.1	11.6	5.21	ul
	X	0400910401	2006-10-18	MOS1	Medium	8.8	4.1	11.6	0.75	ul
	X	0400910401	2006-10-18	MOS2	Medium	8.8	4.4	11.6	0.70	ul
	X	0552950101	2008-10-16	MOS1	Medium	56.6	26.4	13.7	1.13	ul
	X	0552950101	2008-10-16	MOS2	Medium	58.3	24.5	13.7	1.07	ul
	C	6719	2006-08-19	ACIS-I	-	20.2	16.0	7.1	0.18	ul
	C	7545	2007-05-28	HRC-I	-	1.2	0.9	11.7	13.97	ul
	X	0690010101	2012-09-13	PN/FF	Medium	12.8	5.2	13.1	4.52	ul
	X	0690010101	2012-09-13	MOS1	Medium	23.3	11.0	13.1	2.24	ul
J1838–0537	X	0690010101	2012-09-13	MOS2	Medium	23.8	10.3	13.1	2.36	ul
	C	7493	2008-03-09	ACIS-I	-	19.5	18.8	11.6	0.96	ul
	C	12463	2011-02-20	ACIS-S	-	29.4	10.1	0.3	0.31	ul
	C	9084	2008-08-22	ACIS-I	-	10.1	9.1	0.8	0.54	ul
	C	729	2000-07-23	ACIS-S	-	29.6	20.4	3.2	0.15	ul
	C	6732	2006-07-30	ACIS-S	-	25.2	18.6	3.1	0.17	ul
	C	7552	2008-03-03	ACIS-I	-	19.1	16.7	3.9	0.71	ul
	X	0302970301	2006-04-13	PN/EFF	Medium	22.1	13.0	4.7	7.92	ul
	X	0302970301	2006-04-13	MOS1	Medium	26.1	12.0	4.7	4.46	ul
	X	0302970301	2006-04-13	MOS2	Medium	26.5	14.2	4.7	2.38	ul
J1843–0137	X	0301880501	2006-04-07	PN/FF	Medium	6.6	2.0	9.0	29.44	ul
	X	0301880501	2006-04-07	MOS1	Medium	12.7	5.8	9.0	7.80	ul
	X	0301880501	2006-04-07	MOS2	Medium	14.0	6.6	9.0	5.64	ul
	C	2298	2001-05-20	ACIS-I	-	99.9	74.7	6.5	0.04	ul
	C	949	2000-02-25	ACIS-I	-	41.8	37.7	5.2	0.21	ul
	C	1523	2000-02-24	ACIS-I	-	58.5	54.1	5.1	0.13	ul
	C	8169	2008-02-29	ACIS-S	-	3.2	1.8	13.5	3.78	ul
	C	9114	2008-10-31	HRC-S	-	20.1	19.9	0.3	1.45	ul
	X	0602350101	2010-04-14	MOS2	Medium	50.4	16.8	10.8	2.35	ul
	X	0602350201	2010-04-16	MOS2	Medium	42.0	14.5	10.8	1.49	ul
J1844–0310	C	1964	2002-03-03	HRC-I	-	19.7	14.4	12.0	3.11	ul
	C	3897	2003-09-14	ACIS-S	-	11.9	7.2	13.0	0.43	ul
	C	7583	2007-11-05	ACIS-S	-	5.2	2.5	14.2	1.22	ul
	C	7582	2007-09-18	ACIS-S	-	5.1	2.8	14.1	1.10	ul
	C	7579	2007-04-22	ACIS-S	-	5.0	3.7	10.7	0.83	ul
	C	11801	2010-06-17	ACIS-I	-	30.0	25.0	6.4	0.24	ul
	C	11232	2009-08-11	ACIS-I	-	29.9	25.5	4.4	0.25	ul
	C	3897	2003-09-14	ACIS-S	-	11.9	7.3	13.3	0.42	ul
	C	7582	2007-09-18	ACIS-S	-	5.1	3.7	12.2	0.85	ul
	C	8163	2007-05-24	ACIS-S	-	2.8	2.5	5.6	1.16	ul
J1844–0433	X	0306170401	2006-04-03	PN/FF	Medium	17.2	6.9	5.5	4.16	ul
	X	0306170401	2006-04-03	MOS1	Medium	18.5	11.6	5.5	1.85	ul
	X	0306170401	2006-04-03	MOS2	Medium	19.0	12.4	5.5	1.30	ul
	X	0306170401	2006-04-03	PN/FF	Medium	17.2	8.8	9.8	3.78	ul
	X	0306170401	2006-04-03	MOS1	Medium	18.5	11.3	9.8	1.68	ul
J1845–0434	X	0306170401	2006-04-03	MOS2	Medium	19.0	9.3	9.8	2.14	ul
	C	7505	2008-02-27	ACIS-S	-	5.0	1.7	8.3	2.75	ul

Continued on next page

Table 1 – continued from previous page

PSR	satellite ^(α)	obsID	date	instrument ^(β)	filter	$t_{\text{on-axis}}$	$t(\theta)$	$\theta^{(\gamma)}$	count rate ^(δ)	flag ^(δ)
J1846+0919	C	13793	2012-06-12	ACIS-S	-	15.1	14.9	0.1	0.21	ul
J1846-0257	C	748	2000-10-15	ACIS-S	-	37.8	30.4	3.1	0.17	ul
	C	6686	2006-06-07	ACIS-S	-	55.3	52.9	1.7	0.09	ul
	C	7337	2006-06-05	ACIS-S	-	17.8	17.0	1.7	0.25	ul
	C	7338	2006-06-09	ACIS-S	-	40.1	38.4	1.7	0.08	ul
	C	7339	2006-06-12	ACIS-S	-	45.1	43.1	1.7	0.07	ul
J1847-0130	X	0207010201	2004-10-22	PN/FF	Medium	16.9	14.8	1.7	1.47	ul
J1848-0055	C	2786	2002-08-03	ACIS-S	-	61.6	39.0	9.7	0.23	ul
J1848-0123	C	6587	2006-08-15	ACIS-S	-	46.5	29.9	9.1	0.26	ul
J1848-1952	X	0653300101	2011-03-16	PN/LW	Thin	18.2	16.6	1.8	2.56	ul
	X	0653300101	2011-03-16	MOS1	Thin	36.2	35.6	1.8	1.23	ul
	X	0653300101	2011-03-16	MOS2	Thin	37.5	35.5	1.8	0.77	ul
	X	0554140401	2009-03-15	PN/LW	Thin	11.3	10.2	1.8	12.77	ul
	X	0554140401	2009-03-15	MOS1	Thin	9.7	9.2	1.8	2.96	ul
	X	0554140401	2009-03-15	MOS2	Thin	10.8	9.7	1.8	2.78	ul
J1850-0026	X	0136030101	2003-09-25	MOS1	Medium	17.1	15.5	1.3	1.81	ul
	X	0136030101	2003-09-25	MOS2	Medium	17.2	16.2	1.3	1.19	ul
J1850-0031	X	0136030101	2003-09-25	MOS1	Medium	17.2	9.2	7.0	1.51	ul
	X	0136030101	2003-09-25	MOS2	Medium	17.1	7.5	7.0	1.00	ul
J1852+0008	X	0017740401	2003-10-05	PN/FF	Medium	23.3	6.3	13.5	8.25	ul
	X	0017740501	2003-10-21	PN/FF	Medium	17.9	4.9	13.3	4.26	ul
J1852+0031	X	0204970201	2004-10-18	MOS1	Medium	30.8	17.5	8.2	1.06	ul
	X	0204970201	2004-10-18	MOS2	Medium	30.4	19.8	8.2	0.95	ul
	X	0204970301	2004-10-23	MOS1	Medium	30.6	18.4	8.2	1.40	ul
	X	0204970301	2004-10-23	MOS2	Medium	30.6	18.8	8.2	1.43	ul
	X	0400390201	2006-10-08	MOS2	Medium	28.1	18.5	8.0	1.01	ul
	X	0400390301	2007-03-20	MOS1	Medium	33.1	16.3	9.9	1.23	ul
	X	0400390301	2007-03-20	MOS2	Medium	33.8	15.2	9.9	1.36	ul
	X	0550670201	2008-09-19	MOS2	Medium	21.8	14.3	7.8	1.26	ul
	X	0550670301	2008-09-21	MOS2	Medium	30.7	20.2	7.8	1.03	ul
	X	0550670401	2008-09-23	MOS2	Medium	36.0	23.6	7.8	2.00	ul
	X	0550670501	2008-09-29	MOS2	Medium	33.3	21.9	7.8	1.01	ul
	X	0550670601	2008-10-11	MOS2	Medium	36.0	23.5	8.0	1.51	ul
	X	0550671001	2009-03-16	MOS1	Medium	22.5	10.3	9.9	1.74	ul
	X	0550671001	2009-03-16	MOS2	Medium	24.8	11.3	9.9	1.44	ul
	X	0550670901	2009-03-17	MOS1	Medium	25.5	12.0	9.9	1.52	ul
	X	0550670901	2009-03-17	MOS2	Medium	25.3	11.4	9.9	2.39	ul
	X	0550671201	2009-03-23	MOS1	Medium	17.8	9.0	9.9	2.98	ul
	X	0550671201	2009-03-23	MOS2	Medium	22.4	10.0	9.9	1.88	ul
	X	0550671101	2009-03-25	MOS1	Medium	7.5	3.8	9.8	0.81	ul
	X	0550671101	2009-03-25	MOS2	Medium	8.7	3.9	9.8	0.80	ul
	X	0550671301	2009-04-04	MOS1	Medium	22.2	11.4	9.8	2.47	ul
	X	0550671301	2009-04-04	MOS2	Medium	22.9	10.6	9.8	3.24	ul
	X	0550671901	2009-04-10	MOS1	Medium	16.7	8.6	9.7	1.94	ul
	X	0550671901	2009-04-10	MOS2	Medium	17.5	8.2	9.7	1.75	ul
	X	0550671801	2009-04-22	MOS1	Medium	28.5	14.5	9.6	1.27	ul
	X	0550671801	2009-04-22	MOS2	Medium	28.3	14.0	9.6	1.78	ul
	C	1982	2001-07-31	ACIS-I	-	29.9	23.8	8.3	0.46	ul
J1852-0118	X	0652760201	2010-09-20	PN/FF	Medium	25.0	9.2	12.1	4.37	ul
	X	0652760201	2010-09-20	MOS1	Medium	26.4	11.1	12.1	1.74	ul
	X	0652760201	2010-09-20	MOS2	Medium	26.3	9.4	12.1	1.85	ul
J1852-0127	X	0652760201	2010-09-20	PN/FF	Medium	25.0	17.8	2.8	2.47	ul
	X	0652760201	2010-09-20	MOS1	Medium	26.3	23.5	2.8	1.64	ul
	X	0652760201	2010-09-20	MOS2	Medium	26.4	24.5	2.8	1.03	ul

Continued on next page

Table 1 – continued from previous page

PSR	satellite ^(α)	obsID	date	instrument ^(β)	filter	$t_{\text{on-axis}}$	$t(\theta)$	$\theta^{(γ)}$	count rate ^(δ)	flag ^(δ)
J1853+1303	X	0503190301	2008-04-20	MOS1	Medium	14.8	14.6	1.7	2.00	ul
	X	0503190301	2008-04-20	MOS2	Medium	18.5	17.7	1.7	1.44	ul
J1856+0102	X	0112201101	2003-03-27	PN/FF	Medium	2.4	0.9	13.7	3.59	ul
	X	0112201101	2003-03-27	MOS1	Medium	3.3	1.4	13.7	2.20	ul
J1857+0943	X	0112201101	2003-03-27	MOS2	Medium	3.9	1.5	13.7	2.08	ul
	X	0551060101	2009-04-24	PN/FF	Medium	47.0	15.7	13.7	3.37	ul
J1901+0124	X	0551060101	2009-04-24	MOS1	Medium	67.0	25.3	13.7	1.78	ul
	X	0551060101	2009-04-24	MOS2	Medium	67.3	22.6	13.7	1.16	ul
J1901+0435	X	0742520201	2014-09-27	MOS1	Medium	7.8	7.5	1.7	3.15	ul
	X	0742520201	2014-09-27	MOS2	Medium	7.4	6.7	1.7	1.83	ul
J1901+0510	C	12500	2011-03-07	HRC-I	-	1.1	1.1	3.5	3.83	ul
J1905+0709	X	0742820101	2014-10-10	MOS1	Medium	20.6	8.4	10.1	3.15	ul
	X	0742820101	2014-10-10	MOS2	Medium	20.5	9.4	10.1	2.01	ul
J1906+0746	X	0136030201	2003-09-21	MOS1	Medium	13.8	5.6	12.5	2.26	ul
	X	0136030201	2003-09-21	MOS2	Medium	15.3	5.9	12.5	3.45	ul
J1907+0534	C	8147	2007-07-12	ACIS-S	-	2.2	1.3	11.6	1.85	ul
J1907+0918	C	3793	2003-05-26	ACIS-I	-	13.5	12.1	0.2	0.25	ul
J1908+0734	C	7618	2007-08-10	ACIS-I	-	32.0	28.2	0.8	0.11	ul
	C	14821	2013-07-08	ACIS-I	-	57.1	51.2	1.7	0.09	ul
J1908+0839	C	1954	2001-06-17	ACIS-I	-	30.1	20.8	13.0	1.23	ul
	C	6731	2006-06-04	ACIS-I	-	25.0	18.1	13.0	0.17	ul
J1908+0916	C	7049	2006-06-28	ACIS-I	-	10.1	9.0	15.3	0.34	ul
	C	1954	2001-06-17	ACIS-I	-	30.1	27.1	2.4	0.11	ul
J1911+1758	C	3449	2002-03-11	ACIS-S	-	2.7	2.6	2.3	1.11	ul
	C	6731	2006-06-04	ACIS-I	-	25.0	14.4	2.4	0.22	ul
J1911+1114	C	9614	2008-02-28	ACIS-S	-	1.5	0.5	11.5	7.74	ul
J1913+0446	C	8223	2007-06-26	ACIS-S	-	3.5	2.2	7.7	1.43	ul
	C	3481	2002-04-15	ACIS-S	-	1.1	0.7	9.2	4.17	ul
J1913+1011	C	15981	2014-03-16	ACIS-S	-	3.6	3.5	0.2	0.88	ul
	X	0406620201	2007-04-27	MOS1	Medium	52.5	51.5	1.8	-	d
J1921+2153	X	0406620201	2007-04-27	MOS2	Medium	51.7	48.7	1.8	-	d
	X	0075140401	2004-09-30	PN/FF	Medium	29.7	13.2	10.4	3.10	ul
J1926-1314	X	0075140401	2004-09-30	MOS1	Medium	31.8	13.5	10.4	1.79	ul
	X	0075140401	2004-09-30	MOS2	Medium	31.6	17.0	10.4	2.20	ul
J1928+1746	C	3854	2003-07-15	ACIS-S	-	19.8	18.1	0.6	0.33	ul
J1933+2421	X	0670940101	2012-03-20	PN/FF	Thin	4.1	3.6	1.7	7.03	ul
	X	0670940101	2012-03-20	MOS1	Thin	8.2	7.5	1.7	2.10	ul
J1946+3417	X	0670940101	2012-03-20	MOS2	Thin	8.6	8.3	1.7	1.50	ul
	C	15364	2012-12-14	ACIS-I	-	9.8	9.0	0.7	0.55	ul
J1954+2836	X	0742620101	2014-09-29	MOS1	Thin	69.5	63.9	1.7	0.42	ul
	X	0742620101	2014-09-29	MOS2	Thin	71.4	67.9	1.7	0.43	ul
J1954+2923	C	9081	2008-03-01	ACIS-I	-	10.0	9.0	0.8	0.34	ul
J1955+3547	C	7335	2006-07-20	ACIS-S	-	9.4	9.2	0.1	0.53	ul
	C	9115	2007-12-09	HRC-S	-	20.2	19.9	0.3	1.68	ul
J2007+2722	X	0304200301	2006-04-21	PN/LW	Medium	8.7	3.4	10.7	6.04	ul
	X	0304200301	2006-04-21	MOS1	Medium	14.4	5.9	10.7	2.89	ul
J2007+2722	X	0304200301	2006-04-21	MOS2	Medium	14.7	5.8	10.7	4.56	ul
	C	12148	2011-12-26	ACIS-I	-	10.0	0.6	0.9	5.32	ul
J2007+2722	C	12684	2010-12-22	ACIS-S	-	5.1	5.0	0.3	0.62	ul
J2007+2722	X	0556260301	2009-04-16	PN/FF	Medium	43.5	21.2	7.1	2.05	ul
	X	0556260301	2009-04-16	MOS1	Medium	50.0	25.3	7.1	1.03	ul
J2007+2722	X	0556260301	2009-04-16	MOS2	Medium	51.0	28.2	7.1	1.56	ul
	C	6438	2006-12-10	ACIS-I	-	22.9	17.8	5.8	0.17	ul
J2007+2722	C	7254	2006-01-07	ACIS-I	-	21.1	17.9	5.9	0.17	ul

Continued on next page

Table 1 – continued from previous page

PSR	satellite ^(α)	obsID	date	instrument ^(β)	filter	$t_{\text{on-axis}}$	$t(\theta)$	$\theta^{(γ)}$	count rate ^(δ)	flag ^(δ)
	C	8492	2007-01-29	ACIS-I	-	51.1	47.6	6.0	0.06	ul
J2017+0603	C	12537	2011-07-30	ACIS-S	-	10.0	9.9	0.3	-	d
J2043+1711	C	15366	2012-12-18	ACIS-I	-	10.1	9.3	0.7	1.83	ul
J2048+2255	C	15982	2014-01-02	ACIS-S	-	3.3	3.2	0.2	0.90	ul
J2129-5721	X	0406620401	2007-04-19	MOS1	Medium	55.4	54.4	1.7	1.60	ul
	X	0406620401	2007-04-19	MOS2	Medium	55.6	53.6	1.7	0.72	ul
J2144-3933	X	0604550101	2009-10-24	PN/FF	Thin	18.0	15.4	1.7	3.22	ul
	X	0604550101	2009-10-23	MOS1	Thin	28.1	27.6	1.7	0.89	ul
	X	0604550101	2009-10-23	MOS2	Thin	28.0	27.0	1.7	0.91	ul
J2156+2618	C	15983	2013-12-31	ACIS-S	-	3.6	3.5	0.2	0.83	ul
J2222+2923	C	15984	2014-01-15	ACIS-S	-	3.6	3.5	0.2	0.89	ul
J2222-0137	C	12237	2010-09-26	ACIS-S	-	30.0	27.2	0.3	-	d
J2235+1506	C	13798	2011-12-30	ACIS-S	-	3.5	3.4	0.2	0.91	ul
J2238+5903	C	13286	2012-04-21	ACIS-I	-	10.0	8.8	4.1	5.32	ul
J2307+2225	C	15985	2014-05-19	ACIS-S	-	3.3	3.2	0.2	0.96	ul

Notes. ^(α) C:Chandra X:XMM-Newton; ^(β) in the case of XMM-Newton EPIC-PN observations the used observation mode is added (EFF: Extended Full Frame; FF: Full Frame; LW: Large Window; SW: Small Window) ^(γ) off-axis angle; ^(δ) If flagged with *ul* than 2σ upper limit on count rate, otherwise see text.

6.43873E-07,-1.10052e-07,1.29864e-07

Table 5:: Pulsar parameters, flux upper limits and X-ray efficiency upper limits for pulsars for which no X-ray counterpart was detected in the XMM-Newton and Chandra archival data by June 1st 2016.

PSR	DM pc cm ⁻³	P ms	log(Age) yrs	log(\dot{E}) erg s ⁻¹	$N_{\text{H}}/N_{\text{H}}^{\text{LAB}}$ 10^{21} cm^{-2}	d kpc	$f_{0.1-2 \text{ keV}}^{\text{PL}}$ erg s ⁻¹ cm ⁻²	$\log(L_{0.1-2 \text{ keV}}^{\text{PL}})$ erg s ⁻¹	$\mu_{0.1-2 \text{ keV}}^{\text{PL}}$	$\log(T_{\infty})$ K
J0051+0423	13.9	354	8.9	30.8	0.4/7.5	0.6 [2]	4.6×10^{-15}	29.6	$< 6.6 \times 10^{-2}$	5.61
J0134-2937	21.806	136	7.4	33.1	0.7/5.0	0.6 [2]	4.0×10^{-15}	29.5	$< 2.5 \times 10^{-4}$	5.51
J0137+1654	26.6	414	8.7	30.8	0.8/0.5	1.2 [2]	4.8×10^{-15}	30.2	$< 2.5 \times 10^{-1}$	5.70
J0139+5814	73.779	272	5.6	34.3	2.3/0.5	2.6 [1]	7.8×10^{-15}	30.9	$< 3.8 \times 10^{-4}$	5.85
J0157+6212	30.21	2351	5.3	32.8	0.9/8.2	1.7 [2]	5.3×10^{-15}	30.6	$< 6.4 \times 10^{-3}$	5.74
J0248+6021	370	217	4.8	35.3	11.4/7.5	23.2 [3]	2.0×10^{-14}	33.5	$< 1.4 \times 10^{-2}$	6.29
J0335+4555	47.153	269	8.8	31.2	1.5/4.2	1.6 [2]	6.2×10^{-15}	30.7	$< 3.4 \times 10^{-1}$	5.85
J0520-2553	33.77	241	8.1	31.9	1.0/4.4	1.7 [2]	5.3×10^{-15}	30.6	$< 4.5 \times 10^{-2}$	5.81
J0609+2130	38.73	55	9.6	31.7	1.2/7.1	1.2 [2]	4.1×10^{-15}	30.3	$< 3.4 \times 10^{-2}$	5.79
J0622+3749	-	333	5.3	34.4	-/2.2	-	1.4×10^{-14}	-	-	-
J0636+5129	11.11	2	10.1	33.8	0.3/0.9	0.6 [3]	2.4×10^{-14}	30.4	$< 4.2 \times 10^{-4}$	5.65
J0645+5158	18.25	8	10.5	32.4	0.6/0.8	5.1 [3]	3.8×10^{-15}	31.4	$< 9.6 \times 10^{-2}$	5.83
J0656-5449	67.5	183	8.0	32.3	2.1/10.2	3.9 [2]	6.4×10^{-15}	31.2	$< 8.2 \times 10^{-2}$	5.92
J0742-2822	73.782	166	5.2	35.2	2.3/7.6	2.0 [1]	1.7×10^{-14}	31.3	$< 1.2 \times 10^{-4}$	5.89
J0828-3417	52.2	1848	7.5	30.8	1.6/8.5	0.5 [2]	2.3×10^{-15}	29.1	$< 1.9 \times 10^{-2}$	5.63
J0847-4316	292.5	5977	5.9	31.3	9.0/11.7	5.1 [2]	5.3×10^{-15}	31.4	< 1.1	5.97
J0907-5157	103.72	253	6.3	33.6	3.2/8.0	0.9 [2]	2.0×10^{-14}	30.5	$< 6.5 \times 10^{-4}$	5.84
J0940-5428	134.5	87	4.6	36.3	4.2/8.9	3.0 [2]	2.9×10^{-15}	30.6	$< 2.2 \times 10^{-6}$	5.86
J0943+1631	20.32	1087	8.3	30.4	0.6/9.8	0.8 [2]	8.2×10^{-15}	30.1	$< 4.5 \times 10^{-1}$	5.68
J1001-5939	113	7733	6.3	30.7	3.5/0.7	2.8 [2]	2.2×10^{-15}	30.5	$< 5.7 \times 10^{-1}$	5.87
J1038+0032	26.59	28	9.8	32.0	0.8/10.2	1.2 [2]	5.5×10^{-15}	30.3	$< 1.6 \times 10^{-2}$	5.77
J1055-6022	590	947	5.2	33.6	18.2/1.2	12.5 [2]	1.3×10^{-14}	32.5	$< 7.9 \times 10^{-2}$	6.15
J1055-6028	635.9	99	4.7	36.1	19.6/2.4	15.5 [2]	6.9×10^{-15}	32.5	$< 2.4 \times 10^{-4}$	6.04

Continued on next page

Table 5 – continued from previous page

PSR	DM	P	log(Age)	log(\dot{E})	$N_{\text{H}}/N_{\text{H}}^{\text{LAB}}$	d	$f_{0.1-2 \text{ keV}}^{\text{PL}}$	$\log(L_{0.1-2 \text{ keV}}^{\text{PL}})$	$\mu_{0.1-2 \text{ keV}}^{\text{PL}}$	$\log(T_{\infty})$
J1103–5403	103.915	3	10.2	33.6	3.2/12.3	2.5 [2]	7.2×10^{-15}	30.9	$< 2.2 \times 10^{-3}$	5.91
J1104–6103	78.506	280	6.4	33.5	2.4/0.8	1.9 [2]	5.5×10^{-15}	30.5	$< 1.0 \times 10^{-3}$	5.81
J1105–6107	271.01	63	4.8	36.4	8.4/3.7	5.0 [2]	3.5×10^{-15}	31.2	$< 6.0 \times 10^{-6}$	5.75
J1107–5907	40.2	252	8.6	31.3	1.2/1.1	1.3 [2]	1.1×10^{-14}	30.5	$< 1.4 \times 10^{-1}$	5.79
J1115+5030	9.195	1656	7.0	31.3	0.3/3.6	0.4 [2]	8.5×10^{-16}	28.7	$< 2.4 \times 10^{-3}$	5.48
J1157–6224	325.2	400	6.2	33.4	10.0/0.9	4.0 [1]	1.3×10^{-14}	31.8	$< 2.4 \times 10^{-2}$	6.01
J1159–7910	59.24	525	6.5	32.9	1.8/11.5	1.9 [2]	3.2×10^{-14}	31.3	$< 2.6 \times 10^{-2}$	5.88
J1225–6408	415.1	419	6.8	32.7	12.8/12.2	10.4 [2]	1.7×10^{-14}	32.5	$< 6.2 \times 10^{-1}$	6.19
J1253–5820	100.584	255	6.3	33.7	3.1/0.12	2.2 [2]	8.9×10^{-15}	30.9	$< 1.4 \times 10^{-3}$	5.68
J1300+1240	10.16550	6	8.9	34.3	0.3/0.9	0.6 [1]	8.7×10^{-16}	28.8	$< 3.5 \times 10^{-6}$	5.49
J1302–6313	500	967	6.4	32.4	15.4/17.4	8.9 [2]	3.7×10^{-15}	31.7	$< 1.8 \times 10^{-1}$	5.90
J1303–6305	343	2306	7.2	30.8	10.6/3.5	6.2 [2]	1.3×10^{-14}	31.9	$< 1.2 \times 10^{+1}$	6.12
J1305–6256	967	478	6.6	32.9	29.8/18.3	11.9 [2]	7.6×10^{-14}	33.3	< 2.4	6.08
J1306–6242	480	981	6.4	32.4	14.8/8.4	8.2 [2]	7.2×10^{-15}	31.9	$< 3.4 \times 10^{-1}$	5.85
J1309–6526	340	398	8.5	31.1	10.5/0.2	7.6 [2]	3.2×10^{-15}	31.5	< 2.7	5.95
J1317–5759	145.3	2642	6.5	31.4	4.5/18.5	3.1 [2]	8.6×10^{-15}	31.2	$< 5.3 \times 10^{-1}$	5.95
J1317–6302	678.1	261	7.6	32.4	20.9/16.6	12.1 [2]	1.5×10^{-14}	32.6	< 1.7	6.19
J1320–3512	16.42	458	9.6	29.9	0.5/2.9	0.7 [2]	5.2×10^{-15}	29.6	$< 5.3 \times 10^{-1}$	5.64
J1322–6329	659	2764	6.6	31.3	20.3/3.3	12.4 [2]	3.7×10^{-15}	32.0	< 4.8	6.03
J1324–6302	497	2483	7.6	30.4	15.3/15.6	8.2 [2]	1.5×10^{-14}	32.2	$< 7.0 \times 10^{+1}$	6.04
J1333–4449	44.3	345	10.0	29.7	1.4/1.9	1.4 [2]	4.3×10^{-15}	30.1	< 2.7	5.59
J1334–5839	119.2978	107	7.9	32.8	3.7/15.2	2.4 [2]	7.1×10^{-15}	30.9	$< 1.0 \times 10^{-2}$	5.95
J1339–4712	39.9	137	9.6	30.9	1.2/14.2	1.2 [2]	5.4×10^{-15}	30.1	$< 1.7 \times 10^{-1}$	5.75
J1355–5925	354.8	1213	6.5	32.1	10.9/17.2	7.3 [2]	1.0×10^{-14}	32.0	$< 7.2 \times 10^{-1}$	5.93
J1355–6206	547	276	9.2	30.8	16.9/11.8	8.3 [2]	4.4×10^{-15}	31.7	< 9.0	5.87
J1359–6038	293.71	127	5.5	35.1	9.1/7.8	5.0 [1]	3.7×10^{-14}	32.3	$< 1.8 \times 10^{-3}$	6.16
J1406–6121	542.3	213	4.8	35.3	16.7/5.4	8.1 [2]	3.1×10^{-14}	32.5	$< 1.6 \times 10^{-3}$	6.13
J1410–7404	54.24	278	8.8	31.1	1.7/14.3	1.5 [2]	5.4×10^{-15}	30.3	$< 1.8 \times 10^{-1}$	5.83
J1412–6145	514.7	315	4.7	35.1	15.9/1.9	7.8 [2]	9.5×10^{-15}	32.0	$< 8.0 \times 10^{-4}$	6.18
J1413–6141	677	285	4.1	35.8	20.9/12.8	10.1 [2]	1.0×10^{-14}	32.3	$< 3.2 \times 10^{-4}$	6.10
J1425–5723	43.4	353	8.4	31.3	1.3/7.2	1.2 [2]	4.3×10^{-15}	30.0	$< 5.1 \times 10^{-2}$	5.77
J1432–5032	113	2034	6.7	31.4	3.5/2.4	2.8 [2]	7.3×10^{-15}	31.0	$< 3.4 \times 10^{-1}$	5.91
J1444–5941	177.1	2760	6.7	31.2	5.5/1.2	3.3 [2]	3.8×10^{-14}	31.8	< 4.5	6.07
J1453–6413	71.07	179	6.0	34.3	2.2/15.6	2.8 [1]	1.0×10^{-14}	31.3	$< 1.1 \times 10^{-3}$	5.90
J1457–5900	175	1498	6.8	31.6	5.4/10.5	3.2 [2]	2.3×10^{-15}	30.6	$< 9.6 \times 10^{-2}$	5.86
J1457–5902	477.2	390	5.7	33.9	14.7/2.7	6.8 [2]	1.6×10^{-15}	31.1	$< 1.5 \times 10^{-3}$	5.77
J1507–6640	129.8	355	6.7	33.0	4.0/8.3	3.6 [2]	1.0×10^{-14}	31.3	$< 2.2 \times 10^{-2}$	5.90
J1511–5835	332	301	7.1	32.7	10.2/1.1	5.0 [2]	2.6×10^{-15}	31.0	$< 2.2 \times 10^{-2}$	5.81
J1514–5925	194.1	148	5.9	34.5	6.0/7.3	3.5 [2]	4.5×10^{-14}	32.0	$< 2.7 \times 10^{-3}$	6.06
J1517–4636	127.0	886	6.8	32.1	3.9/17.9	3.2 [2]	4.0×10^{-14}	32.4	< 1.9	6.09
J1524–5706	833	1116	4.7	34.0	25.7/1.0	11.4 [2]	1.4×10^{-15}	31.5	$< 3.1 \times 10^{-3}$	5.99
J1529–5611	149	822	6.5	32.5	4.6/4.5	2.7 [2]	1.1×10^{-14}	31.2	$< 4.9 \times 10^{-2}$	6.00
J1535–4114	66.28	432	6.2	33.3	2.0/1.4	2.0 [2]	3.5×10^{-15}	30.9	$< 4.0 \times 10^{-3}$	5.86
J1538–5551	603	104	5.7	35.0	18.6/20.2	7.5 [2]	1.9×10^{-14}	32.8	$< 5.7 \times 10^{-3}$	6.08
J1542–5034	91.0	599	6.4	32.9	2.8/19.7	3.2 [2]	1.7×10^{-14}	32.0	$< 1.4 \times 10^{-1}$	6.06
J1548–4821	126.0	145	9.5	31.0	3.9/1.6	4.4 [2]	8.2×10^{-15}	32.0	< 8.9	6.05
J1549+2113	24.8	1262	7.4	31.2	0.8/12.0	2.1 [2]	7.8×10^{-15}	30.9	$< 4.8 \times 10^{-1}$	5.76
J1549–4848	55.983	288	5.5	34.4	1.7/1.4	2.7 [2]	2.5×10^{-15}	31.0	$< 4.4 \times 10^{-4}$	5.84
J1553–5456	210	1081	6.0	32.7	6.5/2.7	3.8 [2]	1.2×10^{-15}	31.0	$< 2.1 \times 10^{-2}$	6.02
J1554–5512	450	3418	6.2	31.5	13.9/17.2	6.4 [2]	1.1×10^{-15}	31.4	$< 8.7 \times 10^{-1}$	6.10
J1555–2341	51.901	532	7.1	32.3	1.6/6.2	1.9 [2]	4.6×10^{-15}	30.5	$< 1.7 \times 10^{-2}$	5.77
J1604–4909	140.8	327	6.7	33.1	4.3/7.3	5.1 [2]	8.5×10^{-15}	32.1	$< 1.1 \times 10^{-1}$	6.05
J1607–6449	89.39	298	8.3	31.6	2.8/1.5	2.1 [2]	1.2×10^{-14}	31.0	$< 2.5 \times 10^{-1}$	5.87
J1611–5847	79.9	354	9.4	30.3	2.5/15.7	1.7 [2]	6.1×10^{-15}	31.0	< 5.7	5.88

Continued on next page

Table 5 – continued from previous page

PSR	DM	P	log(Age)	log(\dot{E})	$N_{\text{H}}/N_{\text{H}}^{\text{LAB}}$	d	$f_{0.1-2 \text{ keV}}^{\text{PL}}$	$\log(L_{0.1-2 \text{ keV}}^{\text{PL}})$	$\mu_{0.1-2 \text{ keV}}^{\text{PL}}$	$\log(T_{\infty})$
J1613–5211	360.1	457	5.6	33.9	11.1/5.5	6.4 [2]	8.5×10^{-15}	32.3	$< 2.6 \times 10^{-2}$	6.10
J1614–5144	748	1534	6.5	31.9	23.1/0.4	9.9 [2]	1.3×10^{-14}	32.9	< 8.8	6.21
J1616–5109	1160	1219	6.0	32.6	35.8/0.2	15.2 [2]	2.5×10^{-14}	33.5	< 8.2	6.35
J1616–5208	488	1025	5.7	33.0	15.1/0.2	7.8 [2]	1.4×10^{-14}	32.7	$< 4.7 \times 10^{-1}$	6.23
J1620–4927	-	171	5.4	34.9	-/16.9	-	1.7×10^{-14}	-	-	-
J1621–5039	261	1084	6.1	32.6	8.1/18.2	4.6 [2]	6.3×10^{-16}	30.9	$< 1.9 \times 10^{-2}$	5.93
J1622–4944	755	1072	6.0	32.7	23.3/10.0	8.2 [2]	4.0×10^{-15}	32.2	$< 2.9 \times 10^{-1}$	6.19
J1623–4949	183.3	725	5.4	33.6	5.7/18.3	3.6 [2]	1.6×10^{-14}	32.1	$< 2.7 \times 10^{-2}$	5.97
J1625–4904	684.8	460	5.6	33.8	21.1/14.2	7.4 [2]	2.9×10^{-14}	33.0	$< 1.3 \times 10^{-1}$	6.05
J1625–4913	720	355	5.9	33.8	22.2/12.4	7.7 [2]	4.4×10^{-14}	33.2	$< 2.6 \times 10^{-1}$	6.28
J1627–4845	557.8	612	6.4	32.8	17.2/4.8	6.2 [2]	5.6×10^{-15}	32.1	$< 2.0 \times 10^{-1}$	6.07
J1627–5936	99.3	354	8.8	30.9	3.1/12.2	2.2 [2]	5.9×10^{-15}	31.2	< 2.3	5.97
J1632–4757	578	228	5.4	34.7	17.8/1.5	6.3 [2]	8.0×10^{-15}	31.7	$< 1.1 \times 10^{-3}$	6.14
J1633–4805	1120	710	5.2	33.9	34.6/1.7	10.7 [2]	4.7×10^{-15}	32.0	$< 1.1 \times 10^{-2}$	6.15
J1636–4803	503	1204	6.0	32.7	15.5/7.0	5.8 [2]	1.3×10^{-13}	32.9	< 1.6	6.15
J1637–4553	193.23	118	5.8	34.9	6.0/1.9	3.2 [2]	3.5×10^{-14}	31.8	$< 8.1 \times 10^{-4}$	6.05
J1637–4642	417.0	154	4.6	35.8	12.9/1.9	5.1 [2]	1.5×10^{-14}	31.8	$< 1.0 \times 10^{-4}$	6.08
J1637–4721	448	1165	6.6	32.0	13.8/1.9	5.3 [2]	2.8×10^{-15}	31.1	$< 1.2 \times 10^{-1}$	5.84
J1638–4725	552.1	763	6.4	32.6	17.0/14.5	6.1 [2]	2.9×10^{-15}	31.3	$< 4.4 \times 10^{-2}$	6.11
J1640–4648	474	178	6.5	33.7	14.6/2.0	5.5 [2]	1.1×10^{-14}	31.8	$< 1.0 \times 10^{-2}$	6.14
J1643–1224	62.4121	4	9.6	33.9	1.9/10.4	0.4 [1]	3.1×10^{-14}	30.0	$< 1.3 \times 10^{-4}$	5.74
J1646–4346	490.4	231	4.5	35.6	15.1/4.4	5.8 [2]	1.3×10^{-13}	32.9	$< 2.1 \times 10^{-3}$	6.19
J1648–4458	925	629	6.7	32.5	28.5/10.6	9.3 [2]	4.6×10^{-14}	32.8	< 2.3	6.26
J1648–4611	392.9	164	5.0	35.3	12.1/6.8	5.0 [2]	4.0×10^{-15}	31.2	$< 8.1 \times 10^{-5}$	5.99
J1649–4349	398.6	870	8.5	30.4	12.3/10.5	5.0 [2]	1.6×10^{-14}	31.8	$< 2.7 \times 10^{+1}$	5.95
J1650–4341	673	309	8.5	31.3	20.8/0.5	7.5 [2]	7.6×10^{-15}	31.9	< 3.3	6.15
J1652–4406	786	7707	7.1	29.9	24.3/10.2	8.4 [2]	6.4×10^{-14}	32.9	$< 9.5 \times 10^{+2}$	6.27
J1653–4315	337	419	8.6	30.9	10.4/10.6	4.6 [2]	1.0×10^{-14}	31.6	< 4.5	6.09
J1654–4140	307	1273	8.2	30.4	9.5/12.9	4.3 [2]	4.6×10^{-15}	31.2	< 5.9	6.04
J1702–4217	629	227	8.5	31.6	19.4/13.4	7.1 [2]	4.4×10^{-15}	31.6	$< 9.9 \times 10^{-1}$	5.97
J1702–4306	537	215	5.5	34.6	16.6/8.0	6.7 [2]	3.2×10^{-15}	31.4	$< 6.2 \times 10^{-4}$	5.98
J1702–4310	377	240	4.2	35.8	11.6/7.8	5.2 [2]	6.3×10^{-15}	31.5	$< 4.5 \times 10^{-5}$	6.09
J1703–4851	150.29	1396	6.6	31.9	4.6/3.5	3.0 [2]	5.7×10^{-15}	30.9	$< 1.2 \times 10^{-4}$	5.93
J1705–1906	22.907	298	6.1	33.8	0.7/1.0	0.9 [2]	1.4×10^{-14}	30.3	$< 3.1 \times 10^{-4}$	5.69
J1705–4108	1077	861	5.6	33.3	33.2/4.3	11.4 [2]	4.0×10^{-15}	32.0	$< 4.2 \times 10^{-2}$	5.91
J1706–4310	656.1	616	6.2	33.0	20.2/1.9	10.0 [2]	1.8×10^{-13}	33.5	< 2.9	6.27
J1707–4053	360.0	581	6.7	32.6	11.1/12.2	4.0 [1]	6.9×10^{-15}	31.5	$< 7.7 \times 10^{-2}$	6.02
J1709–3626	393.6	447	6.5	33.0	12.1/1.0	5.9 [2]	5.1×10^{-13}	33.5	< 3.1	6.29
J1709–4401	225.8	865	6.3	32.7	7.0/1.4	4.4 [2]	4.8×10^{-14}	32.2	$< 3.5 \times 10^{-1}$	6.08
J1711–3826	376	465	6.0	33.5	11.6/6.6	4.7 [2]	3.0×10^{-15}	31.1	$< 3.9 \times 10^{-3}$	6.00
J1712–2715	92.64	255	6.5	33.5	2.9/11.5	2.1 [2]	7.1×10^{-15}	30.7	$< 1.7 \times 10^{-3}$	5.85
J1715–3859	817	928	6.5	32.3	25.2/8.6	9.5 [2]	8.0×10^{-14}	33.1	< 5.7	6.29
J1716–3720	682.7	630	5.7	33.5	21.1/11.7	7.9 [2]	3.0×10^{-14}	32.5	$< 1.1 \times 10^{-1}$	6.09
J1717–3737	525.8	682	6.3	32.8	16.2/0.8	5.7 [2]	8.1×10^{-15}	31.7	$< 7.0 \times 10^{-2}$	5.96
J1717–4043	452.6	397	5.7	33.9	14.0/12.3	6.3 [2]	1.3×10^{-13}	33.0	$< 1.2 \times 10^{-1}$	6.13
J1718–3714	833	1289	5.9	32.7	25.7/2.0	9.9 [2]	2.0×10^{-15}	31.5	$< 7.1 \times 10^{-2}$	5.97
J1718–4539	254	590	6.1	33.2	7.8/2.8	6.4 [2]	2.5×10^{-14}	32.2	$< 1.2 \times 10^{-1}$	6.14
J1719–1438	36.766	5	10.1	33.2	1.1/6.0	1.2 [2]	7.5×10^{-15}	30.3	$< 1.2 \times 10^{-3}$	5.72
J1720–3659	381.6	351	8.2	31.5	11.8/2.2	4.6 [2]	4.7×10^{-15}	31.2	$< 5.7 \times 10^{-1}$	5.92
J1721–1936	75.7	1004	7.0	31.8	2.3/3.9	1.9 [2]	3.7×10^{-15}	30.4	$< 3.7 \times 10^{-2}$	5.85
J1723–3659	254.2	202	5.6	34.6	7.8/1.4	3.5 [2]	4.9×10^{-14}	32.0	$< 2.8 \times 10^{-3}$	6.04
J1725–3546	744	1032	6.0	32.7	23.0/2.8	8.7 [2]	6.6×10^{-14}	32.9	< 1.6	6.24
J1726–3530	727	1110	4.2	34.5	22.4/5.5	8.4 [2]	9.3×10^{-15}	32.1	$< 3.3 \times 10^{-3}$	6.15
J1730–3350	259	139	4.4	36.1	8.0/3.3	3.5 [2]	5.5×10^{-15}	31.1	$< 9.7 \times 10^{-6}$	6.04

Continued on next page

Table 5 – continued from previous page

PSR	DM	P	log(Age)	log(\dot{E})	$N_{\text{H}}/N_{\text{H}}^{\text{LAB}}$	d	$f_{0.1-2 \text{ keV}}^{\text{PL}}$	$\log(L_{0.1-2 \text{ keV}}^{\text{PL}})$	$\mu_{0.1-2 \text{ keV}}^{\text{PL}}$	$\log(T_{\infty})$
J1730–3353	256	3270	6.4	31.4	7.9/3.3	3.5 [2]	1.3×10^{-14}	31.4	< 1.1	6.05
J1732–3426	513.5	332	7.1	32.6	15.8/6.2	5.8 [2]	4.9×10^{-14}	32.4	$< 6.5 \times 10^{-1}$	6.03
J1733–3030	636	362	6.5	33.1	19.6/6.2	9.5 [2]	6.8×10^{-14}	33.0	$< 7.8 \times 10^{-1}$	6.17
J1733–3322	524.0	1245	6.7	31.9	16.2/6.2	5.8 [2]	2.8×10^{-14}	32.2	< 1.9	6.16
J1733–3716	153.5	337	5.6	34.2	4.7/6.2	2.8 [2]	2.5×10^{-14}	31.5	$< 2.1 \times 10^{-3}$	6.02
J1735–3258	754	350	5.3	34.4	23.3/6.2	9.6 [2]	1.3×10^{-14}	32.3	$< 8.5 \times 10^{-3}$	6.17
J1736–2843	331	6445	6.5	30.6	10.2/6.2	4.9 [2]	3.0×10^{-14}	32.1	$< 2.7 \times 10^{+1}$	6.15
J1739–2903	138.56	322	5.8	34.0	4.3/8.6	2.5 [2]	1.4×10^{-14}	31.2	$< 1.5 \times 10^{-3}$	5.93
J1739–3023	170.0	114	5.2	35.5	5.2/9.3	2.9 [2]	1.2×10^{-14}	31.2	$< 5.7 \times 10^{-5}$	5.97
J1739–3049	573.2	239	6.2	33.8	17.7/5.4	6.4 [2]	3.3×10^{-15}	31.4	$< 3.7 \times 10^{-3}$	6.05
J1739–3951	24.6	341	8.4	31.3	0.8/2.6	0.8 [2]	3.8×10^{-15}	29.6	$< 2.0 \times 10^{-2}$	5.68
J1740–3052	738.78	570	5.5	33.7	22.8/3.5	9.5 [2]	3.9×10^{-15}	31.8	$< 1.1 \times 10^{-2}$	5.97
J1741–2719	361.9	346	7.8	31.9	11.2/4.0	5.2 [2]	2.2×10^{-14}	32.0	< 1.3	6.08
J1741–2733	149.2	892	8.0	30.9	4.6/5.8	2.7 [2]	4.8×10^{-14}	31.8	< 7.3	6.07
J1743–3150	193.05	2414	5.5	32.5	6.0/4.8	3.3 [2]	1.6×10^{-14}	31.5	$< 8.8 \times 10^{-2}$	6.01
J1743–3153	505.7	193	5.5	34.8	15.6/11.9	6.6 [2]	1.4×10^{-14}	32.0	$< 1.8 \times 10^{-3}$	6.04
J1744–3130	192.9	1066	5.9	32.8	6.0/0.7	3.3 [2]	2.2×10^{-14}	31.6	$< 6.1 \times 10^{-2}$	6.06
J1744–3922	148.1	172	9.2	31.1	4.6/8.5	3.1 [2]	2.5×10^{-14}	31.6	< 3.4	5.93
J1745–3040	88.373	367	5.7	33.9	2.7/8.6	1.9 [2]	8.6×10^{-15}	30.7	$< 6.4 \times 10^{-4}$	5.85
J1747–2802	835	2780	7.3	30.6	25.8/8.8	11.1 [2]	5.5×10^{-15}	32.1	$< 2.7 \times 10^{+1}$	6.10
J1748–3009	420.2	9	-	-	13.0/5.0	5.1 [2]	2.2×10^{-14}	32.0	-	6.12
J1749–3002	509.4	609	6.1	33.1	15.7/6.1	5.8 [2]	1.4×10^{-14}	31.9	$< 6.0 \times 10^{-2}$	6.02
J1751–2857	42.808	3	9.7	33.9	1.3/3.0	1.1 [2]	1.9×10^{-14}	30.6	$< 5.4 \times 10^{-4}$	5.79
J1753–1914	105.3	62	8.7	32.5	3.2/2.4	2.2 [2]	5.1×10^{-15}	30.6	$< 1.3 \times 10^{-2}$	5.79
J1754–3443	187.7	361	7.0	32.7	5.8/12.0	4.1 [2]	9.4×10^{-15}	31.4	$< 5.9 \times 10^{-2}$	6.02
J1755–2725	115	261	8.5	31.5	3.5/2.6	2.4 [2]	1.1×10^{-14}	31.0	$< 3.6 \times 10^{-1}$	5.98
J1757–2421	179.454	234	5.5	34.6	5.5/11.9	4.4 [2]	1.4×10^{-14}	31.7	$< 1.2 \times 10^{-3}$	5.98
J1759–2205	177.157	460	5.8	33.6	5.5/2.9	3.6 [2]	6.5×10^{-14}	32.2	$< 3.3 \times 10^{-2}$	6.07
J1759–2302	889	810	6.1	32.9	27.4/3.4	11.6 [2]	2.6×10^{-14}	32.8	$< 7.4 \times 10^{-1}$	6.22
J1759–2307	812.6	558	6.4	32.9	25.1/0.8	10.9 [2]	3.1×10^{-14}	32.8	$< 7.3 \times 10^{-1}$	6.22
J1759–3107	128.6	1078	6.7	32.1	4.0/12.4	2.8 [2]	9.5×10^{-13}	33.1	$< 1.1 \times 10^{+1}$	6.14
J1801–2304	1073.9	415	4.8	34.8	33.1/10.8	4.0 [1]	2.2×10^{-14}	31.8	$< 1.0 \times 10^{-3}$	5.98
J1804–0735	186.316	23	8.9	33.2	5.7/3.2	5.0 [2]	3.3×10^{-15}	31.2	$< 9.6 \times 10^{-3}$	5.94
J1805–1504	225	1181	7.8	30.8	6.9/5.9	4.4 [2]	2.5×10^{-14}	31.9	$< 1.3 \times 10^{+1}$	6.01
J1806–2125	750.4	481	4.8	34.6	23.2/11.1	9.9 [2]	1.3×10^{-14}	32.3	$< 5.2 \times 10^{-3}$	6.07
J1807–0847	112.3802	163	8.0	32.4	3.5/10.4	2.7 [2]	8.1×10^{-15}	31.0	$< 4.0 \times 10^{-2}$	5.94
J1808–2701	95	2457	5.8	32.2	2.9/12.4	1.8 [2]	1.0×10^{-14}	30.7	$< 3.2 \times 10^{-2}$	5.85
J1809–1850	598	1124	6.2	32.5	18.5/1.7	7.2 [2]	5.4×10^{-14}	32.7	< 1.6	6.21
J1809–2004	867.1	434	6.0	33.5	26.8/1.7	10.9 [2]	6.4×10^{-15}	32.1	$< 3.7 \times 10^{-2}$	5.94
J1810–1820	452.2	153	7.7	32.8	14.0/1.7	5.6 [2]	8.2×10^{-15}	31.7	$< 7.9 \times 10^{-2}$	6.00
J1811–1049	253.3	2623	7.7	30.2	7.8/8.7	5.5 [2]	1.5×10^{-13}	32.9	$< 4.3 \times 10^{+2}$	6.06
J1811–1835	761	557	6.1	33.2	23.5/1.3	9.3 [2]	2.1×10^{-14}	32.5	$< 2.2 \times 10^{-1}$	6.11
J1812–1910	892	430	5.3	34.3	27.5/10.9	11.2 [2]	6.2×10^{-14}	33.1	$< 7.3 \times 10^{-2}$	6.29
J1813–1822	60.8	336	8.4	31.3	1.9/11.8	2.9 [2]	6.7×10^{-15}	31.1	$< 6.2 \times 10^{-1}$	5.91
J1814–1744	792	3975	4.9	32.7	24.4/14.3	9.6 [2]	9.0×10^{-14}	33.2	< 3.0	6.26
J1815–1738	728	198	4.6	35.6	22.5/14.7	8.8 [2]	9.4×10^{-14}	33.1	$< 3.2 \times 10^{-3}$	6.26
J1816–5643	52.4	217	9.3	30.9	1.6/4.4	1.5 [2]	5.9×10^{-15}	30.4	$< 3.3 \times 10^{-1}$	5.80
J1817–3618	94.3	387	6.5	33.1	2.9/6.6	2.4 [2]	2.1×10^{-15}	30.3	$< 1.5 \times 10^{-3}$	5.84
J1818–1448	644	281	5.9	34.0	19.9/11.6	7.4 [2]	1.1×10^{-14}	32.0	$< 9.8 \times 10^{-3}$	6.10
J1818–1519	845	939	6.6	32.3	26.1/10.5	9.6 [2]	3.3×10^{-14}	32.7	< 2.6	6.10
J1818–1541	690	551	6.0	33.4	21.3/0.7	7.8 [2]	4.4×10^{-14}	32.7	$< 2.1 \times 10^{-1}$	6.10
J1818–1556	230	952	7.3	31.5	7.1/5.0	3.9 [2]	4.7×10^{-15}	31.1	$< 3.8 \times 10^{-1}$	5.95
J1819–1008	404	301	6.6	33.3	12.5/8.3	7.2 [2]	2.8×10^{-14}	32.4	$< 1.3 \times 10^{-1}$	6.18
J1819–1510	421.7	226	8.7	31.4	13.0/1.8	5.3 [2]	1.7×10^{-14}	31.9	< 3.1	6.14

Continued on next page

Table 5 – continued from previous page

PSR	DM	P	log(Age)	log(\dot{E})	$N_{\text{H}}/N_{\text{H}}^{\text{LAB}}$	d	$f_{0.1-2 \text{ keV}}^{\text{PL}}$	$\log(L_{0.1-2 \text{ keV}}^{\text{PL}})$	$\mu_{0.1-2 \text{ keV}}^{\text{PL}}$	$\log(T_{\infty})$
J1821–1419	1123	1656	4.5	33.9	34.7/12.0	11.3 [2]	3.2×10^{-14}	32.8	$< 9.0 \times 10^{-2}$	6.22
J1821–1432	570	1915	6.8	31.5	17.6/10.6	6.5 [2]	5.0×10^{-15}	31.6	< 1.2	6.06
J1822–1617	647	831	6.8	32.1	20.0/0.4	9.4 [2]	2.1×10^{-12}	34.5	$< 2.5 \times 10^{+2}$	6.43
J1823–1347	1044	617	6.0	33.2	32.2/1.6	10.5 [2]	8.5×10^{-15}	32.2	$< 1.0 \times 10^{-1}$	6.00
J1824–1159	463.4	362	6.0	33.6	14.3/9.5	5.6 [2]	2.4×10^{-14}	32.1	$< 2.9 \times 10^{-2}$	5.97
J1825–1446	357	279	5.3	34.6	11.0/0.4	5.1 [2]	5.7×10^{-15}	31.4	$< 6.1 \times 10^{-4}$	5.97
J1826–1131	320.58	2093	6.8	31.3	9.9/14.2	4.6 [2]	6.3×10^{-15}	31.4	< 1.1	5.84
J1828–1007	302.6	153	6.6	33.8	9.3/6.0	4.4 [2]	1.2×10^{-14}	31.6	$< 6.1 \times 10^{-3}$	6.04
J1828–1057	245	246	5.3	34.7	7.6/15.9	4.0 [2]	1.6×10^{-14}	31.6	$< 7.9 \times 10^{-4}$	6.02
J1828–1101	607.4	72	4.9	36.2	18.7/5.5	6.6 [2]	1.3×10^{-14}	32.0	$< 6.3 \times 10^{-5}$	6.05
J1830–1059	161.50	405	5.0	34.6	5.0/16.4	3.2 [2]	5.0×10^{-14}	31.9	$< 2.4 \times 10^{-3}$	6.06
J1831–0952	247	67	5.1	36.0	7.6/7.3	4.1 [2]	5.9×10^{-14}	32.2	$< 1.5 \times 10^{-4}$	6.12
J1831–1223	342	2857	6.9	31.0	10.6/6.5	5.0 [2]	1.7×10^{-14}	31.9	< 8.2	6.12
J1832+0029	28.3	533	6.7	32.6	0.9/1.7	1.3 [2]	6.8×10^{-16}	29.5	$< 7.2 \times 10^{-4}$	5.66
J1832–1021	475.7	330	6.1	33.7	14.7/16.8	5.8 [2]	2.8×10^{-14}	32.2	$< 3.5 \times 10^{-2}$	6.13
J1833–1055	543	633	7.3	31.9	16.8/15.9	7.1 [2]	1.8×10^{-14}	32.2	< 1.9	6.16
J1835–1106	132.679	165	5.1	35.3	4.1/18.3	2.8 [2]	4.5×10^{-15}	30.8	$< 3.5 \times 10^{-5}$	5.97
J1837–0559	317.8	201	6.0	34.2	9.8/16.7	5.4 [2]	8.8×10^{-15}	31.7	$< 2.8 \times 10^{-3}$	6.10
J1837–0604	462	96	4.5	36.3	14.3/13.2	6.4 [2]	2.9×10^{-14}	32.3	$< 1.0 \times 10^{-4}$	6.18
J1837–0653	316.1	1905	7.6	30.6	9.8/12.5	5.3 [2]	1.0×10^{-14}	31.7	$< 1.1 \times 10^{+1}$	6.09
J1838–0537	-	145	3.7	36.8	-/14.8	-	5.4×10^{-15}	-	-	-
J1838–0549	274	235	5.0	35.0	8.5/15.9	5.1 [2]	1.7×10^{-14}	31.9	$< 7.9 \times 10^{-4}$	6.11
J1840–1419	19.4	6597	7.2	29.9	0.6/3.3	0.8 [2]	1.8×10^{-15}	29.3	$< 2.5 \times 10^{-1}$	5.63
J1841–0345	194.32	204	4.7	35.4	6.0/1.7	4.8 [2]	8.2×10^{-15}	31.5	$< 1.2 \times 10^{-4}$	6.05
J1841–0500	532	912	5.6	33.3	16.4/11.3	7.0 [2]	1.6×10^{-15}	31.1	$< 7.4 \times 10^{-3}$	6.08
J1841–0524	289	445	4.5	35.0	8.9/9.0	5.3 [2]	1.3×10^{-14}	31.8	$< 6.4 \times 10^{-4}$	6.11
J1842–0359	195.98	1839	7.8	30.5	6.0/10.4	4.7 [2]	3.7×10^{-14}	32.1	$< 4.3 \times 10^{+1}$	6.08
J1843–0137	486	669	6.6	32.5	15.0/13.3	7.9 [2]	8.9×10^{-14}	33.1	< 4.0	6.26
J1843–0355	797.6	132	6.3	34.2	24.6/2.1	8.8 [2]	4.3×10^{-16}	30.8	$< 3.2 \times 10^{-4}$	5.92
J1843–0408	246	781	6.7	32.3	7.6/1.1	5.2 [2]	2.5×10^{-15}	31.1	$< 5.9 \times 10^{-2}$	6.02
J1843–1113	59.96	1	9.5	34.8	1.9/11.8	1.7 [2]	3.2×10^{-14}	31.2	$< 2.7 \times 10^{-4}$	5.85
J1844–0244	429	507	5.7	33.7	13.2/8.2	6.6 [2]	2.7×10^{-14}	32.3	$< 4.0 \times 10^{-2}$	6.17
J1844–0310	836.1	525	5.9	33.4	25.8/11.4	9.2 [2]	6.2×10^{-16}	31.0	$< 3.3 \times 10^{-3}$	5.98
J1844–0433	123.158	991	6.6	32.2	3.8/3.8	2.9 [2]	8.3×10^{-15}	31.1	$< 7.7 \times 10^{-2}$	5.91
J1845–0434	230.8	486	5.8	33.6	7.1/16.4	5.1 [2]	1.6×10^{-14}	31.8	$< 1.8 \times 10^{-2}$	6.07
J1846+0919	-	225	5.6	34.5	-/0.5	-	9.5×10^{-16}	-	-	-
J1846–0257	237	4476	5.6	31.8	7.3/16.4	5.2 [2]	1.3×10^{-16}	29.8	$< 8.8 \times 10^{-3}$	5.78
J1847–0130	667	6707	4.9	32.2	20.6/7.4	8.4 [2]	1.2×10^{-14}	32.3	< 1.1	6.18
J1848–0055	1166	274	6.5	33.4	36.0/10.0	14.9 [2]	4.7×10^{-15}	32.4	$< 9.4 \times 10^{-2}$	6.19
J1848–0123	159.531	659	6.3	32.9	4.9/2.8	4.4 [1]	2.8×10^{-15}	30.9	$< 1.1 \times 10^{-2}$	5.94
J1848–1952	18.23	4308	6.5	31.1	0.6/15.5	0.8 [2]	4.5×10^{-15}	29.6	$< 3.8 \times 10^{-2}$	5.58
J1850–0026	947	166	4.8	35.5	29.2/8.5	11.1 [2]	9.0×10^{-15}	32.4	$< 7.8 \times 10^{-4}$	6.02
J1850–0031	895	734	7.0	32.1	27.6/12.3	10.5 [2]	2.2×10^{-14}	32.8	< 4.6	6.23
J1852+0008	254.9	467	6.1	33.3	7.9/14.7	5.7 [2]	2.8×10^{-14}	32.3	$< 9.7 \times 10^{-2}$	6.13
J1852+0031	787	2180	5.6	32.6	24.3/2.5	8.0 [1]	4.9×10^{-15}	31.8	$< 1.6 \times 10^{-1}$	6.12
J1852–0118	286	451	6.6	32.9	8.8/4.5	5.9 [2]	8.8×10^{-15}	31.9	$< 9.6 \times 10^{-2}$	5.96
J1852–0127	431	428	6.1	33.4	13.3/11.9	7.2 [2]	1.3×10^{-14}	32.2	$< 5.9 \times 10^{-2}$	6.16
J1853+1303	30.5701	4	9.9	33.7	0.9/11.3	2.1 [2]	1.0×10^{-14}	31.0	$< 2.1 \times 10^{-3}$	5.81
J1856+0102	554	620	6.9	32.3	17.1/1.5	8.5 [2]	1.6×10^{-14}	32.4	< 1.3	6.20
J1857+0943	13.300	5	9.7	33.7	0.4/3.7	0.9 [1]	1.4×10^{-14}	30.3	$< 4.4 \times 10^{-4}$	5.67
J1901+0124	314.4	318	6.2	33.6	9.7/13.1	5.2 [2]	2.1×10^{-13}	33.1	$< 3.4 \times 10^{-1}$	6.20
J1901+0435	1042.6	690	6.1	33.0	32.2/1.2	19.4 [2]	1.7×10^{-14}	33.2	< 1.4	6.14
J1901+0510	429	614	5.5	33.7	13.2/1.3	7.3 [2]	4.7×10^{-14}	32.8	$< 1.1 \times 10^{-1}$	6.23
J1905+0709	245.34	648	6.3	32.9	7.6/1.9	5.7 [2]	1.5×10^{-14}	32.1	$< 1.6 \times 10^{-1}$	6.02

Continued on next page

Table 5 – continued from previous page

PSR	DM	P	log(Age)	log(\dot{E})	$N_{\text{H}}/N_{\text{H}}^{\text{LAB}}$	d	$f_{0.1-2 \text{ keV}}^{\text{PL}}$	$\log(L_{0.1-2 \text{ keV}}^{\text{PL}})$	$\mu_{0.1-2 \text{ keV}}^{\text{PL}}$	$\log(T_{\infty})$
J1905+0902	433.4	218	6.0	34.1	13.4/4.2	9.1 [2]	3.0×10^{-15}	31.8	$< 4.4 \times 10^{-3}$	6.06
J1906+0746	217.780	144	5.1	35.4	6.7/6.6	5.4 [2]	6.4×10^{-16}	30.6	$< 1.6 \times 10^{-5}$	5.93
J1906+0912	265	775	8.0	31.0	8.2/9.3	6.4 [2]	7.6×10^{-15}	31.9	< 6.6	6.09
J1907+0534	524	1138	6.8	31.9	16.2/4.0	9.6 [2]	4.5×10^{-15}	32.0	< 1.1	6.09
J1907+0918	357.9	226	4.6	35.5	11.0/10.0	7.8 [2]	1.4×10^{-15}	31.3	$< 6.4 \times 10^{-5}$	6.08
J1908+0734	11.104	212	6.6	33.5	0.3/1.2	1.0 [2]	4.3×10^{-14}	31.0	$< 2.9 \times 10^{-3}$	5.77
J1908+0839	512.1	185	6.1	34.2	15.8/1.9	9.3 [2]	1.2×10^{-14}	32.4	$< 1.6 \times 10^{-2}$	6.10
J1908+0916	249.8	830	8.1	30.8	7.7/3.1	5.9 [2]	3.7×10^{-14}	32.5	$< 4.6 \times 10^{+1}$	6.12
J1911+1758	48.971	460	8.7	30.7	1.5/8.6	2.8 [2]	6.2×10^{-15}	31.0	< 2.1	5.90
J1913+0446	109.1	1616	5.0	33.4	3.4/9.1	3.8 [2]	1.2×10^{-14}	31.6	$< 1.6 \times 10^{-2}$	5.96
J1913+1011	178.8	35	5.2	36.5	5.5/1.1	4.8 [2]	3.8×10^{-15}	31.3	$< 6.9 \times 10^{-6}$	6.00
J1921+2153	12.455	1337	7.2	31.3	0.4/0.6	1.1 [2]	4.8×10^{-15}	30.1	$< 6.1 \times 10^{-2}$	5.63
J1926–1314	40.83	4864	6.3	31.1	1.3/6.4	1.5 [2]	2.4×10^{-15}	30.0	$< 7.2 \times 10^{-2}$	5.71
J1928+1746	176.68	68	4.9	36.2	5.5/0.6	5.8 [2]	4.3×10^{-15}	31.5	$< 2.1 \times 10^{-5}$	6.04
J1933+2421	106.03	813	6.2	32.8	3.3/0.2	4.6 [2]	4.7×10^{-15}	31.4	$< 3.9 \times 10^{-2}$	5.97
J1933–6211	11.499	3	10.2	33.5	0.4/0.5	0.5 [2]	2.2×10^{-14}	30.5	$< 1.0 \times 10^{-3}$	5.64
J1946+3417	-	3	10.1	33.7	3.4/7.3	6.4 [3]	1.1×10^{-14}	32.1	$< 2.6 \times 10^{-2}$	5.92
J1954+2836	-	92	4.8	36.0	-/6.4	-	4.4×10^{-14}	-	-	-
J1954+2923	7.932	426	9.6	29.9	0.2/6.4	0.7 [2]	3.3×10^{-15}	29.6	$< 4.3 \times 10^{-1}$	5.57
J2005+3547	401.6	615	7.5	31.7	12.4/6.4	30.0 [3]	3.1×10^{-15}	32.9	$< 1.6 \times 10^{+1}$	6.06
J2007+2722	127.0	24	8.6	33.4	3.9/6.4	5.4 [2]	3.5×10^{-16}	30.4	$< 9.3 \times 10^{-4}$	5.87
J2043+1711	20.70987	2	9.9	34.2	0.6/6.4	1.8 [2]	1.6×10^{-14}	31.1	$< 7.7 \times 10^{-4}$	5.91
J2048+2255	68.8	283	8.5	31.4	2.1/6.4	4.0 [2]	7.0×10^{-15}	31.4	< 1.0	5.95
J2129–5721	31.853	3	9.5	34.2	1.0/6.4	0.4 [1]	7.7×10^{-15}	29.5	$< 2.1 \times 10^{-5}$	5.64
J2144–3933	3.35	8509	8.4	28.5	0.10/6.4	0.2 [1]	3.3×10^{-15}	28.1	$< 4.0 \times 10^{-1}$	5.34
J2156+2618	48.8	498	8.7	30.7	1.5/6.4	3.2 [2]	5.8×10^{-15}	31.1	< 3.0	5.89
J2222+2923	49.38	281	8.9	31.0	1.5/6.4	3.3 [2]	6.2×10^{-15}	31.2	< 1.4	5.91
J2235+1506	18.09	59	9.8	31.5	0.6/6.4	1.1 [2]	5.3×10^{-15}	30.2	$< 4.9 \times 10^{-2}$	5.72
J2238+5903	-	162	4.4	35.9	-/6.4	-	4.4×10^{-14}	-	-	-
J2307+2225	7.08	535	9.0	30.3	0.2/6.4	0.6 [2]	5.1×10^{-15}	29.8	$< 2.7 \times 10^{-1}$	5.59

References. [1] Verbiest et al. (2012); [2] Cordes & Lazio (2002); [3] Taylor & Cordes (1993).

Table 2. Pulsars and coordinates of their potential X-ray counterparts along with their positional discrepancy, chance probability for a false detection, signal-to-noise and X-ray to visual flux ratio.

PSR	RA hh:mm:ss	DEC dd:mm:ss	Δ arcsec	S/N $\sigma_G^{(\alpha)}$	P_{coin}	$\log(f_X/f_V)$
J0101–6422	01 : 01 : 11.11 ± 0.06	−64 : 22 : 30.4 ± 0.4	0.2 ± 0.4	15.9	5.5×10^{-6}	> 0.2
J0117+5914	01 : 17 : 38.5 ± 0.3	+59 : 14 : 38 ± 2	1.6 ± 2.1	16.9	1.3×10^{-4}	> 0.2
J0337+1715	03 : 37 : 43.7 ± 0.1	+17 : 15 : 13 ± 2	1.7 ± 2.1	33.0	3.0×10^{-4}	> −1.1
J0543+2329	05 : 43 : 09.5 ± 0.2	+23 : 29 : 07 ± 2	3.4 ± 4.8	5.9	2.8×10^{-4}	> −0.4
J0922+0638	09 : 22 : 14.16 ± 0.14	+06 : 38 : 24 ± 2	2.4 ± 2.1	17.8	6.3×10^{-4}	> −0.7
J1044–5737	10 : 44 : 32.87 ± 0.05	−57 : 37 : 19.1 ± 0.4	0.6 ± 0.9	12.6	5.9×10^{-5}	> 0.1
J1112–6103	11 : 12 : 14.87 ± 0.03	−61 : 03 : 30.7 ± 0.2	0.6 ± 0.5	43.0	4.1×10^{-4}	> 0.0
J1224–6407	12 : 24 : 21.8 ± 0.3	−64 : 07 : 55 ± 2	2.9 ± 2.3	6.1	2.3×10^{-4}	> −0.3
J1301–6310	13 : 01 : 28.2 ± 0.3	−63 : 10 : 42 ± 2	1.9 ± 2.3	10.4	2.0×10^{-4}	> −0.2
J1341–6220	13 : 41 : 43.1 ± 0.3	−62 : 20 : 18 ± 2	4.2 ± 2.4	6.4	3.4×10^{-3}	> −0.8
J1600–3053	16 : 00 : 51.8 ± 0.2	−30 : 53 : 49 ± 2	0.8 ± 2.4	5.8	3.0×10^{-5}	> −0.6
J1658–5324	16 : 58 : 39.35 ± 0.05	−53 : 24 : 06.8 ± 0.3	0.2 ± 0.3	9.6	6.2×10^{-6}	> −0.1
J1730–2304	17 : 30 : 21.5 ± 0.2	−23 : 04 : 30 ± 2	2.7 ± 2.1	24.4	5.5×10^{-4}	> −0.2
J1731–1847	17 : 31 : 17.7 ± 0.2	−18 : 47 : 31 ± 2	1.2 ± 2.7	5.1	1.1×10^{-4}	> −0.6
J1816+4510	18 : 16 : 35.90 ± 0.03	+45 : 10 : 33.9 ± 0.2	0.3 ± 0.3	6.4	2.9×10^{-5}	> −1.9
J1825–0935	18 : 25 : 30.7 ± 0.2	−09 : 35 : 23 ± 2	1.5 ± 2.3	6.7	2.4×10^{-5}	> −1.1
J1832–0836	18 : 32 : 27.7 ± 0.2	−08 : 36 : 54 ± 2	1.8 ± 2.6	5.9	1.9×10^{-3}	> −0.8
J1911–1114	19 : 11 : 49.5 ± 0.2	−11 : 14 : 23 ± 2	3.1 ± 2.8	6.5	8.7×10^{-4}	> −0.8
J2017+0603	20 : 17 : 22.70 ± 0.01	+06 : 03 : 05.4 ± 0.2	0.2 ± 0.2	8.7	3.6×10^{-6}	> −0.3
J2222–0137	22 : 22 : 05.95 ± 0.01	−01 : 37 : 15.7 ± 0.2	0.1 ± 0.2	8.9	2.0×10^{-5}	> −0.7

^a $\sigma_G = 1 + \sqrt{c_{\text{bg}} + 0.75}$, where c_{bg} are the background counts.

Table 3. Spectral parameters of model spectra fitted to potential pulsar counterparts which were detected with sufficient photon statistics to allow for a brief spectral analysis.

PSR	model	$\chi^2/\text{d.o.f.}$	N_{H} 10^{22} cm^{-2}	Γ/T_{emit} -/keV	Norm ^β	R_{emit} km
J0117+5914	BB ^α	12.2/13	< 0.48	$0.18^{+0.04}_{-0.03}$	$3.7^{+1.3}_{-1.1} \times 10^{-7}$	0.4 ± 0.2
	PL ^α	13.2/13	$0.5^{+0.7}_{-0.5}$	3.3 ± 0.5	$(8 \pm 2) \times 10^{-6}$	-
J0922+0638	PL	4.0/8	< 0.12	$2.3^{+0.8}_{-0.4}$	$1.9^{+0.9}_{-0.4} \times 10^{-6}$	-
J1301-6310	BB ^α	23.8/16	< 0.09	$0.25^{+0.08}_{-0.07}$	$9^{+4}_{-2} \times 10^{-8}$	$0.08^{+0.04}_{-0.03}$
	PL ^α	16.4/16	< 0.39	$3.4^{+0.8}_{-0.6}$	$(3.2 \pm 0.7) \times 10^{-6}$	-
J1341-6220	BB ^α	12.8/23	< 2.2	$1.2^{+1.6}_{-0.4}$	$3^{+4}_{-2} \times 10^{-7}$	$0.04^{+0.06}_{-0.02}$
	PL ^α	13.6/23	4 ± 3	1.1 ± 0.7	$1.5^{+2.1}_{-1.0} \times 10^{-6}$	-
J1730-2304	BB ^α	12.2/18	< 0.53	$0.26^{+0.06}_{-0.21}$	$1.5^{+0.4}_{-0.7} \times 10^{-7}$	$0.026^{+0.009}_{-0.023}$
	PL ^α	17.0/17	< 0.47	$2.7^{+0.9}_{-0.5}$	$3.3^{+0.9}_{-1.2} \times 10^{-6}$	-
J1112-6103	BB	12.7/11	$0^{+0.5}$	$1.18^{+0.17}_{-0.18}$	$6.5^{+1.3}_{-1.1} \times 10^{-7}$	$0.157^{+0.028}_{-0.028}$
	PL	9.7/11	$1.2^{+1.1}_{-1.0}$	1.5 ± 0.7	$1.3^{+2.3}_{-0.8} \times 10^{-5}$	-

^αSpectral parameters were obtained with N_{H} fixed to DM based value and we added the result of N_{H} before fixing.

^βPL: photons keV⁻¹ cm⁻² s⁻¹ at 1 keV; BB: $L[10^{39} \text{ erg/s}]/(D[10 \text{kpc}])^2$, where L is the source luminosity and D the distance to the source.

Table 4. Essential radio pulsar parameters along with the flux, luminosity and X-ray efficiency of the potential X-ray counterparts for thermal (BB) and/or non-thermal (PL) emission.

PSR	DM pc cm ⁻³	P ms	log(Age) yrs	log(\dot{E}) erg s ⁻¹	n_{H} 10 ²¹ cm ⁻²	d kpc	model	$f_{0.1-2 \text{ keV}}$ erg s ⁻¹ cm ⁻²	$L_{0.1-2 \text{ keV}}$ erg s ⁻¹	$\mu_{0.1-2 \text{ keV}}$
J0117+5914	49.423	101	5.4	35.3	1.5	2.2	BB	$(3.1 \pm 0.6) \times 10^{-14}$	$(1.8 \pm 0.4) \times 10^{31}$	$(8 \pm 2) \times 10^{-5}$
							PL	$1.8^{+1.4}_{-0.8} \times 10^{-13}$	$1.1^{+0.9}_{-0.4} \times 10^{32}$	$(5 \pm 2) \times 10^{-4}$
J0337+1715	-	2	9.4	34.5	0.7	1.4	PL ^a	$(2.17 \pm 0.15) \times 10^{-14}$	$5.1^{+0.3}_{-0.4} \times 10^{30}$	$(1.49 \pm 0.10) \times 10^{-4}$
J0543+2329	77.7115	245	5.4	34.6	2.4	2.1	PL ^a	$(8 \pm 2) \times 10^{-15}$	$(4.1 \pm 1.1) \times 10^{30}$	$(10 \pm 3) \times 10^{-5}$
J0922+0638	27.271	430	5.7	33.8	0.8	1.1	PL	$1.2^{+1.4}_{-0.6} \times 10^{-14}$	$1.7^{+2.0}_{-0.9} \times 10^{30}$	$(2.5 \pm 1.4) \times 10^{-4}$
J1224-6407	97.47	216	5.8	34.3	3.0	4.0	PL ^a	$(10 \pm 3) \times 10^{-15}$	$(1.9 \pm 0.5) \times 10^{31}$	$(10 \pm 3) \times 10^{-4}$
J1301-6310	86.1	663	5.3	33.9	2.7	1.9	BB	$(7.4 \pm 1.4) \times 10^{-15}$	$(3.0 \pm 0.6) \times 10^{30}$	$(4.0 \pm 0.8) \times 10^{-4}$
							PL	$9^{+7}_{-4} \times 10^{-14}$	$3^{+3}_{-2} \times 10^{31}$	$(5 \pm 2) \times 10^{-3}$
J1341-6220	717.3	193	4.1	36.1	22.1	11.1	PL	$5^{+4}_{-3} \times 10^{-15}$	$7^{+6}_{-4} \times 10^{31}$	$(5 \pm 3) \times 10^{-5}$
J1600-3053	52.3262	3	9.8	33.9	1.6	2.4	PL ^a	$(6 \pm 2) \times 10^{-15}$	$(4.1 \pm 1.1) \times 10^{30}$	$(5.1 \pm 1.3) \times 10^{-4}$
J1730-2304	9.617	8	9.8	33.2	0.3	0.5	BB	$1.4^{+0.1}_{-0.2} \times 10^{-14}$	$4.9^{+0.4}_{-0.6} \times 10^{29}$	$(3.3 \pm 0.4) \times 10^{-4}$
							PL	$3.5^{+1.8}_{-1.1} \times 10^{-14}$	$1.2^{+0.6}_{-0.4} \times 10^{30}$	$(8 \pm 2) \times 10^{-4}$
J1731-1847	106.56	2	9.2	34.9	3.3	2.6	PL ^a	$(6 \pm 2) \times 10^{-15}$	$(4.4 \pm 1.3) \times 10^{30}$	$(6 \pm 2) \times 10^{-5}$
J1825-0935	19.38	769	5.4	33.7	0.6	0.9	PL ^a	$(1.7 \pm 0.4) \times 10^{-14}$	$(1.6 \pm 0.4) \times 10^{30}$	$(3.4 \pm 0.8) \times 10^{-4}$
J1832-0836	28.18	2	9.7	34.2	0.9	1.1	PL ^a	$(3.8 \pm 1.0) \times 10^{-15}$	$(5.6 \pm 1.5) \times 10^{29}$	$(3.3 \pm 0.9) \times 10^{-5}$
J1911-1114	30.9750	3	9.6	34.1	1.0	1.2	PL ^a	$3.7^{+0.9}_{-0.8} \times 10^{-15}$	$6.5^{+1.6}_{-1.5} \times 10^{29}$	$(5.6 \pm 1.3) \times 10^{-5}$
J0101-6422	11.926	2	9.9	34.1	0.4	0.6	PL ^a	$(3.0 \pm 0.5) \times 10^{-14}$	$(1.1 \pm 0.2) \times 10^{30}$	$(9 \pm 2) \times 10^{-5}$
J1044-5737	-	139	4.6	35.9	1.0	-	PL ^a	$2.4^{+0.5}_{-0.4} \times 10^{-14}$	-	-
J1112-6103	599.1	64	4.5	36.7	18.5	12.3	PL	$4^{+3}_{-2} \times 10^{-14}$	$6^{+5}_{-4} \times 10^{32}$	$(1.4 \pm 0.9) \times 10^{-4}$
J1658-5324	30.8	2	9.5	34.5	1.0	0.9	PL ^a	$(1.6 \pm 0.3) \times 10^{-14}$	$(1.7 \pm 0.3) \times 10^{30}$	$(5.6 \pm 1.1) \times 10^{-5}$
J1816+4510	38.8	3	9.1	34.7	1.2	2.4	PL ^a	$(3.1 \pm 0.8) \times 10^{-15}$	$(2.1 \pm 0.5) \times 10^{30}$	$(4.1 \pm 1.1) \times 10^{-5}$
J2017+0603	23.918	2	9.7	34.1	0.7	1.6	PL ^a	$(1.1 \pm 0.3) \times 10^{-14}$	$(3.3 \pm 0.8) \times 10^{30}$	$(2.4 \pm 0.6) \times 10^{-4}$
J2222-0137	3.27511	32	9.9	31.8	0.10	0.3	PL ^a	$4.5^{+1.0}_{-0.9} \times 10^{-15}$	$(5.2 \pm 1.1) \times 10^{28}$	$(8 \pm 2) \times 10^{-4}$

^aFlux derived using PIMMS with a power law model and a photon index of 1.7.

Table 6. The pulsars with an X-ray efficiency upper limit below 5×10^{-5} .

PSR	$\frac{\dot{E}}{4\pi d^2}$ erg s ⁻¹ cm ⁻²	log(\dot{E}) erg s ⁻¹	$\mu_{0.1-2 \text{ keV}}^{\text{PL}}$	d kpc	log(τ) yrs	B_{surf} G
J0940–5428	1.9×10^{-9}	36.3	2.2×10^{-6}	3.0	4.6	$1.7 \times 10^{+12}$
J1300+1240	4.4×10^{-10}	34.3	3.5×10^{-6}	0.6	8.9	$8.5 \times 10^{+08}$
J1105–6107	8.3×10^{-10}	36.4	6.0×10^{-6}	5.0	4.8	$1.0 \times 10^{+12}$
J1913+1011	1.1×10^{-9}	36.5	6.9×10^{-6}	4.8	5.2	$3.5 \times 10^{+11}$
J1730–3350	8.2×10^{-10}	36.1	9.7×10^{-6}	3.5	4.4	$3.5 \times 10^{+12}$
J1906+0746	7.7×10^{-11}	35.4	1.6×10^{-5}	5.4	5.1	$1.7 \times 10^{+12}$
J2129–5721	8.3×10^{-10}	34.2	2.1×10^{-5}	0.4	9.5	$2.8 \times 10^{+08}$
J1928+1746	3.9×10^{-10}	36.2	2.1×10^{-5}	5.8	4.9	$9.6 \times 10^{+11}$
J1835–1106	1.9×10^{-10}	35.3	3.5×10^{-5}	2.8	5.1	$1.9 \times 10^{+12}$
J1702–4310	2.0×10^{-10}	35.8	4.5×10^{-5}	5.2	4.2	$7.4 \times 10^{+12}$

Table 7. The pulsars with the lowest 3σ temperature upper limit (indicated by a black arrow in the upper panel of Figure 5). *Top:* Young neutron stars with $\tau \leq 5 \times 10^4$ yrs. *Bottom:* Neutron stars with $\tau > 5 \times 10^4$ yrs.

PSR	log(age) yrs	T_{∞} 10^5 K
J0940–5428	4.63	7.3
J1524–5706	4.70	9.8
J1730–3350	4.42	11.0
J1637–4642	4.62	12.1
J1907+0918	4.58	12.1
J1702–4310	4.23	12.3
J1413–6141	4.13	12.6
J1841–0524	4.48	12.8
J1726–3530	4.16	14.1
J1837–0604	4.53	15.2
J1646–4346	4.51	15.6
J0157+6212	5.29	5.5
J1105–6107	4.80	5.7
J1457–5902	5.70	5.8
J1846–0257	5.65	6.0
J0742–2822	5.20	7.8
J1906+0746	5.05	8.4
J1913+0446	4.96	9.2
J1801–2304	4.77	9.6
J1850–0026	4.83	10.6
J1928+1746	4.92	10.9
J1055–6028	4.73	11.1
J1828–1101	4.89	11.1
J1841–0345	4.75	11.3
J1806–2125	4.80	11.7